NASA SP-301

SUPERCRITICAL WING TECHNOLOGY

A Progress Report on Flight Evaluations

A compilation of reports
presented at a symposium held at
NASA Flight Research Center
Edwards, California
February 29, 1972

Prepared by Flight Research Center

Scientific and Technical Information Office 1972
NATIONAL AERONAUTICS AND SPACE ADMINISTRATION
Washington, D.C.

Restriction/
Classification Cancelled

The class: nited status
of this d lies to each
page the s otherwise
marked. ge printouts
MUST be ccordingly.

CLASSIFICATION CHANGE

To UNCLASSIFIED

By authority of [illegible] Date [illegible]

[illegible] Station, NASA
Scientific and Technical Information Facility

[redacted]

PRECEDING PAGE BLANK NOT FILMED

PREFACE

The papers in this compilation were presented at the NASA Symposium on "Supercritical Wing Technology: A Progress Report on Flight Evaluations," held at the NASA Flight Research Center, Edwards, Calif., on February 29, 1972.

The purpose of the symposium was to present timely information on flight results obtained with the F-8 and T-2C supercritical wing configurations, discuss comparisons with wind-tunnel predictions, and project follow-on flight programs planned for the F-8 and F-111 (TACT) airplanes.

Papers were presented by representatives of the NASA Flight Research Center, the NASA Langley Research Center, and North American Rockwell-Columbus Division.

[redacted]

[redacted]

PRECEDING PAGE BLANK NOT FILMED

CONTENTS

[redacted]

1. THE NASA SUPERCRITICAL AIRFOIL AND ITS APPLICATION TO SWEPT WINGS*

By Richard T. Whitcomb
Langley Research Center

INTRODUCTION

The principal feature of each of the configurations to be discussed in this conference is the supercritical airfoil shape. However, in the development of these configurations, substantial attention was given to solving high-speed three-dimensional problems, particularly near the wing-fuselage junction. In this paper the mode of operation and characteristics of the NASA two-dimensional supercritical airfoils and methods for applying them to three-dimensional swept wings are discussed briefly.

DESCRIPTION OF TWO-DIMENSIONAL NASA AIRFOIL

The well-known flow problem for conventional airfoils at high subsonic speeds is illustrated at the top of figure 1. A local region of supersonic or supercritical flow develops above the upper surface of a lifting airfoil which terminates in a strong shock wave. The wave itself causes some increase in drag, but usually the principal effect is separation of the boundary layer with a significant increase in drag, stability problems, and buffet. For the NASA supercritical airfoil shown at the bottom of figure 1, the curvature of the middle region of the upper surface is substantially reduced with a resulting decrease in the strength and extent of the shock wave. The drag associated with the wave is reduced and, more importantly, the onset of separation is substantially delayed. The lift lost by reducing the curvature of the upper surface is regained by substantial camber of the rear portion of the airfoil.

The airfoil also incorporates other features which are important to the total effectiveness of the new shape. The middle region of the lower surface is designed to maintain subcritical flow for all operating conditions of the airfoil, because the pressure rise associated with a shock wave superimposed on the pressure rise caused by the cusp would cause separation of the lower-surface boundary layer. To minimize the surface curvatures and thus the induced velocities on the middle regions of both the upper and lower surfaces, the leading edge is made substantially larger than for previous airfoils. It is approximately 2.5 times that for a 6-series airfoil of the same thickness ratio.

The rear portion of the upper surface is designed to produce a constant or

*Title, Unclassified.

decreasing pressure behind the shock wave for the design condition. This feature stabilizes the boundary layer behind the shock before it enters the subsonic pressure recovery. In particular, it substantially delays the final detachment of the boundary-layer bubble present under the strong shock for high-lift conditions. Results to be presented in paper 2 will define this effect more explicitly. The pressure distribution on the aft portion of the lower surface is designed by the Stratford criteria to obtain the largest increase in lift by the cusp without incurring boundary-layer separation in the cusp. This involves a rapid initial increase in pressure followed by a more gradual increase. Finally, at the trailing edge the slope of the lower surface is made equal to that of the upper surface to reduce to a minimum the required pressure recovery at the upper-surface trailing edge. For most NASA supercritical airfoils tested, the trailing-edge pressure is near ambient.

At Mach numbers or lift coefficients less than the design conditions, the shock wave is farther forward with a substantial increase in velocity aft of the shock to a second velocity peak in the vicinity of the three-quarter chord. This peak must be carefully controlled to prevent the development of a second shock with associated separation on the extreme rearward portion of the airfoil. At Mach numbers higher than the design value, the shock wave moves rearward and becomes stronger. Also, the pressure plateau disappears. As a result, the boundary layer usually separates aft of the shock.

The aft loading (fig. 1) associated with the new shape results, of course, in more negative pitching moments.

The chronological development of the supercritical airfoil is shown in figure 2. Originally it was assumed that a means for stabilizing the boundary layer between the shock wave and the subsonic pressure recovery was required. A slot was placed between the lower and upper surfaces to accomplish this; however, it was found that the required geometric tolerances of the slot would be difficult to produce and maintain in use. Therefore, an integral or unslotted airfoil was developed using the techniques just described. Later, in recognition of the structural problem of the extremely thin trailing edge of the initial integral airfoil, a thickened trailing edge was added. This thickened trailing edge also slightly improved the aerodynamic characteristics of the airfoil by increasing the lift with a relatively small base drag penalty. All the applications to be discussed in this conference incorporate a thickened trailing edge.

TWO-DIMENSIONAL RESULTS

A comparison of the drag variation with Mach number at a normal-force coefficient of 0.7 is shown in figure 3 for a NACA 64A-410 airfoil and a supercritical airfoil. It should be noted that the supercritical airfoils intended for use on sweptback wings have been developed for relatively high-lift coefficients because the effective lift decreases by the cosine of the sweep squared. Results obtained for the 10-percent-thick unslotted airfoil are shown by the solid line (ref. 1). Data for the NACA 64A-410 airfoil are shown by the dashed line (ref. 2). A 6-series airfoil with a relatively high camber was used because it provided the fairest comparison with the highly cambered supercritical airfoil. The final drag rise for the supercritical airfoil occurs more than 0.1 Mach number later than that for the 6-series airfoil. The supercritical airfoil experiences a drag creep of approximately 12 counts at Mach numbers between the

subcritical value of 0.60 to the final drag-rise condition. This drag is associated with the relatively weak shock above the upper surface at these speeds. It is important to note, however, that earlier airfoils produced drag creeps for the same reason. At the final drag rise, the drag-creep increment for the NACA 64A-410 airfoil is the same as that for the comparable supercritical shape. Similar agreement is noted in paper 2.

In the early work with the slotted supercritical airfoil, a dip in the drag creep was achieved at a Mach number just below the final drag rise (ref. 3). Pressure distributions, schlieren photographs, and wake surveys indicated that at this condition the deceleration from supersonic to subsonic flow above the upper surface was essentially shockless. However, because of the very limited speed extent of this shockless condition, it was considered to be of little practical significance. In the later development of the unslotted airfoil, no attempt was made to attain such a condition; rather, the effort was to reduce the level of drag creep between the critical speed and final drag rise.

In figure 4 the Mach number for the onset of severe separation, that is, for buffet or abrupt drag rise, is plotted against normal-force coefficient for the same airfoils as in the previous figure. The results indicate that not only does the supercritical airfoil delay drag rise at near cruise lift coefficients but it also substantially increases both the Mach number and lift coefficient at the characteristic high-lift corner of the curve. This effect, which results primarily from the stabilization of the bubble under the shock wave as discussed earlier, is particularly important for improving maneuverability.

Recent airplane designs incorporate airfoils with somewhat higher drag rise than the NACA 6-series shown here. However, it has been difficult to acquire two-dimensional data for such airfoils. Results obtained with a C-5A airplane model in the Langley Research Center 8-foot tunnel indicate that one of these new shapes, the Pearcey peaky airfoil, delays the drag-rise Mach number 0.02 or 0.03 compared with the NACA 6-series airfoil but at a loss in the maximum lift.

As demonstrated in paper 2, supercritical technology can also be used to substantially increase the thickness ratios of an airfoil without an associated reduction in the Mach number for separation onset. Obviously, the increased thickness allows a weight reduction or an increase in aspect ratio and provides added volume for fuel or other required equipment in the wing. The three flight demonstration programs to be described in this conference are intended to demonstrate the three principal advantages of the supercritical airfoil: increased thickness ratio using the T-2C airplane; increased cruise speed using the F-8 airplane; and improved maneuverability using the F-111 airplane.

THEORETICAL AND EXPERIMENTAL TECHNIQUES

Before these supercritical airfoils can be most effectively utilized in actual airplane design, theoretical methods for describing the shapes and characteristics of such airfoils and a body of systematic experimental data should be provided. At present a method for geometrically defining the shape is available. This method, which allows for variations of thickness ratios and cambers, was used to define the airfoils for the F-8 and F-111 demonstration vehicles to be described. A number of outstanding

theoretical investigators in this country and Europe have been working on aerodynamic analysis of two-dimensional supercritical flow (references 4 to 7, for example). In this country the work is being done in industry, the universities, and the NASA Langley and Ames Research Centers. At least for the two-dimensional use, the applications of the theory to practical designs is close at hand. However, the complementary systematic experimental data are not yet available.

It should be strongly emphasized that any meaningful theoretical analysis of NASA supercritical airfoils must include the effect of the boundary layer. The importance of this effect is illustrated in figure 5. The varying boundary-layer displacement substantially changes the effective shape of the airfoil. In particular, it greatly reduces the aft camber with reductions of the trailing-edge slopes for both the upper and lower surfaces. Also, the new shape produces steep increasing pressure gradients near the trailing edge of the upper surface and ahead of the cusp on the lower surface (fig. 1). Obviously, separation will occur if these gradients are made too severe. Further, it is now well established that the position and strength of a shock wave above the upper surface of any airfoil at supercritical speeds is strongly influenced by the presence of the boundary layer.

Because of the strong effect of the boundary layer on the operation of the supercritical airfoils, it is also important that such airfoils be developed at relatively high Reynolds numbers or that full-scale boundary-layer conditions be simulated in the wind tunnel. Such a method of simulation has been used in the wind-tunnel tests of each of the configurations to be described.

The technique is illustrated in figure 6 for a conventional airfoil. As shown by the top sketch, boundary-layer-transition strips in wind-tunnel tests are normally near the airfoil leading edge. At the relatively low wind-tunnel Reynolds numbers, a fairly thick turbulent boundary layer develops which results in a forward shock location. In flight, as indicated in the middle sketch, although boundary-layer transition naturally occurs well forward on the airfoil, the higher flight Reynolds numbers result in a thinner boundary layer and the shock wave is farther rearward. The bottom sketch illustrates the technique used to simulate full-scale conditions for wind-tunnel tests where supercritical flows are expected. In this approach, the transition is somewhat rearward and the wing ahead of the trip was kept very smooth in order to maintain laminar flow ahead of the trip. The actual trip location is based on a criterion designed to provide, in the wind tunnel, the same relative boundary-layer-displacement thickness at the trailing edge as would exist in full-scale flight. Earlier investigations with a 6-series airfoil (ref. 8) showed that, based upon this approach, similar shock-wave locations and associated separation can be achieved.

For conditions where laminar flow cannot be maintained ahead of this trip location, such as when a shock or steep adverse pressure is present in this forward region, this technique is not effective. In fact, it may be detrimental. The laminar flow may separate at conditions for which the fully turbulent flow at full-scale Reynolds numbers would not. Consequently, the boundary-layer trip is moved forward to the normal forward location for such conditions.

APPLICATION TO THREE-DIMENSIONAL WINGS

Explicit methods for designing three-dimensional swept-wing configurations,

particularly for the near-sonic flight speeds allowed by the supercritical airfoils, are not as fully developed as those for two-dimensional configurations. However, some rational qualitative approaches have been developed which will be discussed briefly.

For wings of reasonably high aspect ratio such as those of the configurations to be described in this conference, the sections of the midsemispan and outboard regions can be the same as those of the two-dimensional airfoils. On the wing developed for the F-8 flight demonstration and shown in figure 7 (ref. 9), such an agreement holds even for sections on the outboard part of the nontrapezoidal region of the wing. The section near the wing-fuselage juncture is substantially different in detail from the two-dimensional section. However, even here some aft camber provided the most satisfactory results. A similar situation was found for the F-111 supercritical wing panels. The optimum shape of the inboard region must be arrived at experimentally for each configuration. However, it should be recognized that this has also been true for configurations with more conventional airfoils at Mach numbers near the drag rise.

Substantial wing twist is usually required for the best overall performance of supercritical swept wings, as for previous swept wings intended for high-speed flight. Experiments at the Langley Research Center and in industry have indicated that for both previous and supercritical swept wings a twist significantly greater than that which theoretically provides an elliptical load distribution provides the best overall design. Further, theory and experiment indicate that with an increase in the design Mach number toward 1.0 the magnitude of the optimum twist increases. Thus the optimum twist for supercritical wings designed for higher speeds is greater than for lower-speed designs. This large amount of twist substantially reduces or eliminates the trim penalty associated with the greater negative pitching moment for the supercritical airfoil for a sweptback wing.

As for many previous swept wings, the most effective operation of swept supercritical wings is achieved with a progressive increase in camber from inboard to outboard sections.

The planform as shown in figure 7 is an important part of obtaining a high drag-rise Mach number as well as a practical structure for a swept wing. The rearward extension of the root section allows for the attachment of landing gear in a transport application of such a wing. The glove extending forward is an attempt to provide the same drag-rise Mach number for the root sections as for the outboard regions of the wing. Experiments and theory have indicated that at supercritical speeds the isobars on any sweptback wing move rearward near the root sooner and more rapidly than outboard, with a resulting premature drag rise for this region. The forward root extension turns the isobars forward for subcritical conditions, so that at supercritical design conditions the sweeps of the isobars of the inboard region more nearly match those of the outboard region.

Also, as with conventional airfoils, the high-speed characteristics of a swept supercritical wing are improved by designing it so that the primary forward shock wave has more sweep than the wing elements.

Considerable interest has been shown in applying the supercritical airfoils to thin, lower aspect ratio wings intended for supersonic flight. No method for designing such a configuration has yet been developed.

The problem of incorporating a supercritical wing into a total airplane design for near-sonic flight is extremely complex. This area is being explored. One of the approaches is discussed in paper 9.

REFERENCES

1. Harris, Charles D.: Wind-Tunnel Investigation of Effects of Trailing-Edge Geometry on a NASA Supercritical Airfoil Section. NASA TM X-2336, 1971.

2. Stivers, Louis S., Jr.: Effects of Subsonic Mach Number on the Forces and Pressure Distributions on Four NACA 64A-Series Airfoil Sections at Angles of Attack as High as 28°. NACA TN 3162, 1954.

3. Whitcomb, Richard T.; and Clark, Larry R.: An Airfoil Shape for Efficient Flight at Supercritical Mach Numbers. NASA TM X-1109, 1965.

4. Magnus, R.; Gallaher, W.; and Yoshihara, H.: Inviscid Supercritical Airfoil Theory. AGARD C.P. 35, 1968.

5. Garabedian, P. R.; and Korn, D. G.: Numerical Design of Transonic Airfoils. Numerical Solution of Partial Differential Equations-II, Bert Hubbard, ed., Academic Press, Inc., 1971, pp. 253-271.

6. Murman, E. M.; and Cole, J. D.: Calculation of Plane Steady Transonic Flows. AIAA Paper No. 70-188, 1970.

7. Steger, J. L.; and Lomax, H.: Numerical Calculation of Transonic Flow About Two-Dimensional Airfoils by Relaxation Procedures. AIAA Paper No. 71-569, 1971.

8. Blackwell, James A., Jr.: Preliminary Study of Effects of Reynolds Number and Boundary-Layer Transition Location on Shock-Induced Separation. NASA TN D-5003, 1969.

9. Bartlett, Dennis W.; and Re, Richard J.: Wind-Tunnel Investigation of Basic Aerodynamic Characteristics of a Supercritical-Wing Research Airplane Configuration. NASA TM X-2470, 1972.

SYMBOLS

C_p	pressure coefficient
c_d	section drag coefficient
c_n	section normal-force coefficient
M	Mach number

[redacted]

M_{DR}	drag-rise Mach number
R	Reynolds number
t/c	airfoil thickness-to-chord ratio

[redacted]

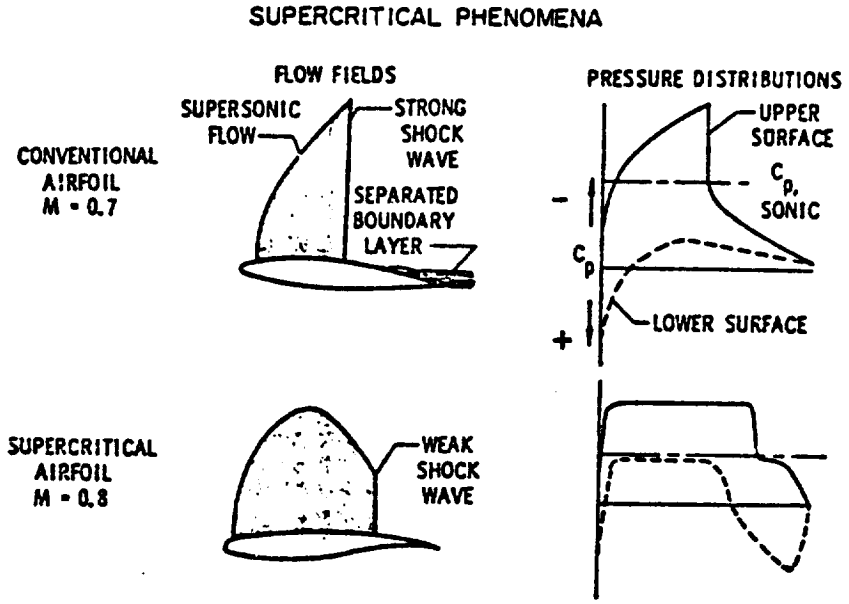

Figure 1

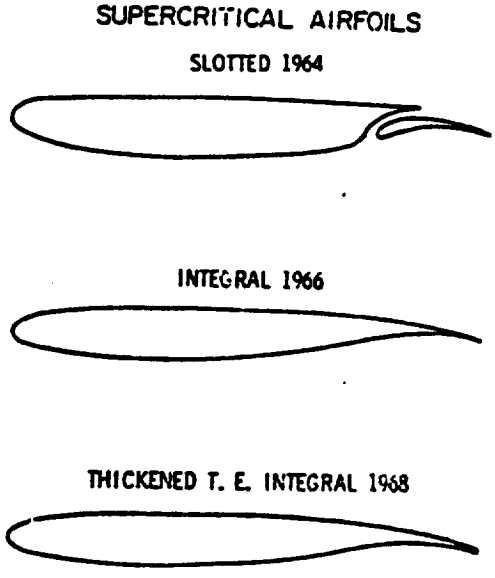

Figure 2

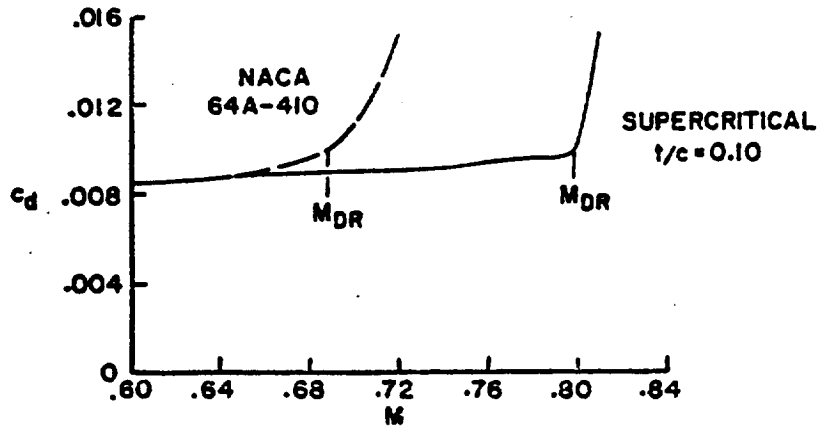

Figure 3

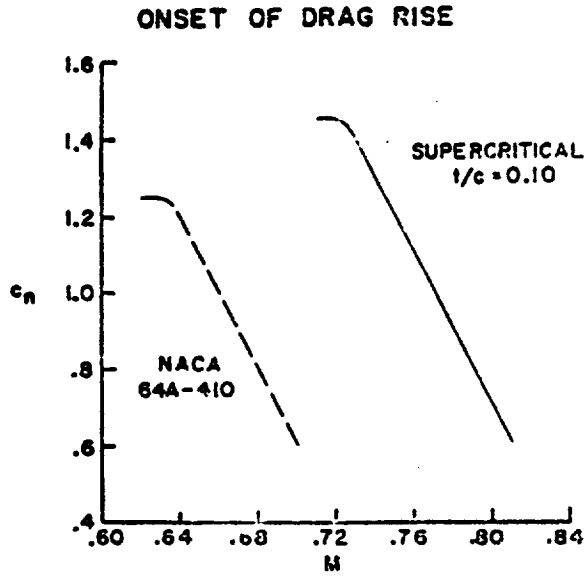

Figure 4

INFLUENCE OF BOUNDARY- LAYER DISPLACEMENT
ON EFFECTIVE CAMBER OF SUPERCRITICAL AIRFOIL

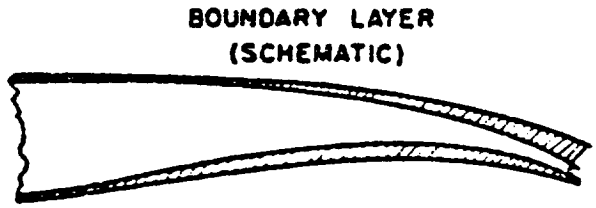

Figure 5

TRANSITION APPLICATION FOR SUPERCRITICAL FLOWS

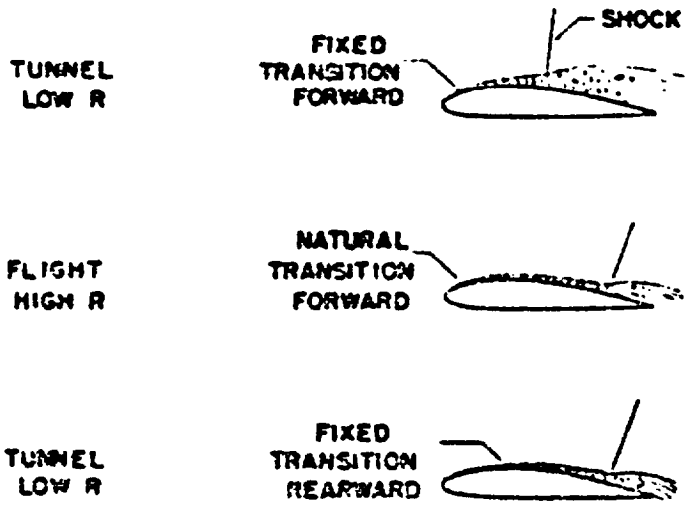

Figure 6

SUPERCRITICAL WING ON F-8 RESEARCH AIRPLANE

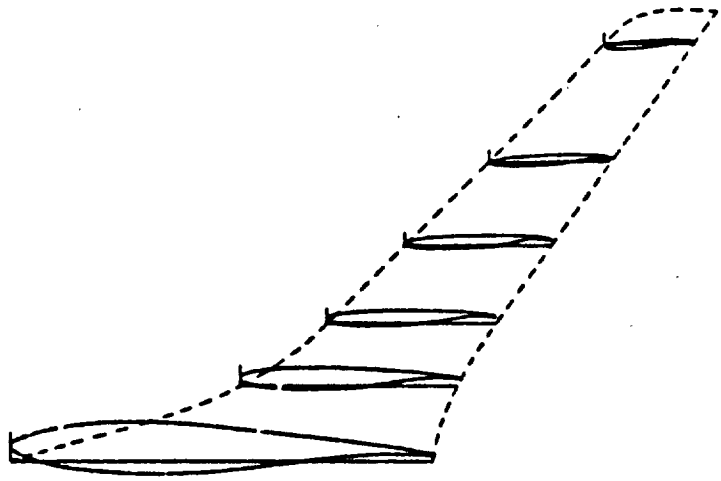

Figure 7

2. SUMMARY OF T-2C SUPERCRITICAL WING PROGRAM*

By William E. Palmer and Donald W. Elliott
North American Rockwell

INTRODUCTION

If the supercritical airfoil concept is applied to subsonic transports and other long-endurance airplanes, wing thickness can be increased without causing a reduction in drag-divergence Mach number that normally results when the thickness ratio of conventional airfoils is increased. The benefits to be realized from an increase in wing thickness are: (1) improved structural efficiency (and attendant reduced weight), and (2) increased internal wing volume. If a wing of 17-percent thickness can be designed to have the cruise efficiency of a 12-percent-thick wing with a conventional airfoil, the internal wing volume is increased approximately 40 percent and the amount of the wing volume that can be devoted to fuel may be increased on the order of 50 percent or more. For V/STOL aircraft, the added volume may also be useful for ducting.

Several supercritical airfoils were designed analytically and tested in the wind tunnel to determine the increase in thickness that might be achieved relative to NACA 6-series airfoils without degrading performance at high subsonic speeds. Wings with thickness ratios of 12 percent to 15 percent were designed to operate under supercritical flow conditions and tested in the North American Rockwell 7-foot Trisonic Wind Tunnel on a semispan model with a high-aspect-ratio, low-sweep planform. A conventional NACA 64A-412 airfoil was tested with the same planform for purposes of comparison. The camber of all the wings was approximately the same. Based upon the results of these tests, a similar wing incorporating a supercritical airfoil of 17-percent thickness was designed and tested on the same semispan model. The test results showed that the drag-divergence Mach number of the thicker wing was at least as great at moderate and high lift coefficients as that of the conventional wing and that the lift coefficient at the onset of buffet was significantly higher through a wide range of Mach numbers. At low speed, the stall angle of attack was increased considerably, with an attendant increase in the maximum lift coefficient.

The development of the airfoil was aided by consultation with Richard T. Whitcomb of the Langley Research Center and study of his test results on thinner airfoils with regard to the tolerable bluntness of the leading edge and the limits of pressure gradient and pressure rise imposed by flow separation.

Figure 1 shows the drag-divergence Mach number obtained in the tests of the 17-percent-thick airfoil and the NACA 64A-412 airfoil at a given lift coefficient. Also shown are data for a number of other airfoils tested by NASA, NACA, and Northrop. The lines drawn through the points are believed to indicate approximately the amount of

*Title, Unclassified.

increase in either drag-divergence Mach number or thickness ratio that can be obtained relative to conventional airfoils with airfoils designed to operate under supercritical conditions.

To determine whether gains obtained in the wind tunnel could also be achieved in flight, a T-2C Navy/North American Rockwell jet trainer aircraft was modified to have the 17-percent-thick-airfoil shape. The characteristics of the modified airplane were compared with those of a standard T-2C, which has a NACA 64A-212 airfoil. This airplane was considered well suited to the study because (1) the wing, having low sweep, would have negligible spanwise flow and hence approximate the two-dimensional conditions for which the analytical derivation was made and (2) the wing alone could be changed with no other aircraft modification which might affect the results.

An 0.09-scale model of the T-2C was also built with the 17-percent-thick airfoil and tested in the Langley 8-foot transonic pressure tunnel for comparison with the flight data. Grit was placed near the 35-percent chord of the model wing to simulate the flight boundary-layer thickness at the trailing edge.

This paper briefly presents the results of this investigation, which was sponsored jointly by NASA and the Naval Air Systems Command. The study is discussed in more detail in reference 1.

TEST CONFIGURATION

The T-2C airplane is a twin-jet configuration with a midwing of aspect ratio 5 and zero sweep of the 40-percent-chord line. Figure 2 is a photograph of the standard T-2C and the modified airplane. The tip tanks were retained in the test version. The landing gear retract into the wing, which necessitated moving the gear-door hinges out to the new mold line.

For the modification, the basic T-2 wing was replaced by another T-2 wing that was covered from the fuselage juncture to the tip tanks with balsa wood coated with a thin layer of fiber glass. No other changes were made to the airplane; even the engines were unchanged to preclude any differences in thrust. The shapes of the NACA 64A-212 airfoil of the basic T-2C airplane and the thicker supercritical airfoil are shown in figure 3. As shown, the NACA 64A-212 airfoil extends outside the contour of the thicker section in the lower aft region. By drooping the flaps and ailerons approximately 8° and decreasing the relative angle of incidence of the basic airfoil, the desired airfoil shape was achieved without altering the basic wing structure. Figure 4 shows that the wing incidence was approximately 0.75° greater at the mean aerodynamic chord for the supercritical wing than for the basic T-2C wing. Some reduction in twist was also desired in order to achieve more nearly two-dimensional results at the design condition.

The flaps were entirely encapsulated and were inoperative. It was necessary that the ailerons be operable to provide lateral control for the aircraft. Aileron hinge moment balance was maintained by an internal seal and paddle, and the difference in mass balancing was compensated for by changing the counterbalancing weights.

Figure 5 shows a representative cross section of the buildup. Thin layers of foam rubber were bonded to the wing surface and were used as expansion joints at 0.6-inch-er

(2-foot) intervals. This permitted the wing to flex and reduced the effects of the added material on the structural load distributions. Complete reanalysis of the airframe structure was therefore unnecessary.

To control the new contour to close tolerances, the wings were removed from the airplane and placed in a simple jig. The jig is illustrated in figure 6. It consisted of a reference plane, a mounting bracket which held the wings in a known position relative to the plane, and a series of female templates of the desired shape which could be positioned precisely relative to the reference plane. After positioning the templates about the wing in the desired positions, male templates, bonded to the wing surface at 0.6-meter (2-foot) intervals, were cut 0.038 centimeter (0.015 inch) smaller than the female templates (the thickness of the fiber glass coating). The female templates were then removed, and the balsa filler was added to build up the contour on the wing to the level of the templates. Straight-line elements were used between template stations. A photograph of the partially completed lower surface of the wing is shown in figure 7. The thickness of the balsa varied over the surface from 0 to as much as 15 centimeters (6 inches). This means of modifying the wing contour was generally satisfactory but did result in surface waviness of as much as 0.15-centimeter (0.060-inch) deviation from the mold line. This deviation did not appear to affect wing performance, particularly not on the upper surface.

TEST CONDITIONS

The flight test conditions for the basic wing evaluation are shown in figure 8. Pressure distributions and static lift, drag, and pitching-moment characteristics were determined for each condition during stabilized, constant-g turns. Normal-load factors up to buffet onset or 4.5g were obtained.

In subsequent tests, the handling qualities were investigated briefly. Maneuvers performed included steady sideslip, various banks and turns, aileron inputs after buffet onset, and rudder kicks. These tests indicated that the handling characteristics were similar to those of the basic T-2C airplane, including stalling characteristics, and that lateral control after stall was good.

INSTRUMENTATION

A plan view of the airplane is shown in figure 9 to illustrate the 96 wing-surface static-pressure taps and four accelerometers. The accelerometers were used for detecting buffet at the center of gravity and near the wingtips. Additional indication of buffet was obtained from strain gages installed on the horizontal tail. A pressure rake was installed at the wing trailing edge near the 40-percent semispan to determine the airfoil section drag. This rake measured the total- and static-pressure distributions at the 5-percent chord back of the wing trailing edge. Sufficient instrumentation was utilized to obtain, in addition to the flight conditions, the lift, thrust, longitudinal and normal accelerations, control-surface positions, and aileron hinge moments as well as angle of attack and angle of sideslip. Engine thrust was determined from known static thrust-stand calibrations and measured inlet and nozzle pressures and temperatures. Drag was then calculated from a balance of forces.

TEST RESULTS

The flight test results of the modified airplane were compared with wind-tunnel data for the 0.09-scale model of the modified airplane and with the characteristics of the basic T-2C airplane. Figure 10 shows representative lift curves of the modified airplane and the model. No consistent difference due to Reynolds number was apparent within the band of scatter of the flight data. Correlation between the lift-curve slopes of the flight and wind-tunnel data is good.

A representative comparison of the drag polars from wind-tunnel and flight tests on the modified airplane is presented in figure 11 for a Mach number of 0.70. At lift coefficients greater than approximately 0.4, the drag was generally less in the flight data than in the wind-tunnel data. At this condition, chordwise pressure distributions at the trailing edge also showed generally better recovery in flight. At low lift, however, there is a large increase in drag in the flight data that was apparently affected by Reynolds number, suggesting flow separation on the lower surface. A similar condition also occurred at a Mach number of 0.73, as shown in figure 12. The solid line in figures 11 and 12 represents the drag polar that it is assumed would occur at a Reynolds number of 20 million if the added drag were not present. Figure 13 is a photograph showing the pattern of wool tufts on the wing lower surface at a Mach number of 0.73, a lift coefficient of approximately 0.25, and a Reynolds number of 20 million. Flow seperation is clearly indicated on the inboard half of the span. A separate disturbance can be seen near the 50-percent span, which is the outer edge of the landing-gear door. In contrast, the wing flow is smooth farther outboard, even behind the aileron hinge, indicating that the disturbance of the flow is not inherent in the airfoil.

The disturbance and added drag on the airplane is attributed to a combination of factors: (1) adverse wing-fuselage interference, (2) engine compartment vents exiting in that region, (3) surface roughness and earlier boundary-layer transition on the airplane, and (4) landing-gear doors which protruded outside the airfoil contour mold line as much as 0.32 centimeter (0.125 inch) as a result of pressures induced in flight.

Subsequent flights at a Mach number of 0.70, a lift coefficient of 0.15, and a Reynolds number of 20 million with the gear doors carefully matched to the airfoil showed a reduction in drag coefficient of approximately 10 counts ($\Delta C_D = 0.0010$). A small additional drag reduction was obtained by installing a single vortex generator 10 centimeters (4 inches) from the wing-fuselage juncture at the 20-percent chord. This vortex generator, which had a square planform 7.1 centimeters (2.8 inches) on a side and was canted with its trailing edge 15° away from the fuselage, had been selected from several that were tested on the model in the Langley 8-foot wind tunnel, where it reduced drag by approximately 10 counts over a wide range of lift coefficients and Mach numbers.

Oil-flow pictures of the model showed a region of flow separation next to the fuselage that was much smaller than that existing in flight. Figure 14 shows a comparison of the chordwise pressure distributions on the airplane and the model at two span stations. The pressure recovery on the lower surface is better on the model at the inboard station and better on the airplane at the outboard station, which is approximately at the center of the aileron span. Recovery on the upper surface at the trailing edge is better on the airplane at both stations.

Since fuselage interference or protruding gear doors do not produce flow separation on the basic T-2C wing, greater care must be taken with the supercritical airfoil than with a conventional airfoil to avoid extraneous flow interference where pressure gradients on the wing are steepest.

Values taken from the drag polars at constant lift coefficients of 0.4, 0.5, and 0.6 are plotted against Mach number in figure 15. Also shown are the comparable values for the basic T-2C airplane. Maximum lift-drag ratio occurs at a lift coefficient of 0.5. The drag increases with Mach number and reaches a plateau for the modified airplane when local shock waves occur on the wing. In this speed range the modified airplane has a drag penalty of approximately 15 counts. Near the drag-divergence Mach number, however, the levels of drag for the basic and modified airplanes are approximately equal.

A drag plateau also appears in figure 16 for the airfoil section drag for constant values of normal-force coefficient near the 40-percent-span station. The trend of the drag is similar for the wind-tunnel and flight data, although the drag levels are lower at full scale, as expected. Comparison of figures 15 and 16 shows that the drag-rise Mach number for the wing section is in good agreement with that for the airplane. Figure 17 shows a comparison of the drag-divergence Mach number (defined when $\frac{\partial C_D}{\partial M} = 0.1$) for the basic T-2C airplane and the modified airplane at lift coefficients from 0 to 0.6. The values shown for the modified T-2 airplane at lift coefficients less than 0.4 correspond to the assumed drag polar with no lower-surface flow separation. The decrement for the modified wing at low lift is due to the higher design camber and the fact that the lower surface of the wing experiences supercritical flow. Maneuvering with this wing at low lift coefficients may be penalized at the higher Mach numbers. By proper use of flaps to change the effective camber, this effect might be corrected. Further analyses and tests are required in this off-design flight condition.

Pitching-moment characteristics are compared in figure 18. Without the horizontal tail, the nose-down moment for the modified (supercritical) airplane is much larger than that of the basic T-2C airplane. With the tail on and at zero elevator deflection, however, the difference is more than offset by increased downwash at the tail. The pitching moments in flight at zero elevator deflection were obtained by adjusting for the measured elevator deflection at trim for each airplane and the previously determined elevator effectiveness of the basic T-2C airplane. Values with the tail off were, of course, obtained in the wind tunnel. The downwash was computed from wind-tunnel data at different horizontal-stabilizer deflections. Wind-tunnel and flight data for the modified airplane are in close agreement.

One benefit of the modified airfoil is an increase in the lift coefficient for buffet onset, as shown in figure 19. The increase in buffet-onset lift coefficient is as much as 45 percent at the low Mach numbers and decreases with increase in Mach number until drag rise, at which point the lift coefficient for buffet onset for the two airplanes is approximately the same. Also shown in the figure is a curve representing the buffet-onset boundary of the basic T-2C airplane with stall strips removed. (Stall strips are 2.5-centimeter (1-inch) spoilers 25.4 centimeters (10 inches) wide positioned at the leading edge at about the 20-percent span. The strips are on the basic production T-2C airplane to give stall warning.) The curve for the airplane without stall strips gives a

more valid comparison for the supercritical wing, which also was without stall strips.

The symbols in figure 19 correspond to the different indices that were used to determine the onset of buffet. The pilot was asked to note the point at which he estimated the amplitude of oscillation to be ±0.1 g. Because he was near the center of gravity, there was a close correlation of his opinion with the amplitude measured at the center of gravity. Accelerometers just inboard of the wingtip tanks were understandably much more sensitive than either of the indices near the center of gravity. For this airplane it was determined that an amplitude of 0.5g near the wingtip corresponded well with an amplitude of 0.1 g at the center of gravity. Strain gages arranged on the horizontal tail to read bending moment and elevator hinge moments were sensitive indicators of buffet onset but showed onset at essentially the same values of lift coefficient and are therefore not presented.

The lift curves at low speeds representative of the landing condition for the modified and basic airplane are shown in figure 20. The increase in maximum lift coefficient for the modified aircraft is due to both an increase in the effective camber of the airfoil and an increase in the stall angle of attack from 18° for the basic T-2C airplane to 21° for the modified airplane. At this higher angle of attack, the maximum lift coefficient of the modified wing without high-lift devices slightly exceeds that of the basic wing with trailing-edge flap despite the greater down load on the horizontal tail required for trim. With stall strips, the angle of stall of the basic airplane is reduced approximately 1° either with or without flaps.

Chordwise pressure distributions from flight and wind-tunnel tests are compared in figures 21 and 22 for subcritical and supercritical flow conditions, respectively. These data are for the 40-percent-wing-span station. Agreement between wind-tunnel (at a Reynolds number of 3.8 million) and flight data is generally good, and the effects of change in flight Reynolds number from 10 million to 20 million did not cause significant change in the pressure distribution even at the shock. These data do not indicate the shift in shock-wave position with increase in Reynolds number that is characteristic of most transonic data obtained on standard airfoils.

In subsequent flight tests, the general handling qualities of the modified airplane were compared with those of the basic T-2C airplane. This evaluation, which is described in detail in reference 2, showed that the frequencies and damping of short-period and Dutch roll modes of motion were similar to those of the basic T-2C airplane and that the stall characteristics were also similar. Stall was abrupt and characteristic of leading-edge stall, but the wing showed little tendency to drop off and the post-stall aileron control was good.

The study on the supercritical T-2 wing was recently extended to include determination of the boundary-layer characteristics through the shock wave and for some distance downstream. Total-pressure distributions were measured with the traversing probe shown mounted on the wing in figure 23. This probe, which was made available by the Boeing Company, had an arm which rotated about the body axis to achieve translations approximately normal to the wing surface. A static-pressure probe was attached to the probe head, but it was determined that its minimum height (7.6 centimeters (3 inches) from the surface) was too great for it to be used for static-pressure measurements through the boundary layer. It was determined in reference 3, however, that static pressure remains essentially constant through the boundary layer. Surface static pressure was therefore used to determine the velocities in the boundary layer.

These measurements were made at a free-stream Mach number of approximately 0.74 and at angles of attack which produced peak local Mach numbers of 1.15 to 1.40 just upstream of the shock, M_1. At greater shock strengths, the flow remained separated downstream of the shock, and the resulting buffet prevented accurate measurements.

Figure 24 shows the chordwise surface pressure distribution for a representative case in which the shock Mach number was 1.37, the Reynolds number was 20 million based on the wing chord, and the shock was located near the 50-percent chord. Velocity distributions through the boundary layer for this case are shown in figure 25 for several positions relative to the shock wave. There is a separation bubble indicated by profile D at the 7-percent chord downstream of the shock, followed by reattachment and a region of strong profile distortion as far as the 17-percent chord downstream. It is interesting that the profile at the shock is only slightly altered by the shock, and at 1 percent farther downstream the separation bubble has not yet formed. This trend agrees with the results in reference 3 for a flat plate.

Figure 26 presents the variation of shape parameter, H, and θ/δ_u with position relative to the shock location. Also shown are the comparable values from reference 3 for tests on a flat plate. The agreement in levels and curve shapes is considered good and is attributed to the fact that the pressure distribution of the airfoil, like that of the flat plate, has essentially neutral gradients both upstream and downstream of the shock. This feature is perhaps the chief reason that the supercritical airfoils are able to withstand stronger shocks without sustained separation than conventional airfoils. As a general rule, it is suggested that the start of the theoretical adverse pressure gradient be essentially zero to a distance at least $20\delta_u$ downstream of the shock position.

CONCLUDING REMARKS

The 17-percent-thick supercritical airfoil is considered to be generally satisfactory for use on a production aircraft. High-lift characteristics are good. Handling qualities and stall are similar to those of the NACA 64A-212 airfoil at flight conditions below drag rise, ailerons are effective even at lift coefficients greater than that for buffet onset, and the drag level at the design condition is equal to that of the 12-percent-thick conventional airfoil. However, it has objectionable qualities in that (1) it is more sensitive than conventional airfoils to the effects of protuberances and adverse fuselage flow interference near the steep adverse pressure gradients that are designed into the airfoil, (2) the rise in level of drag when the shock appears on the wing causes a drag penalty that is not overcome until the Mach number increases to approximately that for drag rise, where conditions may be uncomfortably close to shock-induced stall, (3) the greater nose-down pitching moment creates added horizontal-tail loads for trim and hence may cause somewhat greater structural weight of the tail for unswept configurations as for the T-2C airplane, and (4) for a tactical aircraft, maneuverability at negative lift coefficients may be restricted at high speed. In this case, however, analysis indicates that maneuvering flaps might be very effective.

The flight characteristics were generally well predicted by the wind-tunnel data, including shock strength and shock position, when the relative boundary-layer thicknesses were approximately equal. It is believed, however, that better representation of the lower-surface flow disturbance might have been obtained if the roughness had been

applied farther forward on the model wing so that the boundary layer would have matched that for full scale at the location where separation was likely to occur rather than at the wing trailing edge.

The results of boundary-layer measurements are in good agreement with results obtained in a wind tunnel on a flat plate with zero pressure gradient when differences in upstream boundary-layer thickness are considered. This agreement indicates that the effects of surface curvature are small compared with the other parameters affecting shock-induced flow separation. It also indicates that the growth in momentum thickness relative to the initial boundary-layer thickness and the velocity shape parameter can be predicted from low Reynolds number data when the differences in boundary-layer thickness are considered.

The buildup of balsa wood covered with fiber glass proved to be a generally satisfactory way of achieving the wing contour change at minimum cost. However, surface waviness was a problem in working such a large area with balsa. Performance of the wing did not appear to be appreciably degraded by this waviness, particularly on the upper surface.

REFERENCES

1. Palmer, W. E.; Elliott, D. W.; and White, J. E.: Flight and Wind Tunnel Evaluation of a 17% Thick Supercritical Airfoil on a T-2C Airplane. Vol. I-Basic Report. NR71H-50, North American Rockwell, July 31, 1971.

2. Elliott, D. W.: Flying Qualities Evaluations of a 17% Thick Supercritical Wing on a T-2C Airplane. NR71H-331, North American Rockwell, July 1971.

3. Seddon, J.: The Flow Produced by Interaction of a Turbulent Boundary Layer With a Normal Shock Wave of Strength Sufficient to Cause Separation. R. & M No. 3502, British A.R.C., March 1960.

SYMBOLS

C_D	drag coefficient
ΔC_D	change in drag coefficient
C_L	lift coefficient
$(C_M)_{0.25}$	pitching moment about 0.25 MAC
C_N	airfoil section normal-force coefficient
C_p	local surface pressure coefficient
H	boundary-layer-shape parameter, δ^*/Θ

M	Mach number
MAC	wing mean aerodynamic chord
M_1	Mach number at the shock wave
R	Reynolds number based on MAC
R_1	Reynolds number based on distance from wing leading edge to shock position
u/V	velocity in the boundary layer relative to velocity just outside the boundary layer
x/c	distance from wing leading edge relative to local wing chord
$\Delta x/c$	distance from shock position relative to wing chord
Z	distance from wing surface, cm (in.)
α	angle of attack of airplane fuselage reference plane, deg
α_i	angle of attack of local wing section, deg
Δx	distance from shock position, cm (in.)
δ^*	boundary-layer displacement thickness, cm (in.)
δ_H	longitudinal control deflection, deg
δ_u	boundary-layer-velocity thickness at the shock wave, cm (in.)
η	spanwise distance from plane of symmetry relative to total wing span
Θ	boundary-layer momentum thickness, cm (in.)
$\frac{\partial C_D}{\partial M}$	rate of change of drag coefficient with Mach number

Drag-Divergence Mach Number Variation with Airfoil Thickness

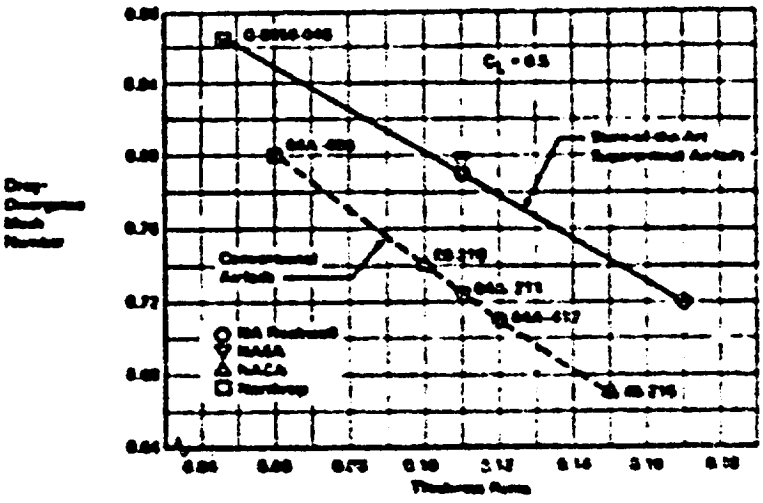

Figure 1

Production and Modified T-2C Aircraft

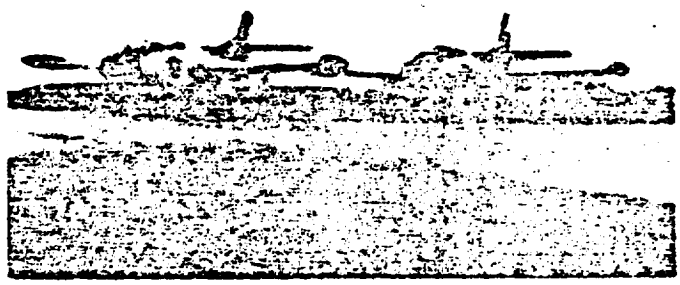

Figure 2

Comparison of Airfoil Shapes

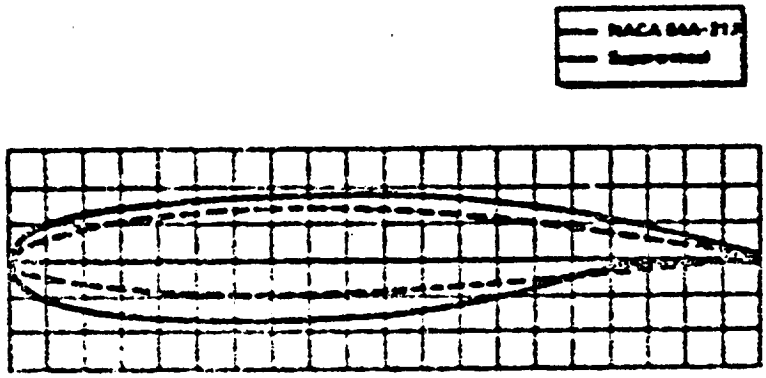

Figure 3

Comparison of Local Wing Incidence for the Basic and Modified Wings

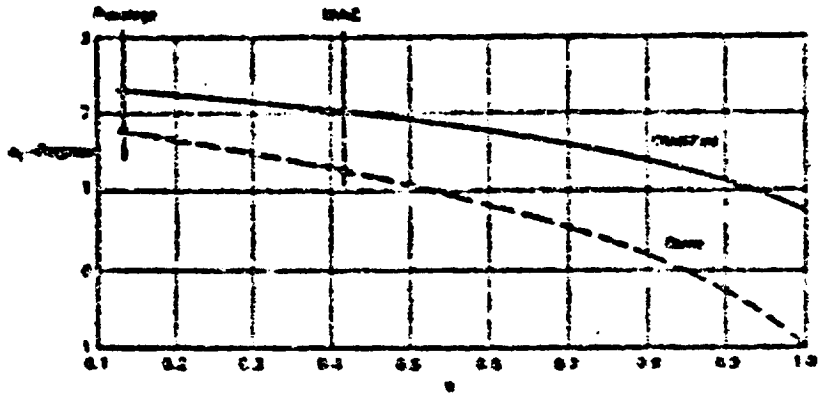

Figure 4

Typical Wing Buildup

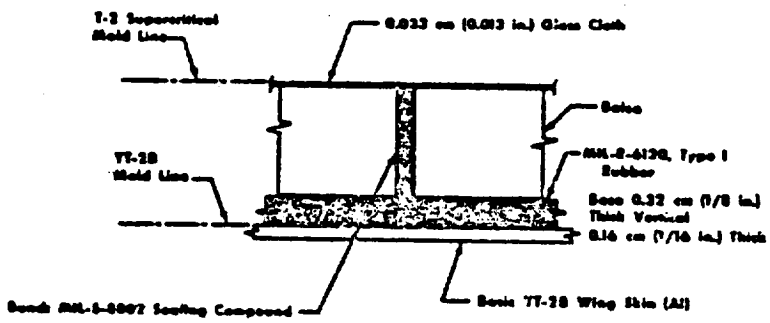

Figure 5

Wing Buildup Technique

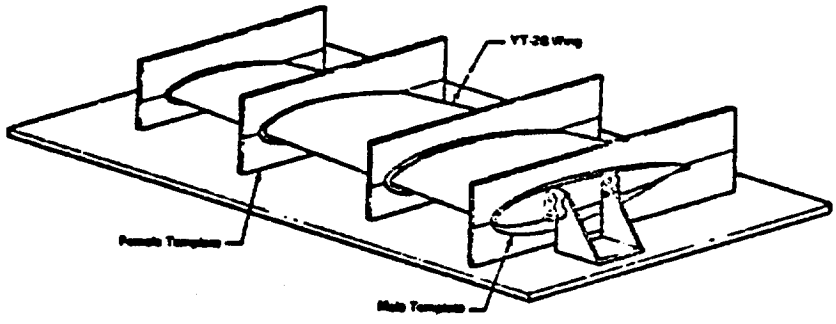

Figure 6

Buildup of Supercritical Airfoil on T-2C Wing

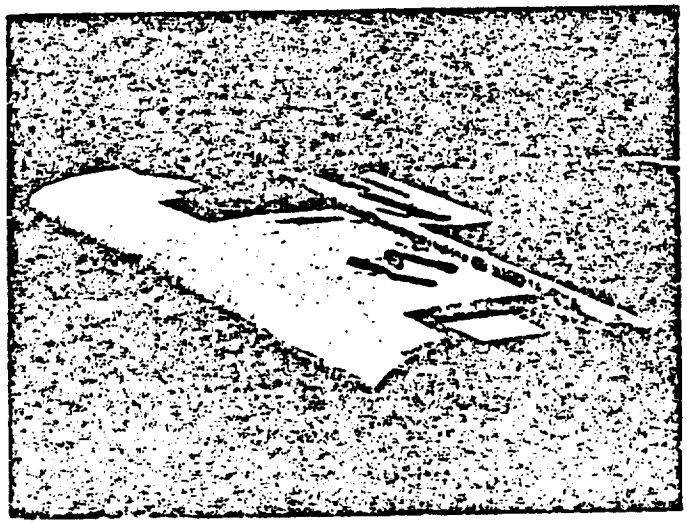

Figure 7

Flight Test Program

Test Conditions

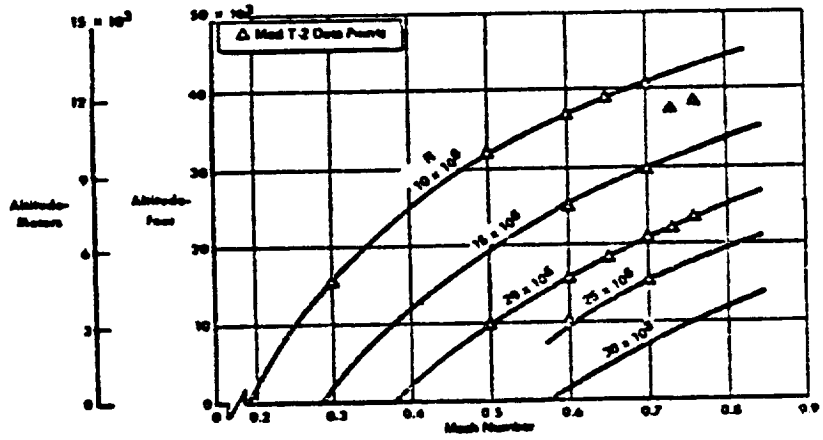

Figure 8

Flight Test Program

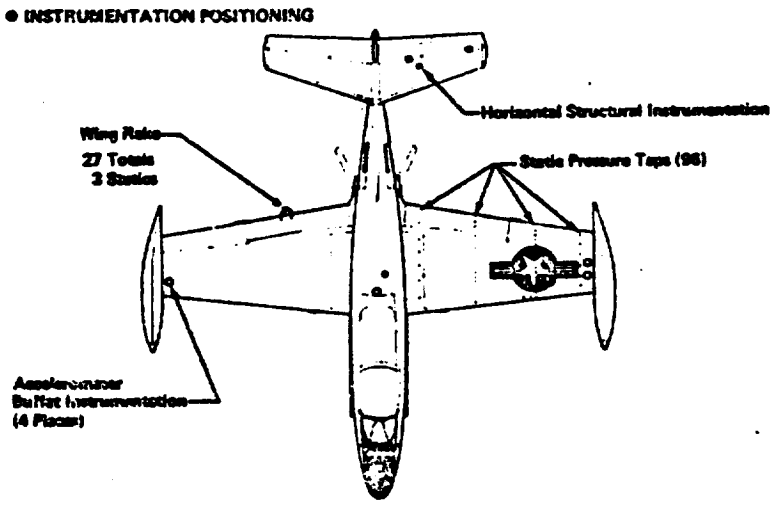

Figure 9

Variation of Lift with Angle of Attack

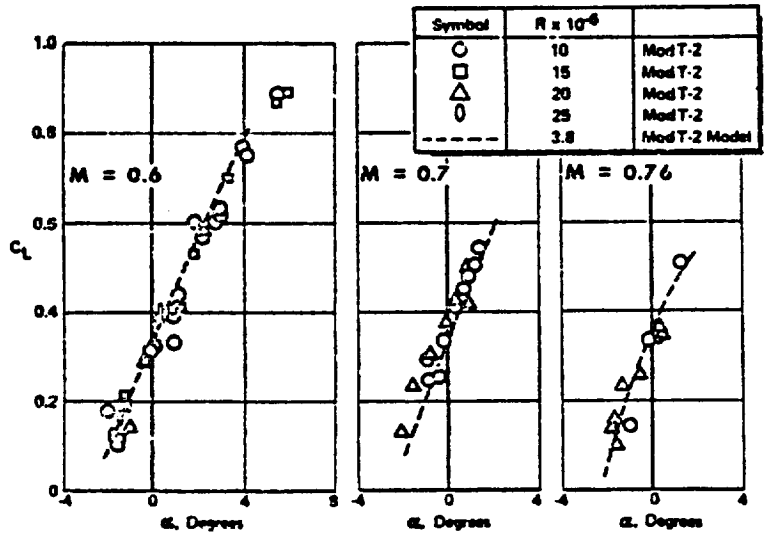

Figure 10

Variation of Lift with Drag for Modified Aircraft, M = 0.70

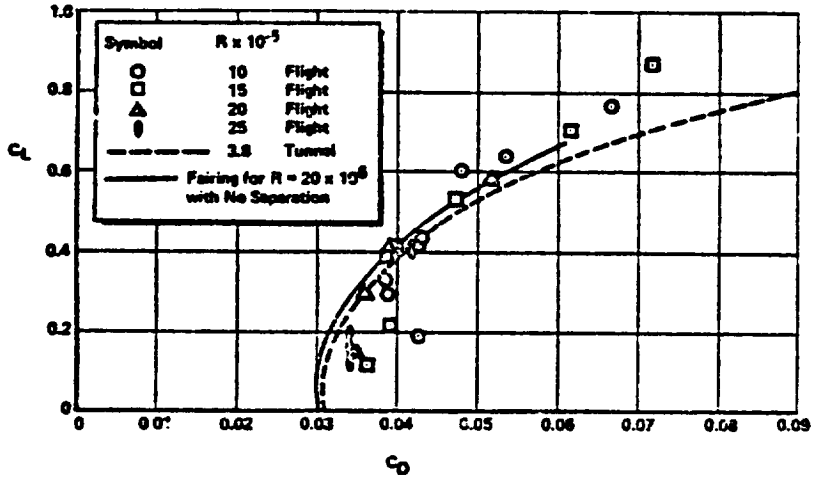

Figure 11

Comparison of Flight and Wind Tunnel Model Drag at M = 0.73

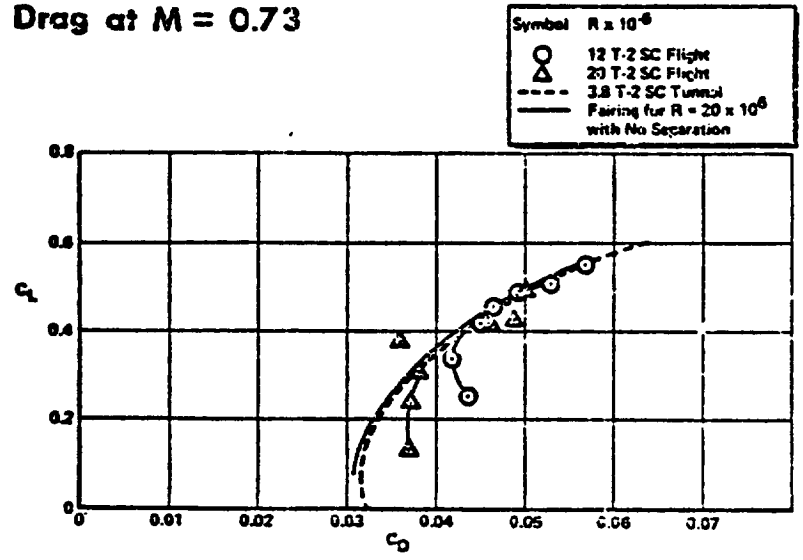

Figure 12

Tuft Observation on Wing Undersurface - M = 0.73, C_L = 0.25

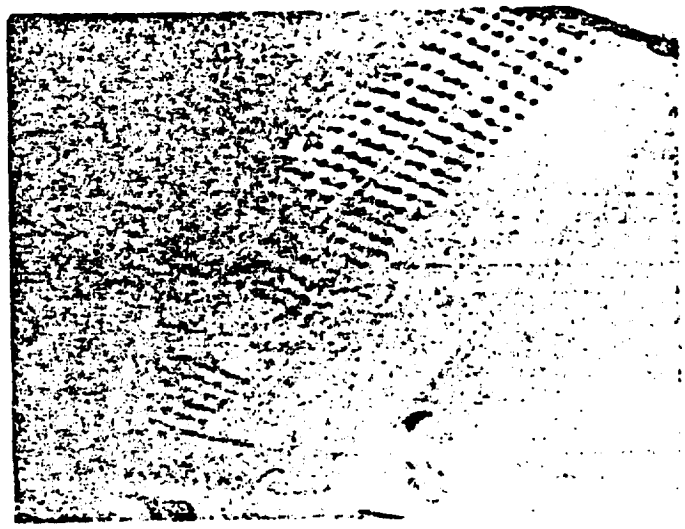

Figure 13

Reynolds Number Effect on Pressure Distribution

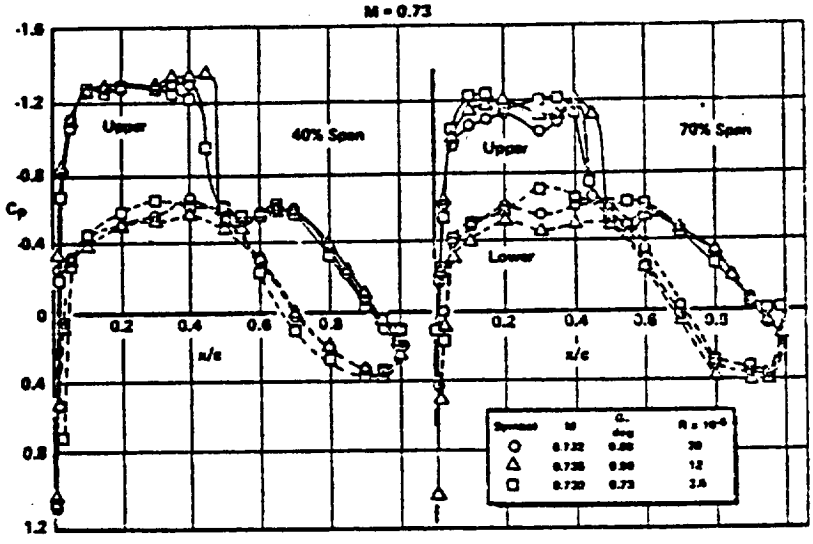

Figure 14

Comparison of Total Aircraft Drag for T-2C and Modified T-2

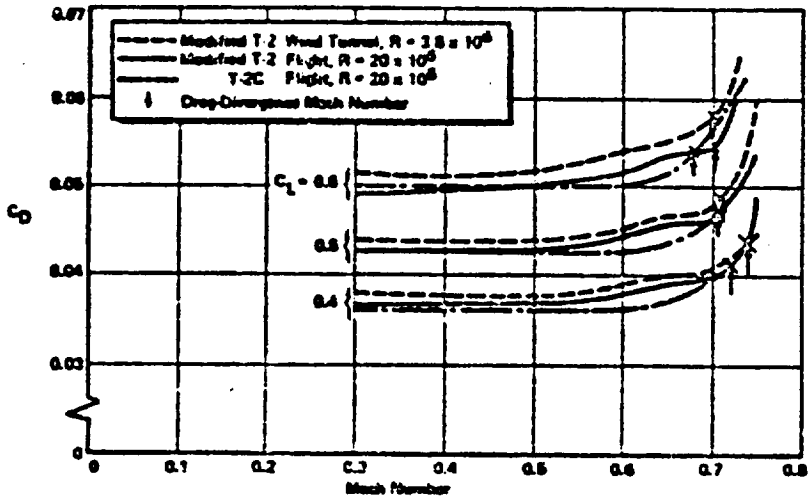

Figure 15

Comparison of Flight and Wind Tunnel Model Section Drag at C_N = 0.40 and 0.50

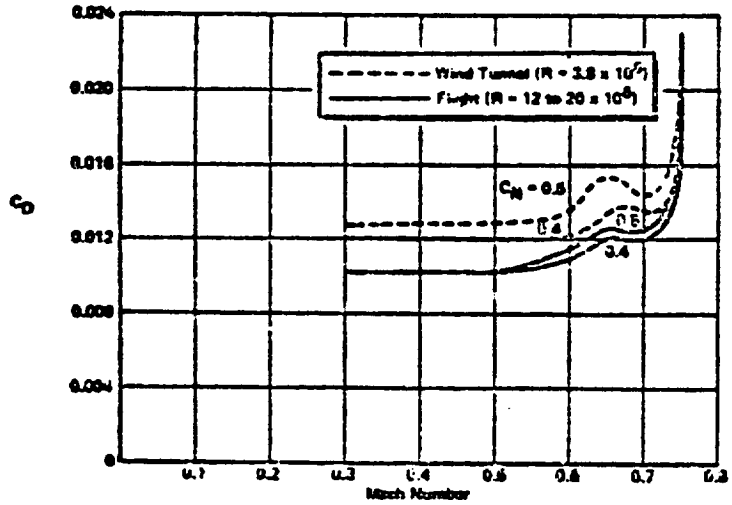

Figure 16

Variation of Drag-Divergence Mach Number with Lift Coefficient

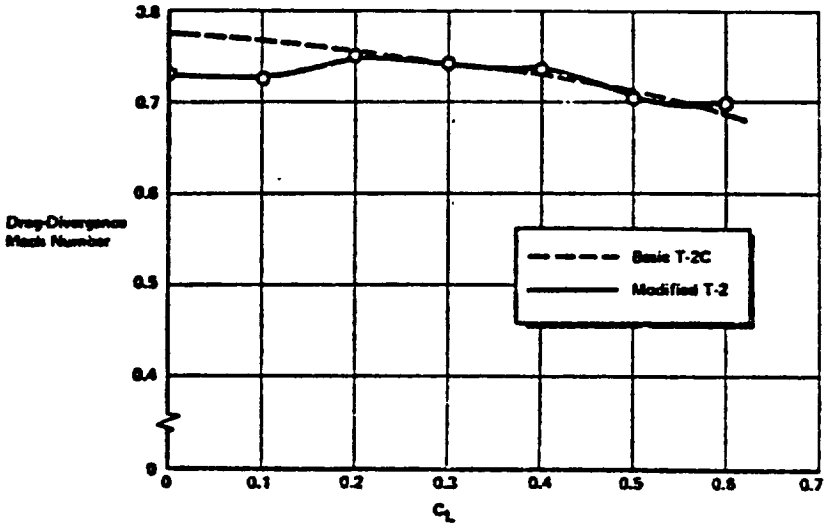

Figure 17

Variation of Pitching Moment and Lift

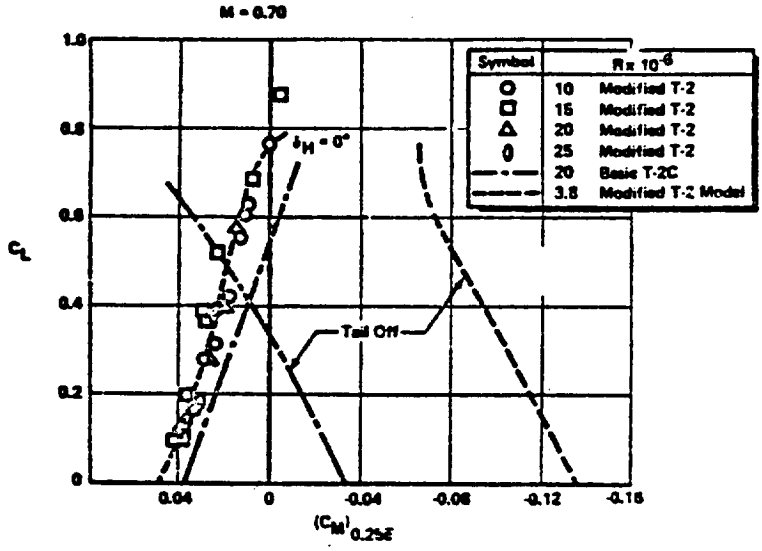

Figure 18

Comparison of Buffet Onset Lift Coefficient for T-2C and Modified T-2 Aircraft

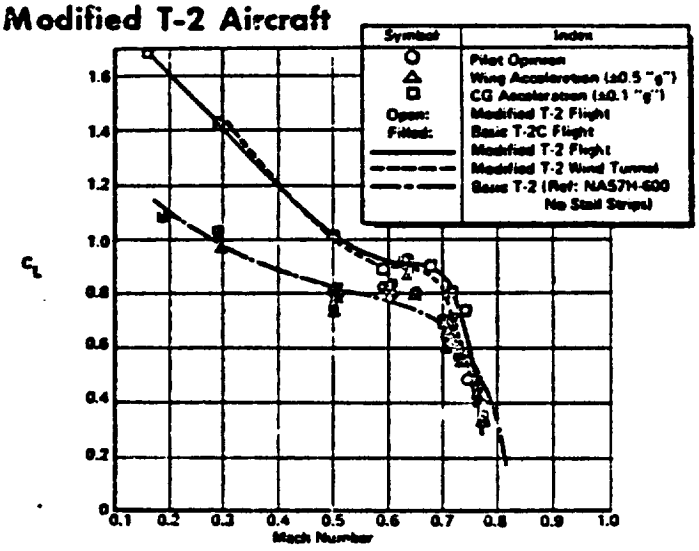

Figure 19

Comparison of Low-Speed Lift Characteristics for T-2C and Modified T-2, Idle Power Flight

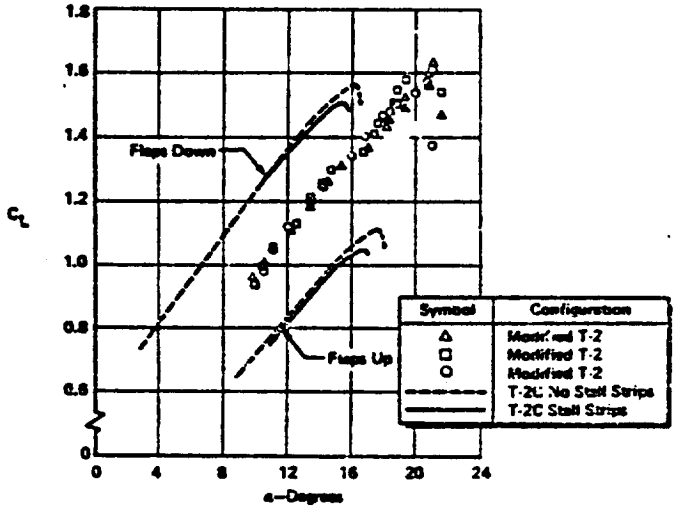

Figure 20

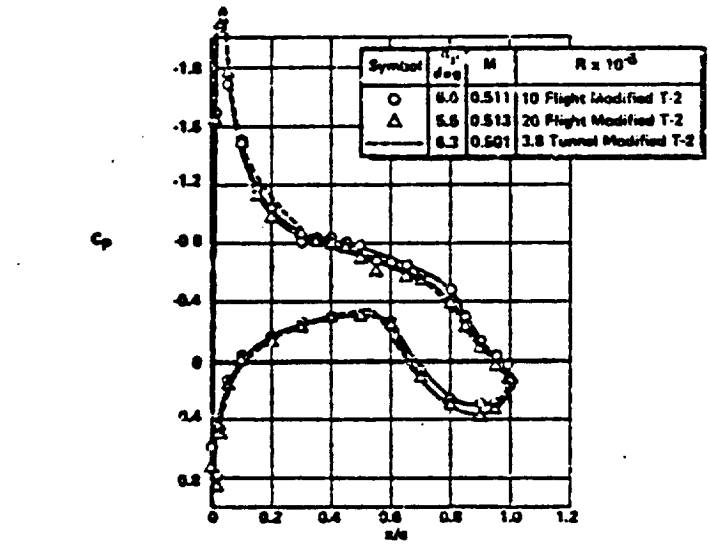

Figure 21

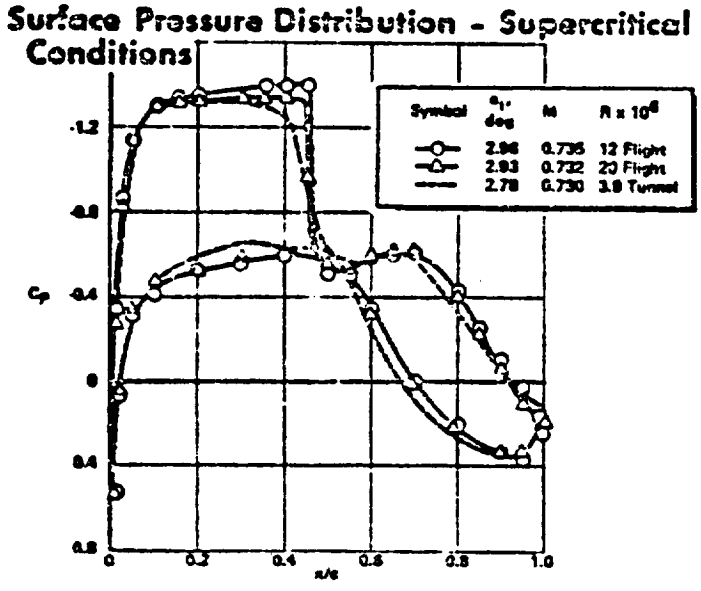

Figure 22

Traversing Probe Mounted on T-2C Wing

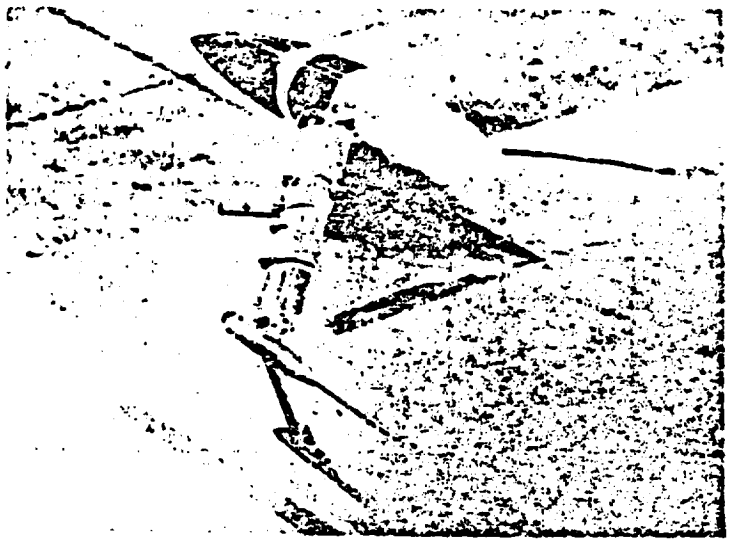

Figure 23

Surface Pressure Distribution for Boundary-Layer Comparison

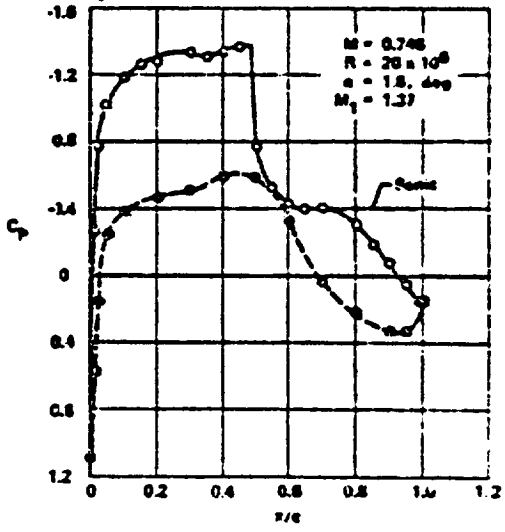

Figure 24

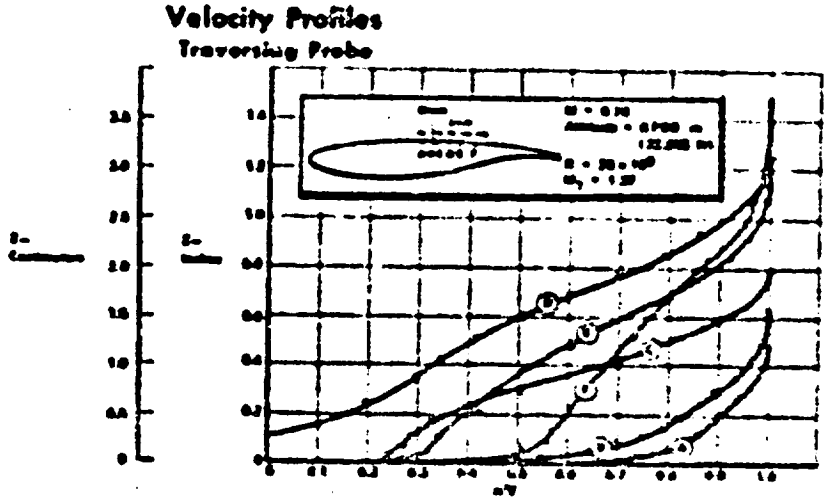

Figure 25

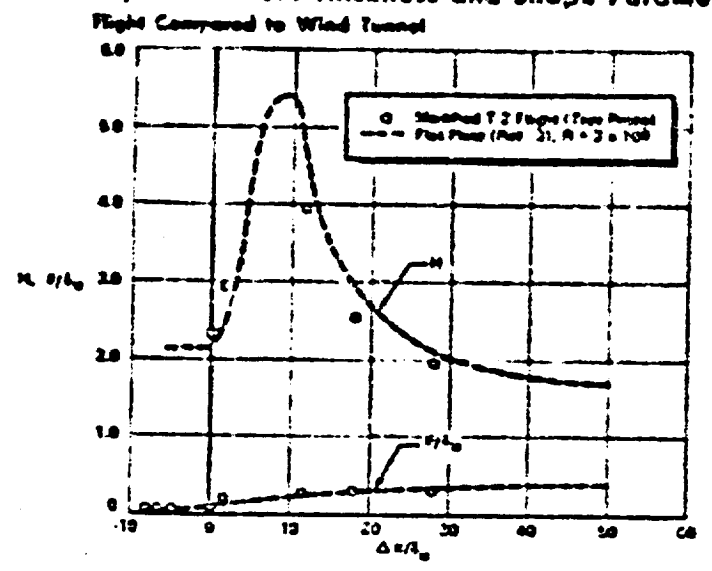

Figure 26

3. EVOLUTION OF THE F-8 SUPERCRITICAL WING CONFIGURATION*

By Thomas C. Kelly and Richard T. Whitcomb
Langley Research Center

INTRODUCTION

In paper 1 it was noted that one of the potential gains of the supercritical airfoil relative to conventional airfoils of comparable thickness was an increase in performance or cruise speed. This gain, which has been indicated in wind-tunnel investigations, could have a significant impact on the performance of transport aircraft if achievable in flight. This paper describes the evolution of the F-8 configuration which was designed to demonstrate in flight the advantage of optimum cruise performance.

PROGRAM DEVELOPMENT

Figure 1 indicates some significant events which led to the development of the F-8 supercritical wing configuration. In early 1967, after the initial development of the two-dimensional integral supercritical section, consideration was given to a proof-of-concept flight test which would be directed to demonstrating optimum cruise performance for a transport-type wing. A number of flight program objectives designed to answer questions related to this new concept were defined. These objectives, which are discussed in paper 4, were essentially associated with determining whether high force-break Mach numbers indicated in wind-tunnel tests could be obtained in flight, and with such characteristics as maneuvering and speed margins, off-design performance, the application and performance of lateral controls, and the sensitivity of the wing to contour variations.

Several test-bed aircraft were considered for use in a flight program. The F-8 airplane was selected as particularly suitable for several reasons: The wing was easily removable; the airplane had sufficient thrust available to explore the accelerated level and overspeed cases; the structural design was compatible with the intent to determine the buffet boundary; the gear retracted into the fuselage; and there were no apparent inlet-wing interference problems. Also, and perhaps most important, the airplane appeared to be available. As noted in figure 1, model design was initiated in 1967, and a joint program between the Flight Research Center and the Langley Research Center was established in early 1968. Model tests were started about mid-1968, and the wing coordinates were finalized in late 1969.

*Title, Unclassified.

CONFIGURATION DEVELOPMENT

The initial model configuration, shown in figure 2, was designed with the wing geometry intended to represent that of an advanced transport designed for near-sonic cruise flight. The configuration has supercritical airfoil sections and the forward wing glove mentioned in paper 1. A number of constraints were involved with the wing sizing, primarily the trade-offs between keeping takeoff and landing speeds from becoming too high and achieving the level-flight design cruise point at or below an altitude of 15,240 meters (50,000 feet). In addition, an attempt was made to keep the ratio of wing span to fuselage width representative of transport aircraft. The wing longitudinal location was selected on the basis of early two-dimensional pitching-moment results.

During development of the F-8 configuration, extensive investigations were conducted in the Langley facilities which were associated not only with what has been called "tuning" or small contour changes but also with the inputs required for structural design and simulator and safety of flight studies. Other configuration changes were required as the design progressed. An example would be the addition of aileron hinge fairings to the lower surface of the wing when the structural design dictated a hinge point below the wing lower-surface line.

The extent of some of these configuration changes is indicated by comparing figure 3, a photograph of the final model configuration tested, with figure 2, a photograph of the initial configuration. The final model also included a simulation of the major protuberances on the full-scale airplane. The different photo angles make direct comparison difficult. However, the main changes included an increase in wing incidence from 0° to 1.5° to reduce takeoff and landing speeds, the addition of a vortex generator to the leading edge of the wing lower surface to improve pitch characteristics at moderate lift coefficients, modification of the inboard trailing-edge shape, and addition of a rear upper-surface fuselage fairing. This fuselage modification and other changes are discussed in greater detail later.

Figure 4 presents some of the geometric characteristics of the full-scale configuration. The wing has an area of slightly less than 26 square meters (275 square feet), an aspect ratio of about 6.8, and a sweep of the quarter-chord line of 42.24°. The wing sweep was selected on the basis of the two-dimensional results and a consideration of local induced flow-field effects near the speed of sound to provide a drag-rise Mach number of approximately 1.0 for the wing. It was believed that this drag-rise Mach number could be obtained for an optimized total configuration, or one which had both supercritical sections and area ruling and an equivalent-body fineness ratio somewhat higher than that of the F-8 configuration.

Figure 5 shows the spanwise variation of thickness and twist distributions for the model wing. Streamwise thickness-to-chord ratios vary from about 11 percent at the wing-body juncture to 9 percent at the mean geometric chord location, and about 7 percent at the tip. These thickness ratios are based on the local streamwise chords which become large inboard because of the glove. The dashed curve indicates thickness ratios which would be obtained by using as a reference the chords formed by straight-line extensions of the outboard leading and trailing edges to these inboard locations.

In the right-hand plot of figure 5 the model wing twist distribution is shown for the test condition corresponding to the 1-g cruise design condition. The overall twist, or washout, from root to tip is about 7°, which is significant. It would be well at this point to consider a contract requirement which specified that the model wing twist had to be matched in flight under the 1-g cruise condition. This requirement was included in the contract so that the best correlation between wind tunnel and flight could be achieved. In other words, the intent was to remove a major variable in the comparison of wind-tunnel and flight results for the wing at the cruise point. As far as it was possible to determine in the wind-tunnel tests, supercritical wing performance on the F-8 airplane is not unduly sensitive to moderate variations in twist, except that increased twist does delay pitchup, as would be expected. (See, for example, reference 1.)

Some further discussion concerning the addition of the rear-fuselage upper-surface fairing is necessary. Figure 6 shows the area distribution for the F-8 airplane, with the components identified. In the early wind-tunnel tests, what was considered to be an excessive, premature drag rise was experienced. Tests of the configuration with the horizontal tails removed indicated that this drag rise was related to the abrupt corner in the area distribution associated with the buildup of the horizontal- and vertical-tail-surface area. Addition of the rear upper fairing served the dual purpose of smoothing the abrupt corner in the area diagram caused by the area buildup and of covering the wing rear attachment fittings which are approximately in line with the wing-root trailing edge. It should be emphasized that the rear-fuselage fairing does not result in either a "coke-bottle" fuselage shape or an ideal area distribution, but, rather, provides a fuselage area progression actually closer to that which would exist on a transport configuration with a cylindrical fuselage. In effect, it modifies the test-bed F-8 airplane to provide an environment which allows the wing to perform without a significant penalty due to the test-bed vehicle itself.

WIND-TUNNEL INVESTIGATIONS

Many of the papers that follow present comparisons of wind-tunnel and flight results; therefore, the remainder of this paper will illustrate only a few basic characteristics and some selected wind-tunnel results associated with the configuration development. It should be noted that in most of the wind-tunnel tests the new method of transition trip application described in reference 2 was used. It was found in the wind-tunnel tests, however, that the flow over the wing glove could not be kept laminar, so transition strips over that region were moved forward. At the lower Mach numbers it was also necessary to move the trip forward on the upper surface of the outer wing panel in order to eliminate a laminar separation bubble which developed rearward of the leading edge.

As noted earlier, vortex generators were added to the lower surface of the wing to alleviate an unstable pitch break which occurred at moderate lift coefficients. Figure 7 shows the effect of the vortex generators on pitching-moment characteristics at Mach numbers of 0.25 and 0.99. A single vortex generator, shown in the sketch at the top of the figure, was mounted at the 60-percent-semispan station on each panel and was swept forward about 42° with respect to the vertical. The streamwise airfoil section was a 10-percent-thick Clark Y with the flat lower surface facing inboard. The figure shows pitching-moment coefficient plotted against lift coefficient for Mach numbers

of 0.25 and 0.99. Fairly sizable effects of the vortex generators are shown for both Mach numbers. These results are for the configuration with the horizontal tail. Limited tests were also made with the tail off, and part of the effect noted is associated with changes in the flow field over the tail. Significant changes in the flow over the wing may be noted in figure 8 which shows comparison photographs of the upper-surface boundary-layer flow at a Mach number of 0.95 and a lift coefficient of approximately 0.93. These boundary-layer-flow photographs were obtained by using the technique described in reference 3. In these photographs, as indicated by the small sketch in the upper right corner, the airflow direction is downward and the view is of the upper surface of the left-wing panel. The midsemispan region of the panel is shown, with the glove just outside the photo to the upper right and the left wingtip just beyond the lower left corner of the photo. The photograph for the configuration with the vortex generator off shows the spanwise boundary-layer flow to be extensive at this condition with separation indicated over the outer wing panel. The right-hand photograph shows that the vortex generator provides a barrier to the spanwise flow, resulting in better characteristics over the outer panel and the improvement in pitch characteristics noted in figure 7. The penalty associated with adding the vortex generators was about 5 drag counts at cruise lift coefficients; however, significant drag reductions occurred at the higher lift coefficients because of the reduced outboard separation. Later results have indicated that the penalty at cruise may be reduced somewhat by toeing-in the generators. The effect of these vortex generators is similar to the effect of a leading-edge extension such as that on the original F-8 wing. The penalty at cruise lift coefficients, however, appears to be significantly less for this vortex generator configuration.

Figures 9 and 10 present some basic results which have been obtained in the wind tunnel for the final configuration with the vortex generators. Streamwise pressure distributions are shown at several spanwise locations for the design cruise point, which is at a Mach number of 0.99 and a lift coefficient of approximately 0.40. Results similar to these are compared with flight results in paper 6, but some general observations can be made with regard to these figures.

Over the two outboard stations, the pressure distributions are similar in appearance to those obtained in two-dimensional tests of the supercritical airfoil, and the presence of a shock wave is indicated at about the 70-percent-chord station. The pressure distribution for the 80-percent-semispan station, for example, is close to that shown in paper 1 in the description of the two-dimensional supercritical airfoil. At stations farther inboard the pressure distributions begin to resemble those obtained at lower relative Mach numbers in the two-dimensional tests, and the presence of a significant shock wave is not apparent. The forward loading of the glove sections inboard is apparent, however. Figure 11 is an oil-flow photograph for this same condition. Relatively clean boundary-layer flow may be noted over most of the upper surface. Also noticeable is the outboard wave at about the 70-percent-semispan station and a slight amount of trailing-edge separation which appears to be restricted to about the last few percent of the chord.

Figure 12 is a summary of the drag characteristics for the final model configuration. Drag coefficient is plotted against Mach number for lift coefficients from 0.2 to 0.6; the design cruise lift coefficient of 0.4 is shown as a solid line. These results are for a horizontal-tail angle of -2.5°, which was the tail angle selected during the wind-tunnel tests for trim at the cruise point with a center-of-gravity location at about 35 percent of the mean geometric chord. The vertical dashed curve connects the points

on each curve at the Mach number at which the change in drag coefficient with Mach number is 0.1; this point has been used to define the drag-divergence Mach number. For the cruise lift coefficient, the drag-divergence Mach number is about 0.97 and, as will be shown later, this drag rise is associated with the total configuration and its developing shock-wave system. An interesting point in this figure is that drag-divergence Mach number does not vary significantly with lift coefficient; the value for a lift coefficient of 0.6 is about 0.95. It is also of interest that the highest drag-rise Mach number is obtained at a lift coefficient of 0.4, the lift coefficient for which the wing was "tuned." These results are, of course, for a fixed horizontal-tail angle, and the possibility exists that trimmed drag curves would show somewhat greater variations with lift coefficient than those indicated, depending upon a selected center-of-gravity location.

On the surface these results for the complete configuration appear to be in conflict with earlier pressure distribution and oil-flow results which indicated good wing performance at a Mach number of 0.99. It should be recalled that the wing design was aimed at optimum performance near a Mach number of 1.0 for a configuration having an equivalent-body fineness ratio higher than that of the F-8 airplane.

Because the performance of the wing was of prime importance, an effort was made in the wind tunnel to determine the drag rise for the wing by testing the F-8 fuselage with the wing replaced by an equivalent body having the same area progression as the wing. As indicated by the equation in figure 13, results for this equivalent-body configuration were then subtracted from corresponding results for the complete wing-body combination, and the difference, which is the drag associated with the wing, was plotted for several lift coefficients as a function of Mach number. The drag shown represents the friction, induced, wave, and separation drag for the wing and indicates efficient wing performance up to sonic speeds at the cruise lift coefficient of 0.4. It is hoped that this result will be verified in full-scale flight wing rake tests, which are planned for the near future.

CONCLUDING REMARKS

This paper has attempted to indicate some of the considerations involved in determining the present F-8 supercritical wing configuration. The evolution of the configuration has been the result of extensive wind-tunnel investigations; however, it may well be that the final evolution may extend over a relatively long time as more is learned from both wind-tunnel and flight tests.

REFERENCES

1. Bartlett, Dennis W.; and Re, Richard J.: Wind-Tunnel Investigation of Basic Aerodynamic Characteristics of a Supercritical-Wing Research Airplane Configuration. NASA TM X-2470, 1972.

2. Blackwell, James A., Jr.: Preliminary Study of Effects of Reynolds Number and Boundary-Layer Transition Location on Shock-Induced Separation. NASA TN D-5003, 1969.

3. Loving, Donald L.; and Katzoff, S.: The Fluorescent-Oil Film Method and Other Techniques for Boundary-Layer Flow Visualization. NASA Memo 3-17-59L, 1959.

SYMBOLS

AR	aspect ratio, b^2/S
b	wing span, m (ft)
C_D	drag coefficient
C_L	lift coefficient
C_m	pitching-moment coefficient
C_p	pressure coefficient
c	local streamwise chord of basic wing panel, m (ft)
i_t	horizontal-tail incidence, relative to fuselage reference line, deg
M	Mach number
S	wing area, m^2 (ft^2)
t/c	airfoil thickness-to-chord ratio
W	weight, kg (lb)
x	chordwise distance rearward of leading edge, m (ft)
y	spanwise distance, measured from plane of symmetry, m (ft)
ϵ	local wing chord incidence, relative to fuselage reference line, deg
Subscripts:	
cr	cruise
tot	total

EVOLUTION OF F-8 SUPERCRITICAL WING CONFIGURATION

EARLY 1967	• CONSIDERATION OF "PROOF-OF-CONCEPT" FLIGHT TEST
	• FLIGHT PROGRAM OBJECTIVES DEFINED
	• SELECTION OF F-8 AS TEST-BED AIRCRAFT
	• MODEL DESIGN INITIATED
EARLY 1968	• JOINT FRC-LRC PROGRAM ESTABLISHED
MID 1968	• FIRST WIND-TUNNEL TEST
LATE 1969	• WING COORDINATES FINALIZED

Figure 1

INITIAL MODEL CONFIGURATION

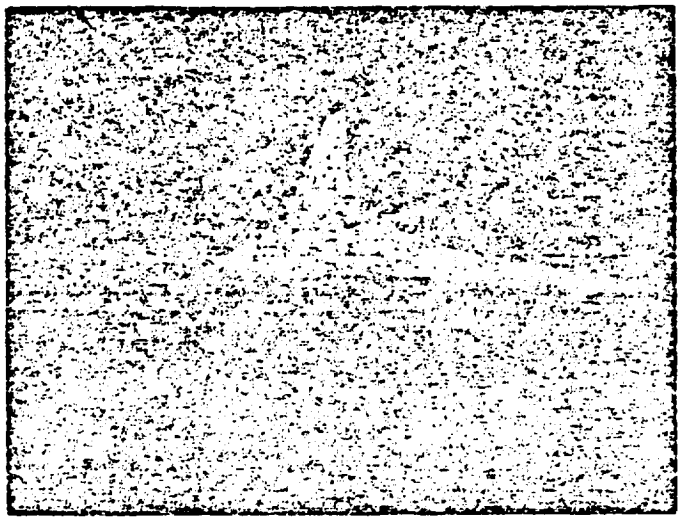

Figure 2

FINAL MODEL CONFIGURATION

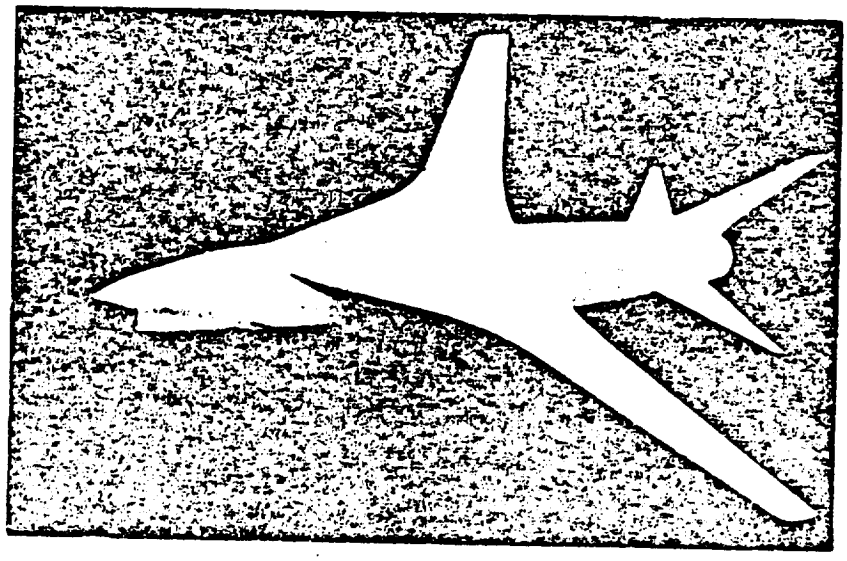

Figure 3

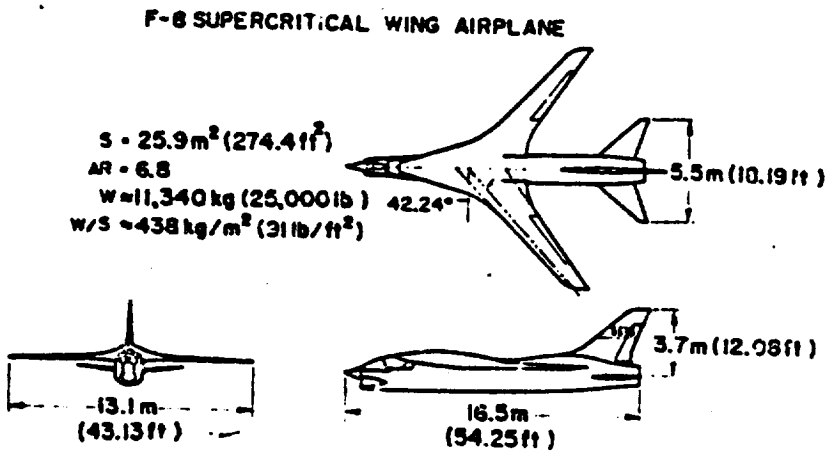

Figure 4

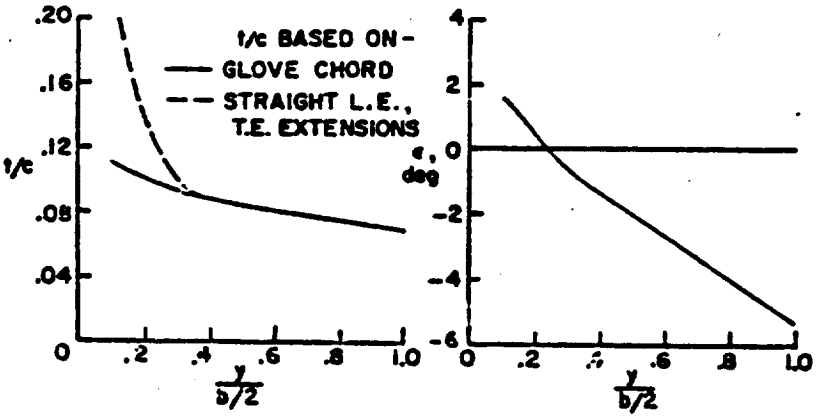

Figure 5

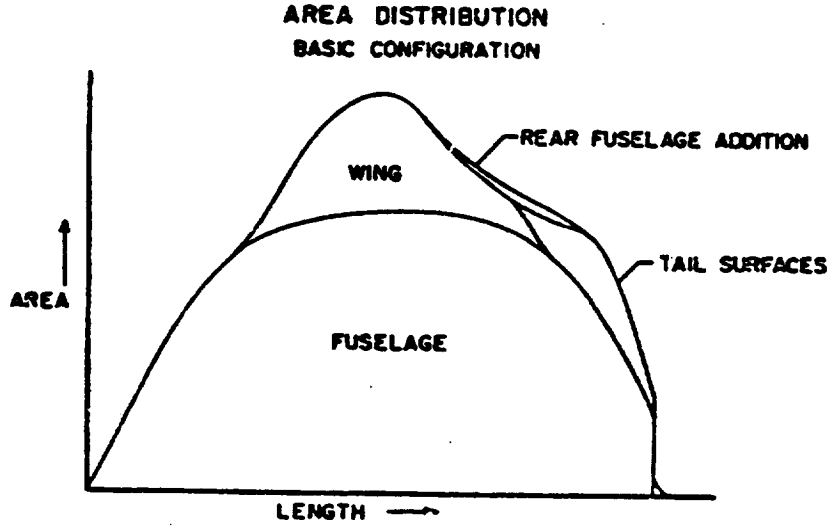

Figure 6

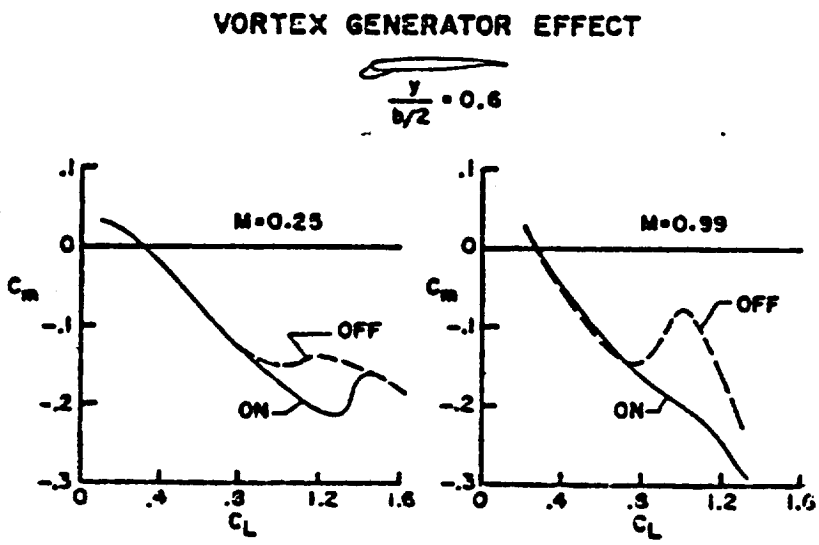

Figure 7

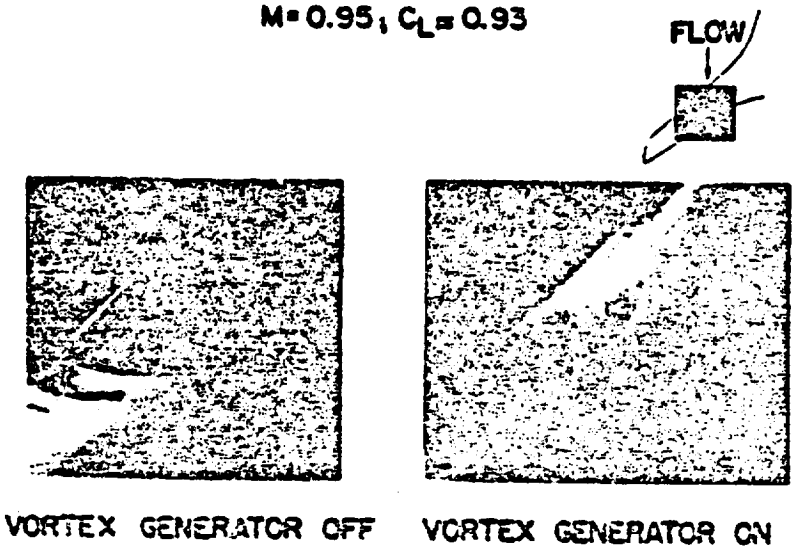

Figure 8

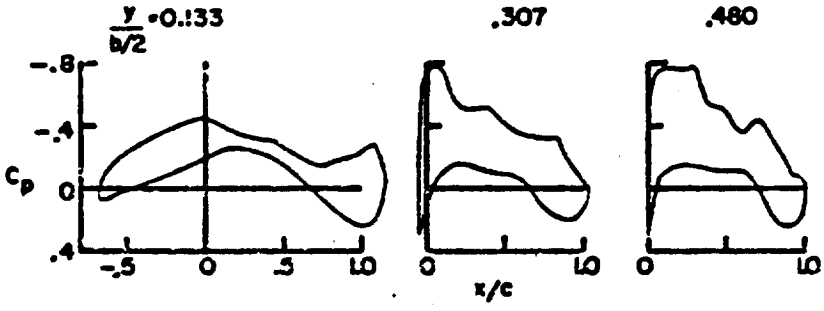

Figure 9

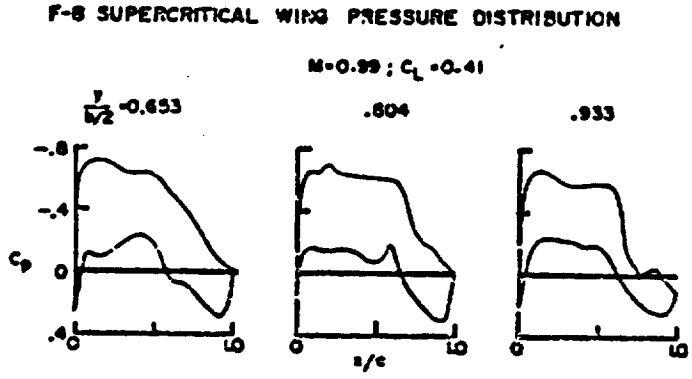

Figure 10

OIL FLOW
BASIC CONFIGURATION
M=0.99 ; $C_L \approx 0.40$

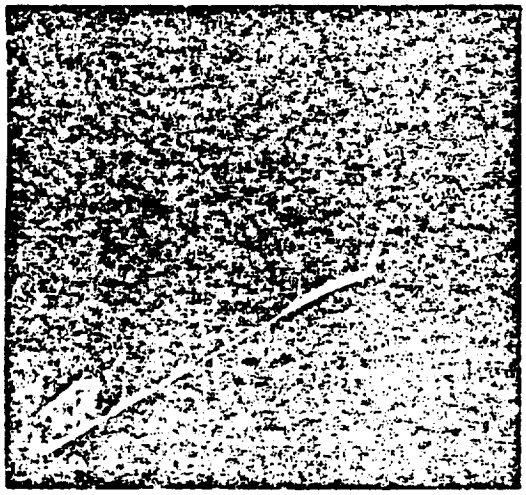

Figure 11

F-8 SCW MODEL
DRAG CHARACTERISTICS
$i_t = -2.5°$

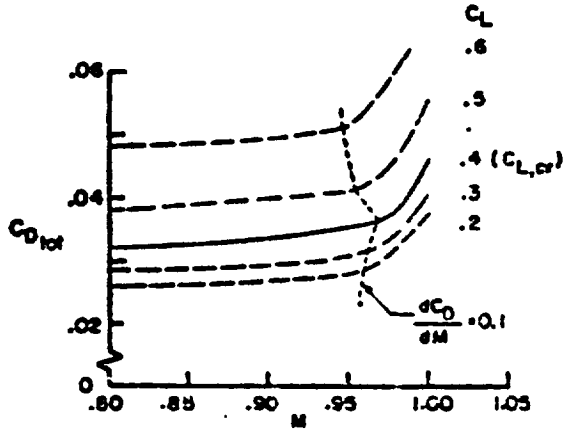

Figure 12

SUPERCRITICAL WING ON F-8

$C_{D,WING} = C_{D,WING\ FUS.} - C_{D,FUS.\ (EQUIV.)}$

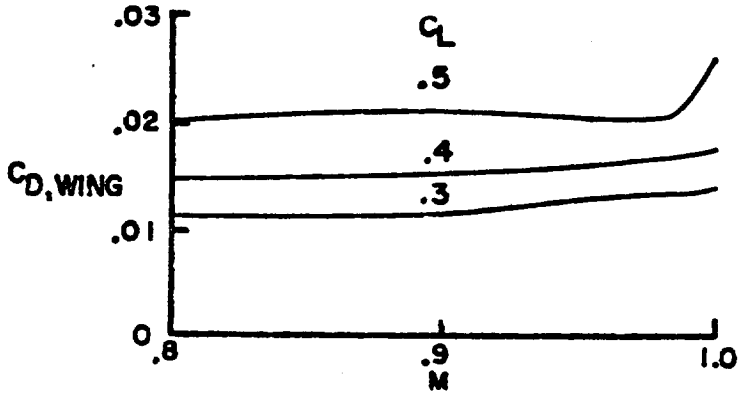

Figure 13

D4

X72-10200

PRECEDING PAGE BLANK NOT FILMED

4. STATUS OF THE F-8 SUPERCRITICAL WING PROGRAM*

By William H. Andrews
Flight Research Center

INTRODUCTION

The decision to proceed with a full-scale flight test evaluation of a sweptwing version of the supercritical wing concept led to the selection of a TF-8A airplane as a test bed. As mentioned in paper 3, an initial assessment revealed that the basic airplane wing could be replaced readily with one incorporating supercritical wing airfoil sections and a scaled transport planform. Further, the projected operational requirements dictated testing in the transonic speed range where propulsion system performance is usually limited. In this regard the TF-8A performance potential appeared equal to the task.

The first of several program milestones leading to the initial flight occurred in May 1969 when the test-bed airplane was obtained from the U. S. Navy. From May to September the details of the airplane modifications were defined. In September 1969 contracts were awarded to North American Rockwell and Ling-Temco-Vought to support the airplane modification and wing manufacturing. Simulator studies indicated that longitudinal stability augmentation as well as other minor modifications to the lateral and directional control systems would be required. Sperry Rand was awarded a contract to manufacture the longitudinal augmentation system components. In November 1970 the new wing was delivered to the Flight Research Center, and soon after a series of structural vibration and proof loads tests was performed. The wing installation, fuselage, and control systems modifications were completed, and the airplane was prepared for the first flight, which was performed on March 9, 1971.

This paper discusses the modifications incorporated in the test airplane and the status of the program.

Figures 1 and 2 are photographs of the basic TF-8A airplane and the supercritical wing test-bed airplane. The wing, of course, is the major difference in the two configurations. The original wing had a variable incidence to improve takeoff and landing performance. The geometry of the supercritical wing was not conducive to this feature and, as a consequence, the takeoff and landing performance of the test airplane was sacrificed. The rationale related to the installation of the wing fairings was discussed in paper 3. The forward fairing, or glove section, which covers the wing center section and extends forward to the cockpit canopy, and the aft fuselage fairings are constructed of Fiberglas.

*Title, Unclassified.

200

WING DESIGN AND STATIC TESTS

Wing Structure and Design Criteria

The wing structure consists of a two-cell main box section with attached leading- and trailing-edge sections (fig. 3). The construction material is primarily aluminum; however, the wingtips and sections of the leading edge are made of Fiberglas. A Styrofoam fill was used to develop the desired contour on the undersurface in the root area to approximately a 10-percent-span location. The wing-surface skins are tapered and vary in thickness from approximately 1.78 centimeter (0.7 inch) at the root to approximately 0.32 centimeter (0.125 inch) near the tips.

The wing structure, fairings, and attachment fittings were designed to standard margins of safety for symmetric load conditions ranging from 4.0g to -2.0g and a dynamic pressure of 38.30 kN/m^2 (800 lb/ft^2). The estimated service life of the structure was 1000 hours for the projected range of test conditions anticipated during the demonstration of the concept.

In addition to the design load specifications, a stringent requirement was set that the deformed shape of the wing was to duplicate that of the wind-tunnel model at the design cruise condition. This was essential for comparing the pressure-distribution data. Thus the wing was assembled with the deflection and twist necessary to compensate for the difference between the shape of the wind-tunnel-model wing and that predicted for the full-scale wing when the design cruise load distribution was applied to the unloaded basic structure. The wing structural design tolerances for a cruise Mach number of 0.99 and a lift coefficient of 0.40 specified that the differential twist between the root ribs was not to exceed 0.1°; the differential twist between wingtips not to exceed 0.3°; and the streamwise twist of the wingtip relative to the root was to be within ±0.5° of the predicted value. A goal, although not a requirement, was that the out-of-plane deflection of the trailing edge was not to exceed 0.15 centimeter (0.06 inch).

Proof Loads Tests

To be certain that the design criteria had been met, a series of proof loads tests was performed on the wing before its installation on the airplane. Figure 4 is a photograph of the test setup. The wing was mounted on a test fixture in an inverted position. Strain gages in the wing structure were monitored for safety purposes. Also, because the primary purpose of the test was to verify the deflection and twist of the structure under a simulated design cruise 1-g load distribution, deflection measurements were made at various spanwise and chordwise stations under the wing. Shot bags were used to produce the required distributed load.

The measured and predicted streamwise twist derived during the proof loads tests for the cruise load distribution are shown in the following table:

	θ_{root}, deg	θ_{tip}, deg	$\theta_{root}-\theta_{tip}$, deg
Predicted	0.14	1.45	1.31
Right wing panel	0.15	1.49	1.34
Left wing panel	0.14	1.46	1.32

The predicted values were derived from a standard North American Rockwell computer program used to predict structural behavior under various load conditions, on the basis of the design characteristics of the basic structure. From the streamwise twist, measured on the right and left wing panels, it can be seen that the difference between the predicted and measured wingtip rotations is well within the specified tolerance of ±0.5°. The measured differential twist between the root ribs is considerably less than the 0.1° specified, and the wingtip differential twist is less than the 0.3° tolerance limit specified in the initial design stage. The out-of-plane deflections of the trailing edge are presented in figure 5. The schematic shows the location of the reference plane and the corresponding points of the deflection measurements. From these data it appears that the root section is the only region where the specified deflection of 0.15 centimeter (0.06 inch) was exceeded.

Structural Vibration Test

In conjunction with the proof loads tests, a structural vibration test was performed on the assembled test airplane to identify the wing, fuselage, and control-surface structural-mode-response frequencies and respective mode shapes. The results of these tests were used to upgrade the structural-mode input data pertinent to the wing flutter analysis and to establish the filter requirements related to the flight-control-system modifications. Figure 6 is a photograph of the test arrangement. The airplane was mounted on an air-bag suspension system under the main and nose gear. Vibration units, capable of producing sinusoidal inputs over the frequency range of 0.1 cps to 1000 cps, were located at strategic points over the airplane and connected to the structure by vacuum pads. The structural response was recorded from accelerometers distributed on the airplane. The overall test was conducted from a van which included a console for controlling the vibration input and a recording system to monitor the accelerometer responses.

No flutter model tests were performed, so it was necessary to estimate flutter boundaries through analysis. The classical flutter analysis used took into account subsonic and supersonic aerodynamics and transonic compressibility effects. The results indicated that the flutter boundary would be well outside the projected flight envelope. On the other hand, a single-degree-of-freedom flutter analysis that considered the bending and twisting action of a swept wing at supersonic speeds predicted potential instability for the first wing symmetric bending mode (approximately 6 cps) at altitudes above 12.19 kilometers (40,000 feet) and Mach numbers of 1.0 to 1.05. As a consequence, the aeroelastic damping of this mode was investigated during the flight envelope expansion program. In figure 7 a portion of the flight results is summarized and compared with the supersonic analytical predictions in terms of the damping ratio of the first wing bending mode as a function of Mach number and altitude. It should be noted that the critical flutter speed would correspond to a damping ratio of zero. Subsonically, between a Mach number of 0.8 and 0.95, at an altitude of 10.67 kilometers (35,000 feet), it is evident that the damping decreases by approximately 34 percent. The damping is further reduced (by approximately 15 percent) as the design cruise condition at 14.02 kilometers (46,000 feet) is approached and it is minimum near a Mach number of 1. Considerably more data were obtained supersonically than are presented here. In general, the data scatter is similar to that presented in the figure, and in this region of the flight envelope the damping appeared to be generally higher than predicted.

FLIGHT-CONTROL-SYSTEM MODIFICATIONS

As mentioned, the preliminary fixed-base simulation studies of the modified F-8 configuration revealed a potential longitudinal instability over the projected flight envelope and indicated a need for stability augmentation. The longitudinal control system designed to control this instability is a blend of pitch rate and normal acceleration measured at the pilot's station. This scheme of control-system mechanization is commonly referred to as the C* concept. The system is essentially a fail-operational, fail-safe design which uses three separate channels for system reliability and failure detection.

Figure 8 is a simplified block diagram of the modifications incorporated in the longitudinal control system. The pilot's command through the force stick provides an input to the basic F-8 mechanical system and the command augmentation system electronic network. Within this network the electrical signal is proportional to the stick-force input. The pitch rate and normal acceleration are shaped, gain controlled, and summed to produce the C* feedback error signal. The error signal is gain controlled and positions the pitch servo to augment the basic airplane pitch damping. To operate the servo around a central position, an auto-trim network is provided. This network moves the stabilizer to the trim position and transmits signals to the C* feedback that drives the error signal to zero and in turn centers the servo. In addition, the trim network provides some shaping which aids in augmenting the longitudinal stability.

Lateral control is provided through segmented ailerons which are drooped and serve as flaps during takeoff and landing operations. The lateral-directional stability augmentation system is similar to those included on the basic TF-8A airplane. However, minor modifications were made to the respective control-surface deflections and augmentation authority to provide compatibility with the configuration changes. In addition, as for the longitudinal system, the variable-gain controls installed in the cockpit are accessible to the pilot.

FLIGHT TEST OBJECTIVES AND PROGRAM STATUS

The objectives of the flight test program include definition of the drag-rise Mach number, determination of the wing pressure distribution and acquisition of corresponding boundary-layer and wing-wake data, investigation of the maneuvering and speed margins associated with the buffet characteristics, and evaluation of the stability and control behavior at the design cruise conditions for the wing. In addition, the sensitivity of wing performance to control-surface deflections, aeroelastic deformation, wing-surface roughness, and other off-design operations is to be assessed. The ultimate objective, however, is to prove the concept by correlating flight information with wind-tunnel predictions where corresponding data exist.

Twenty-seven flights have been performed with the test-bed airplane. Figure 9 shows the flight envelope that has been defined. Essentially, the airplane has been flown to a maximum altitude of 15.55 kilometers (51,000 feet), a Mach number of 1.21, and a dynamic pressure of 25.62 kN/m^2 (535 lb/ft^2). Figure 10 shows the flight and

wind-tunnel Reynolds number envelopes, based on the mean aerodynamic chord, covered in the flight tests as a function of Mach number. Most of the data related to the drag and wing pressures were obtained near the design cruise point. Future testing will extend to higher Reynolds numbers. The first 10 flights in the program were devoted to expanding the flight envelope to the specified supercritical wing design point and beyond. During these flights the basic stability, control, handling qualities, performance, and flutter characteristics of the airplane were evaluated. In the second phase of the program, additional data of these types were obtained; however, most of this test time was devoted to accumulating total drag and wing pressure data. Throughout both test phases, airplane center of gravity varied from approximately 22 percent to 26 percent of the mean aerodynamic chord.

CONCLUDING REMARKS

The flight program of the F-8 supercritical wing test-bed airplane has proceeded in an orderly manner, particularly in view of the difficulties of testing in the transonic speed range in either wind tunnels or flight. An attempt has been made to acquire accurate data from precise state-of-the-art instrumentation and test techniques.

SYMBOLS

C_{L_A}	total airplane lift coefficient
K_{C^*}	C* gain, deg/g
K_{n_z}	normal-acceleration feedback gain, deg/g
K_q	pitch-rate feedback gain, deg/deg/sec
n_{z_p}	normal acceleration at pilot's station, g units
q	pitching velocity, deg/sec
$\bar{q}$	dynamic pressure, kN/m^2 (lb/ft^2)
Θ_{root}	twist of root chord about local 35-percent-chord location, deg
Θ_{tip}	twist of the tip chord about the local 35-percent-chord location, deg

BASIC TF-8A AIRPLANE

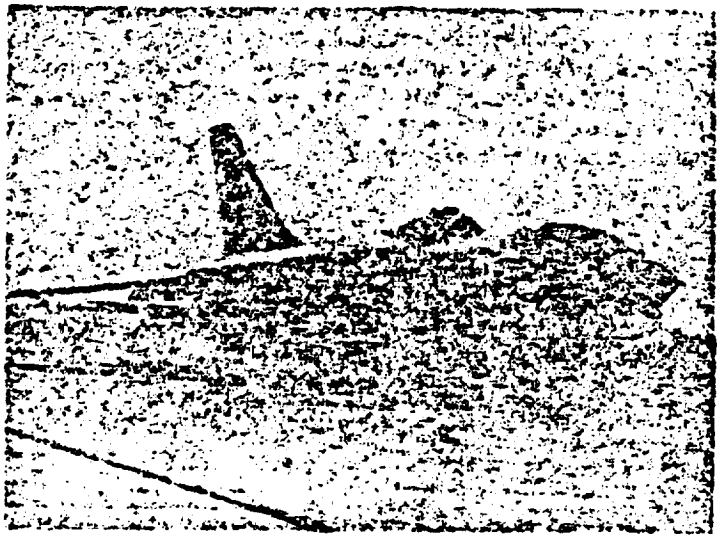

Figure 1

F-8 SUPERCRITICAL WING TEST-BED AIRPLANE

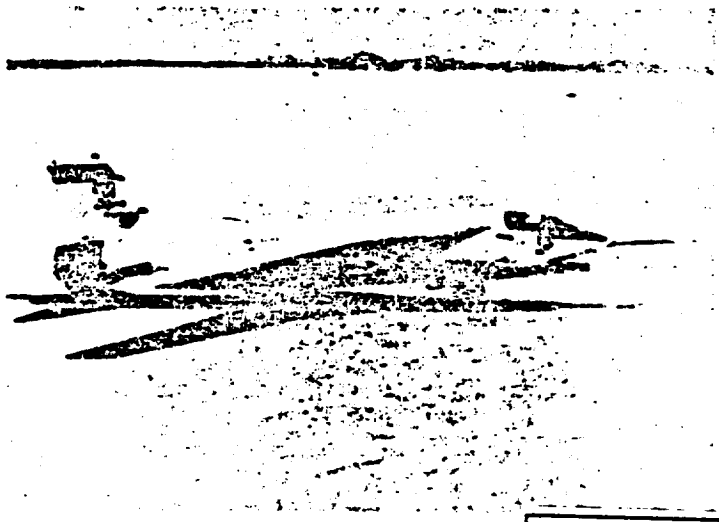

Figure 2

SCHEMATIC OF WING CONSTRUCTION

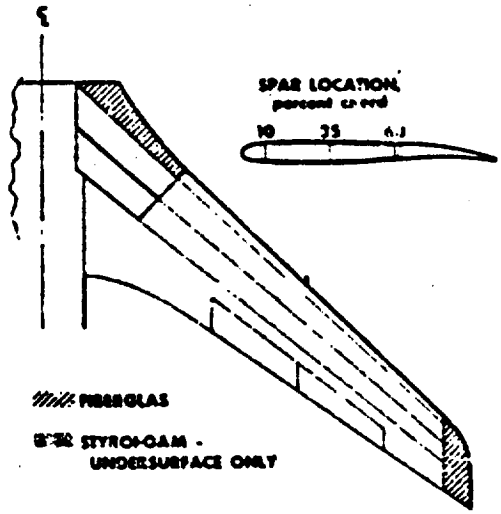

Figure 3

WING PROOF LOADS TEST SETUP

Figure 4

PROOF LOADS TEST - TRAILING-EDGE DEFLECTIONS

CRUISE LOAD DISTRIBUTION

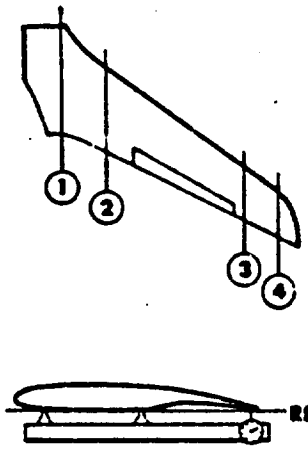

WING STATION	DEFLECTION, CM (IN.)
1	0.36 (0.14)
2	0.15 (0.06)
3	0.05 (0.02)
4	0.025 (0.01)

Figure 5

STRUCTURAL VIBRATION TEST SETUP

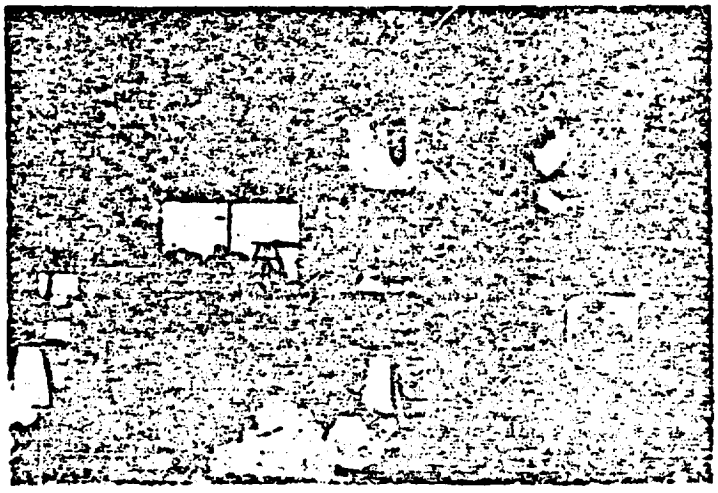

Figure 6

SUPERCRITICAL WING STRUCTURAL DAMPING

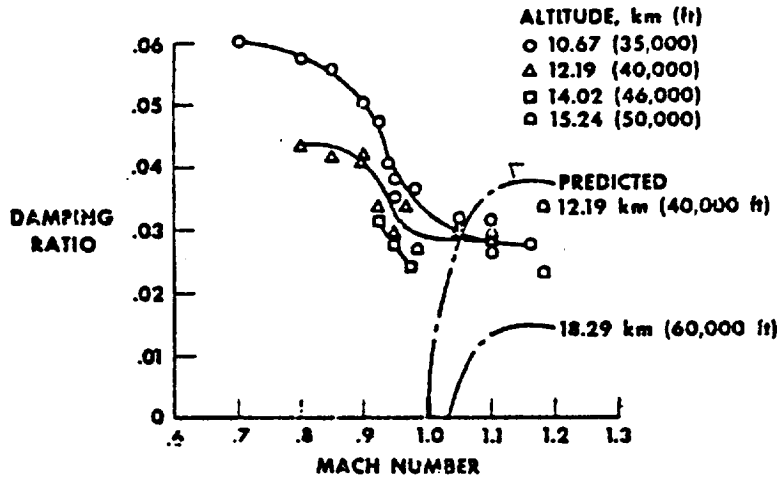

Figure 7

MODIFIED LONGITUDINAL CONTROL SYSTEM BLOCK DIAGRAM

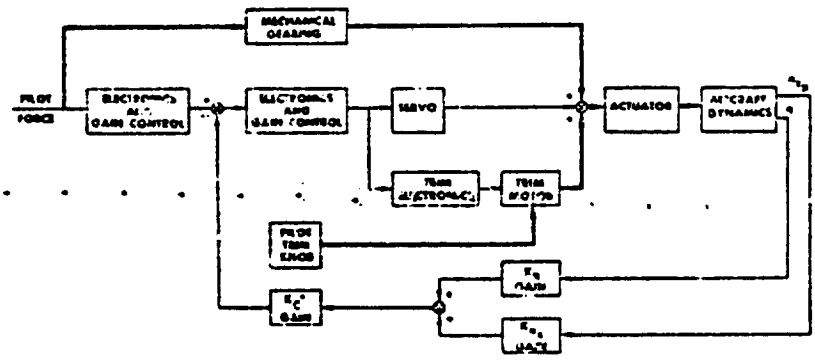

Figure 8

C.2

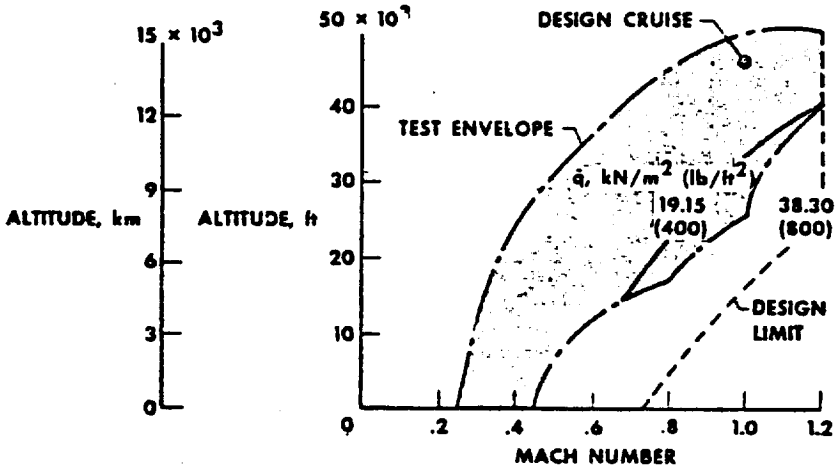

Figure 9

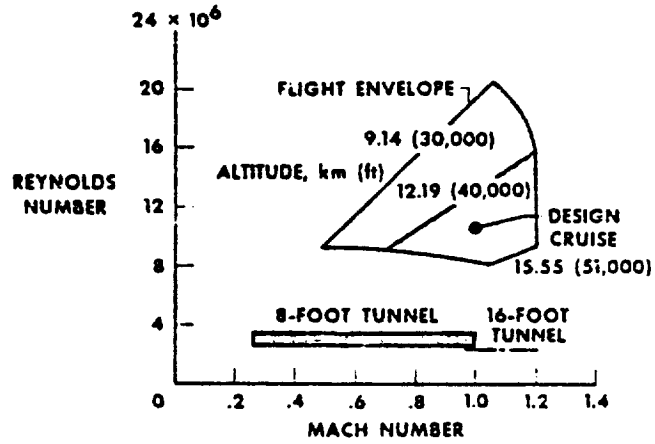

Figure 10

[redacted] X72-10201

5. PRELIMINARY LIFT AND DRAG CHARACTERISTICS OF THE F-8 SUPERCRITICAL WING AIRPLANE*

By Jon S. Pyle
Flight Research Center

[redacted]

INTRODUCTION

A flight research program is being conducted using a supercritical wing attached to a modified F-8 fuselage to demonstrate the potential benefits of the supercritical wing concept in a realistic cruise flight environment. One of the primary goals of the flight program is to determine the drag-divergence Mach number, that is, the Mach number at which the total vehicle drag increases significantly. Another objective of the program is to show how well wind-tunnel data can be used to predict the performance of a supercritical wing configuration in the transonic Mach number region from 0.9 to 1.0. Comparisons of this nature are important in view of the uncertainties in the present methods for extrapolating wind-tunnel-model data to flight Reynolds numbers, determining the effect of wall interference on the model results, and simulating the flow separation characteristics on the model wing to correspond to the large-scale wing. However, in comparing these wind-tunnel and flight results, it must be taken into account that this supercritical wing test configuration is of only intermediate scale and that a full-scale transport would have Reynolds numbers three to five times larger.

[redacted]

This paper reviews the lift and drag results obtained from the first series of flights with the F-8 supercritical wing configuration. To concentrate on the performance of the wing and eliminate extraneous effects of the fuselage and propulsion system, the internal drag and base drag components have been removed from the flight and wind-tunnel data. Although removing these variables provides for the best comparison of the wind-tunnel and flight wing drag, which is the immediate purpose of this paper, it is somewhat unreal for purposes of assessing the ability of a designer to use wind-tunnel results to predict the absolute drag level of a complete airplane.

ACCURACY AND METHOD

The drag-divergence Mach number has been established as being of prime importance to this study; thus the ability to measure Mach number accurately becomes very significant. Figure 1 presents the Mach number position correction as a function of indicated Mach number, which was determined in flight tests (similar to those reported in ref. 1) of the F-8 supercritical wing configuration by using a compensated pitot-static probe. This airspeed probe was designed at the Langley Research Center, on the

*Title, Unclassified.

[redacted]

basis of principles described in reference 2, to compensate for the position error in Mach number for this particular wing-fuselage configuration. The compensated probe was also designed for reduced angle-of-attack sensitivity between -2° and 8°, the region of most importance to this study. The estimated accuracy of the flight Mach number is shown in the figure by the band about the solid curve and is calculated to be within ±0.003 Mach number in the transonic region. The maneuvers used in making the flight calibration consisted of constant-altitude accelerations and decelerations. True ambient pressure was obtained by determining the precise altitude of the airplane with radar tracking and calculating the ambient pressure for that altitude from radiosonde balloon measurements. This calibration was later checked against a calibrated airspeed system on an Air Force PACER aircraft for steady-state flight at specific Mach numbers between 0.7 and 0.95.

Although the compensated pitot-static probe slightly overcompensated the Mach number position error, it improved the pilot's ability to achieve a desired speed by reducing the position error between the indicated and true velocity usually provided by the standard NACA pitot-static probe. This calibration was used to correct all flight Mach numbers in this paper.

The level of confidence in the measurement of Mach number has been determined, thus the ability to determine total drag should be examined closely. The parameters that contribute to the random error in the flight lift and drag results are listed in the following table for a Mach number of 0.97, a lift coefficient of 0.4, and an altitude of 16.2 kilometers (45,000 feet):

Parameter	Measurement error	Error in C_L, percent	Error in C_D, percent
Weight	±4.4 kN (±100 lb)	0.4	---
Dynamic pressure	±0.06 kN/m^2 (±1.3 lb/ft^2)	0.6	0.6
Net thrust	±0.36 kN (±80 lb)	---	3.8
Normal acceleration	±0.01 g	1.0	0.6
Longitudinal acceleration	±0.001 g	---	1.2
Angle of attack	±0.25°	---	5.0
	Root-sum-squared error	1.3 percent	6.4 percent

The estimated random measurement errors are presented for each parameter used in the lift and drag determination based on cruise lift conditions. The contribution of the individual parameters to the random error in the determination of C_L and C_D is presented in the right two columns. The values shown in these two columns represent

the limits within which approximately two-thirds of the data points should occur based only on the individual parameter source. It should be noted that the largest contributions to the scatter in the flight values are uncertainties in the measurement of angle of attack and thrust. The root-sum-squared error shown at the bottom of the table is indicative of the limits within which most of the final computed values of C_L and C_D should occur.

An example of flight lift- and drag-coefficient measurements for a Mach number of 0.9 is presented in figure 2. This figure indicates the repeatability of the flight results by presenting a plot of the actual data points obtained during nine separate maneuvers on four flights. Most of the data points are within the limits set by the total root-sum-squared error shown in the preceding table. These limits are shown as a shaded area at a lift coefficient of 0.4.

Many ground and in-flight calibrations have been used to eliminate nonrandom errors that could affect the flight lift and drag results. Therefore, in addition to the normal corrections made for individual and system component calibrations, preflight and post-flight tare variations, and weight changes, special attention was given to ground thrust-stand calibrations of the thrust instrumentation and an in-flight calibration of angle of attack. The latter calibration consisted of special quasi-stabilized maneuvers at various Mach numbers to determine the true airplane angle of attack with a sensitive accelerometer.

There remain possible bias uncertainties which have not been removed by calibration procedures or tare corrections. For Mach numbers below 0.95, the possible bias error is estimated to be within about 3 percent of the drag coefficient at a lift coefficient of 0.4. The main cause of this 3-percent uncertainty is the thrust determination. The J57-P-4 engine which was used in this airplane is particularly well suited for the thrust measuring and calibration techniques which were used, and thus permitted this relatively small nonrandom uncertainty. At the higher Mach numbers the bias uncertainty in drag coefficient in this study is about 6 percent. This increase is primarily due to the difficulty of defining angle of attack in this speed region.

The primary condition at which lift and drag results were obtained consisted of level flight at a quasi-stabilized airspeed and angle of attack. Additional data to provide drag polar segments were obtained during increasing normal "g" coordinated turns, utilizing the accelerometer method (ref. 3). These "windup" turns were performed at very slow rates to assure that the vehicle would remain close to a trimmed flight condition. The quasi-stabilized maneuver was, however, considered to be the most important flight condition for lift and drag determination because the F-8 supercritical wing, in terms of aspect ratio and thickness, was configured with cruise flight in mind.

DISCUSSION

Lift

Figures 3 and 4 present the flight and wind-tunnel lift curves for selected Mach numbers between 0.90 and 1.2. A comparison of the variation of flight and wind-tunnel lift coefficient with angle of attack is presented for each Mach number. The Langley 8-foot wind-tunnel results were obtained with an 0.087-scale model of the test configuration. The wind-tunnel data are trimmed about the same center-of-gravity location as

the flight data. The solid symbol represents a data point obtained in the Langley 16-foot wind tunnel. These data were obtained at only one horizontal-stabilizer deflection, so the 16-foot wind-tunnel results are compared with flight data only at the condition where the model data represent a trimmed condition.

In general, the flight lift curves are close to the wind-tunnel results except for the data for Mach numbers of 0.95 and 0.99, where the lift coefficient for the wind-tunnel results is higher at any given angle of attack than for the flight results.

The lift-curve slope, C_{L_α}, is presented as a function of Mach number in figure 5. The flight-determined values of lift-curve slope are generally higher than those determined in the 8-foot wind tunnel for Mach numbers between 0.8 and 0.99. Flight-determined lift-curve slopes were not available for Mach numbers from 1.0 to 1.08 because of the difficulty of maintaining constant-Mach-number maneuvers in this speed range. At Mach numbers above 0.99, the F-8 airplane required the use of the jet engine afterburner. However, the extra thrust produced by the afterburner could not be controlled precisely enough to obtain stabilized flight in this Mach number range.

Drag

Before examining the drag measurements, adjustments to the results should be discussed. As stated earlier, the internal drag and base drag were removed from the wind-tunnel and flight drag values. The model used in the 8-foot wind-tunnel tests was an accurate geometric simulation of the flight vehicle and included scaled versions of the actual flight vehicle antennas, anticollision lights, nose boom, and other protuberances that might contribute to the drag of the airplane. Personnel of the Langley 8-foot wind tunnel adjusted the wind-tunnel data to account for the differences in Reynolds numbers, which varied from 3 million for the wind-tunnel results to 10 million for flight data. They also made adjustments, using methods described in reference 4, to account for the presence of surface irregularities on the airplane such as gaps, slots, and rivets, which could not be simulated on a small-scale model.

An earlier version of the 0.087-scale model of the test configuration without the scaled protuberances, leading-edge vortex generators, and aileron hinge fairings was used for the 16-foot wind-tunnel tests. An increment of drag was added to the 16-foot wind-tunnel results to account for these protuberances. Additional adjustments were made by the wind-tunnel personnel to account for the Reynolds number differences and surface irregularities of the model wing.

Figures 6 and 7 present the variation of drag coefficient with lift coefficient for trimmed conditions at selected Mach numbers from 0.90 to 1.2. The flight results are compared with 8-foot and 16-foot wind-tunnel results where these were available. The most notable feature of the comparison is the difference in the shape of the drag polar curves. The flight results show a smaller variation of drag with lift than predicted by the 8-foot wind-tunnel results. The drag level at the lower lift coefficients is higher in the flight data than in the wind-tunnel results. These higher flight drag values become more obvious as Mach number increases up to 0.99.

The flight results showed that a larger horizontal-stabilizer deflection was needed to trim the vehicle than the wind-tunnel data had indicated. In addition, pressure

measurements were obtained on the boattail portion of the test configuration during the 8-foot wind-tunnel tests and the flight tests. These pressure measurements indicated that a higher boattail drag was measured on the aft-sloping boattail surfaces in flight than had been predicted by the wind-tunnel results. The long-short-long dashed line plotted with the $M = 0.97$ curves represents the wind-tunnel data adjusted to the flight horizontal-stabilizer deflections and the added drag increment due to the difference between the flight and wind-tunnel boattail measurements. Although the adjustment compensates for some of the differences between flight and wind-tunnel drag level at the lower lift coefficients, it does not account for the differences in the drag polar shapes. However, it should be noted that the flight and wind-tunnel drag polars intersect near the design cruise lift coefficient of 0.4.

The variation of drag coefficient with Mach number is presented in figure 8 at the design lift coefficient of 0.4 and illustrates the comparison of drag-divergence Mach number for flight and wind-tunnel results. The flight and 8-foot wind-tunnel results were obtained from the previous drag comparisons, and the 16-foot wind-tunnel results were extrapolated to a lift coefficient of 0.4 by the wind-tunnel personnel. For the flight results the drag-divergence Mach number, M_{DR}, is approximately 0.96; for the 8-foot wind-tunnel data it is closer to 0.97.

The Mach number region where some typical commercial transports experience the drag rise is shown by the shaded area (ref. 5 and unpublished data). The supercritical wing test configuration was not optimized to represent a true transport configuration. This is evident from a comparison of the test configuration fineness ratio of 7.5 with the much higher fineness ratios of typical transport configurations. Thus the transport drag coefficients for $C_L = 0.4$ are expected to be lower than those for the test configuration. The comparison indicates a favorable increase in drag-divergence Mach number for the supercritical wing configuration when compared with the results obtained with current jet transports.

An attempt will now be made to explain some of the differences shown in figure 8 between the absolute drag level measured in flight and in the 8-foot wind tunnel. The 8-foot wind-tunnel results shown in figure 9 were adjusted to account for the larger horizontal-stabilizer deflections required in flight and the higher drag measured on the boattail of the flight vehicle, as discussed previously with regard to the polar shown for $M = 0.97$. These adjustments were made so that it was possible to focus on the wing drag and to reduce the effect of those drag differences which were not directly related to the wing. The adjustments produced close agreement between the levels of absolute drag found in flight and in the wind tunnel at the design lift coefficient as well as close agreement in the flight and wind-tunnel drag-divergence Mach number. In the previous comparison of flight and adjusted wind-tunnel model drag polars at a Mach number of 0.97 (fig. 6), it was noted that the model drag polar intersected the flight results near the design lift coefficient of 0.4. In view of the differences in the polar shapes of the wind-tunnel and flight results, the relationship of the absolute drag levels at the design condition in figure 9 is so close as to be deceptive if considered by itself.

CONCLUDING REMARKS

Flight tests of a supercritical wing attached to an F-8 fuselage showed that the drag-divergence Mach number was approximately 0.96 in the flight data and closer to 0.97 in

the 8-foot wind-tunnel data. Also, the drag-divergence Mach number was significantly higher for the supercritical wing installation on the F-8 airplane than for typical operational jet transports.

A significant difference in the shape of the drag polar curves in the flight and 8-foot wind-tunnel results was apparent. The increase of drag with lift was greater on the model than in flight at the lower lift coefficients.

In general, the flight lift curves are close to the wind-tunnel results except for the data for Mach numbers of 0.95 and 0.99, where the lift coefficient for the wind-tunnel results is higher at any given angle of attack than for the flight results.

REFERENCES

1. Larson, Terry J.; and Webb, Lannie D.: Calibrations and Comparisons of Pressure-Type Airspeed-Altitude Systems of the X-15 Airplane From Subsonic to High Supersonic Speeds. NASA TN D-1724, 1963.

2. Ritchie, Virgil S.: Several Methods for Aerodynamic Reduction of Static-Pressure Sensing Errors for Aircraft at Subsonic, Near-Sonic, and Low Supersonic Speeds. NASA TR R-18, 1959.

3. Beeler, De E.; Bellman, Donald R.; and Saltzman, Edwin J.: Flight Techniques for Determining Airplane Drag at High Mach Numbers. NACA TN 3821, 1956.

4. Horton, Elmer A.; and Tetervin, Neal: Measured Surface Defects on Typical Transonic Airplanes and Analysis of Their Drag Contribution. NASA TN D-1024, 1962.

5. Tambor, Ronald: Flight Investigation of the Lift and Drag Characteristics of a Swept-Wing, Multijet, Transport-Type Airplane. NASA TN D-30, 1960.

SYMBOLS

C_D	drag coefficient
$\Delta C_D/\Delta M$	slope of the drag coefficient with respect to Mach number
C_L	lift coefficient
C_{L_α}	lift-curve slope
h_p	altitude, m (ft)
M	free-stream Mach number
ΔM	compensated probe position correction for indicated Mach number, $M_T - M_i$

M_{DR}	drag-divergence Mach number, $\Delta C_D/\Delta M = 0.1$
M_I	indicated Mach number
M_T	true Mach number
α	angle of attack, deg

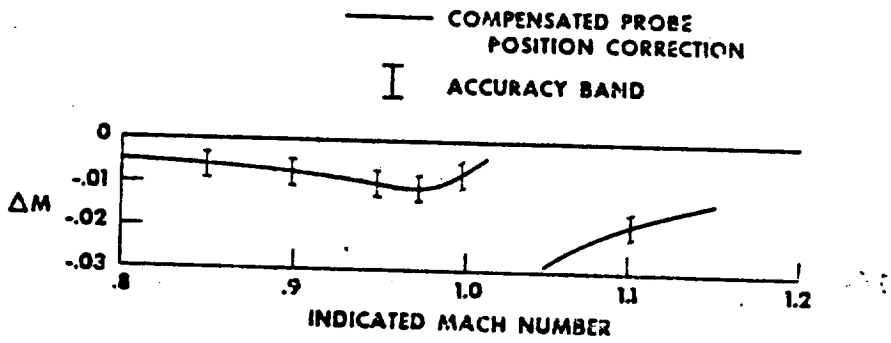

Figure 1

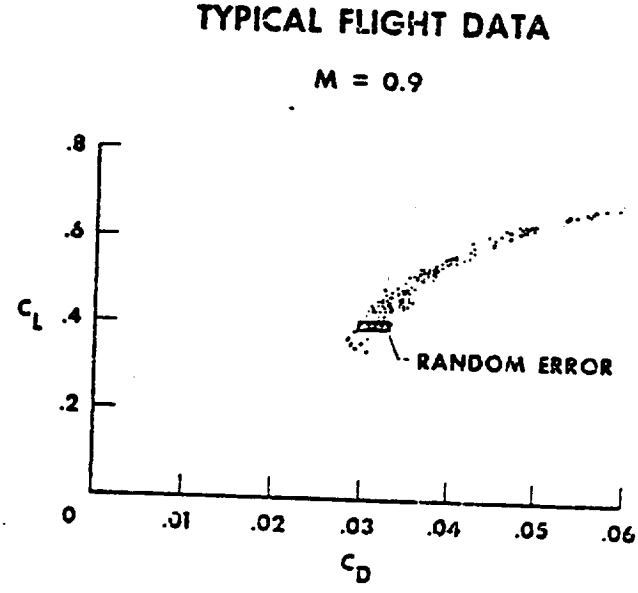

Figure 2

LIFT-CURVE RESULTS

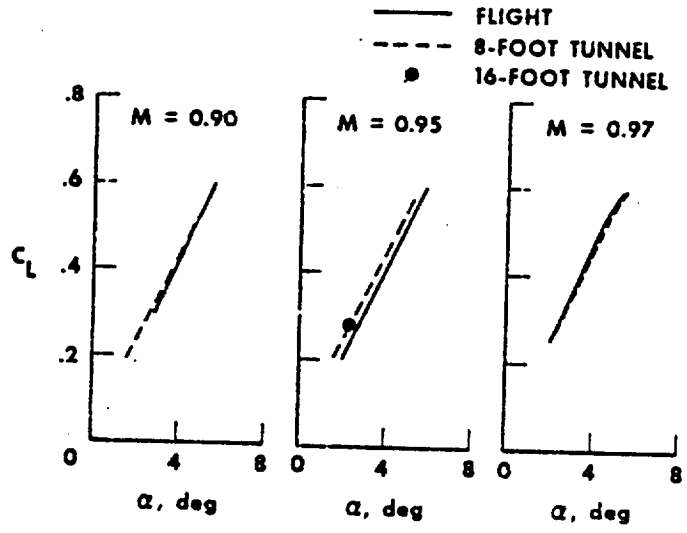

Figure 3

LIFT-CURVE RESULTS

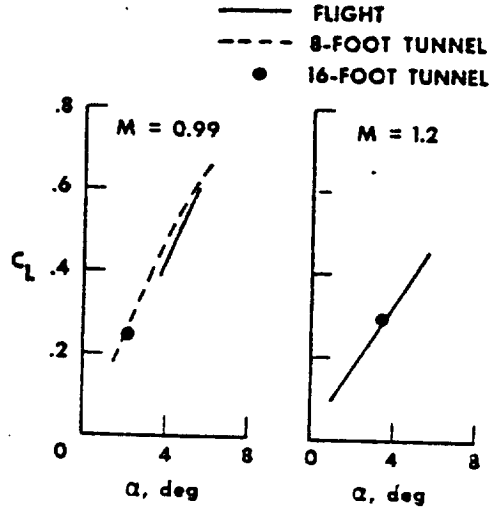

Figure 4

EFFECT OF MACH NUMBER ON LIFT-CURVE SLOPE

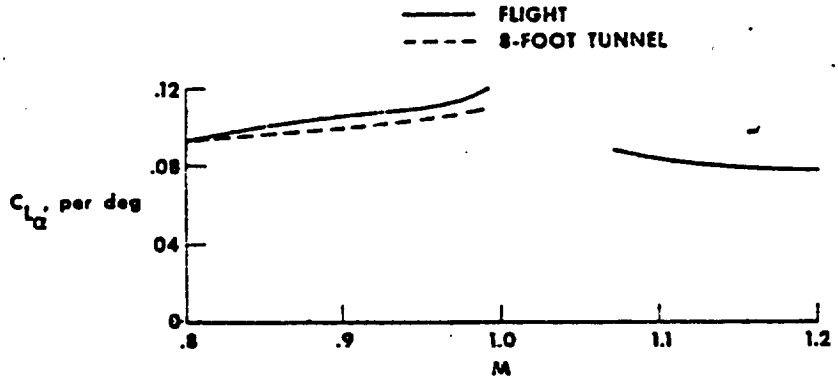

Figure 5

DRAG POLARS

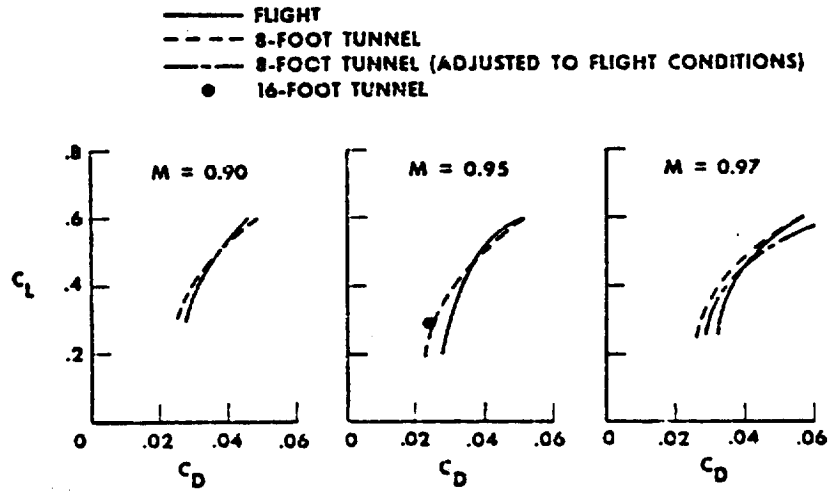

Figure 6

DRAG POLARS

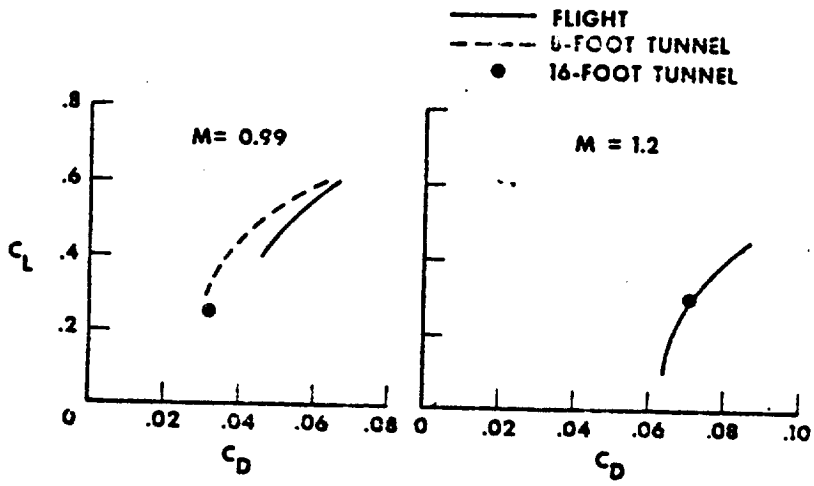

Figure 7

EFFECT OF MACH NUMBER ON DRAG
C_L = 0.4

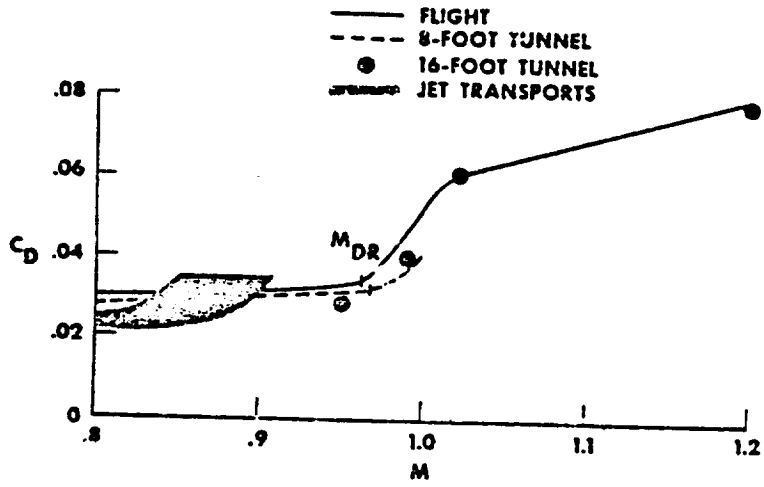

Figure 8

COMPARISON OF ADJUSTED DRAG RESULTS

$C_L = 0.4$

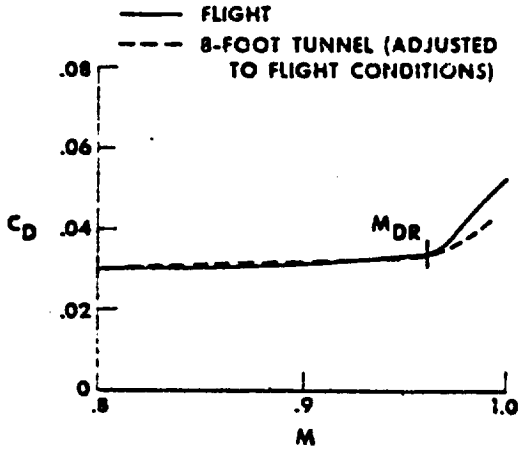

Figure 9

6. F-8 SUPERCRITICAL WING PRESSURE DISTRIBUTION EVALUATION*

By Lawrence C. Montoya and Richard D. Banner
Flight Research Center

INTRODUCTION

In paper 5 the total lift and drag characteristics of the full-scale supercritical wing F-8 airplane and the wind-tunnel model were presented and compared. In those data the drag-rise Mach number for the complete configuration was approximately 0.96. However, the model wing performed well, with only a small amount of separation, up to a Mach number of 0.99. This Mach number was chosen as the design condition for the wing.

The details of the flow characteristics over the wing are also of interest, particularly where flows are mixed and contain shocks and adverse pressure gradients that might compromise the design if their effects are not properly predicted. To evaluate the wind-tunnel wing data, wing pressure measurements were made in flight. This paper presents some of these data, compares them with Langley 8-foot wind-tunnel results, and relates the measurements to the drag and buffet characteristics of the complete configuration.

WING CONFIGURATION

The flight wing pressure measurements were obtained from six rows of orifices on both the top and bottom surfaces at span stations shown in figure 1. These span stations were identical to those used for the pressure survey on the model.

The wing planforms of the airplane and model were identical. The full-scale and the model wings were constructed so that they had the same twist distribution at the design conditions—a Mach number of 0.99 and a total airplane normal-force coefficient of 0.40. The model wing also incorporated the leading-edge vortex generator and aileron hinge fairings that existed on the full-scale wing. The airplane wing surfaces were filled and sanded so that they were as close to the model in smoothness and surface contour as practical.

To simulate the boundary-layer characteristics in flight, artificial trips were used on the model. The position of the boundary-layer trips, which were placed on both the upper and lower surfaces of the model wing, is shown in figure 2.

At Mach numbers equal to or greater than 0.95, the trips were placed at the

*Title, Unclassified.

31-percent chord on both the upper and lower surfaces of the outer wing panel (shown at the top of fig. 2). This trip location was used to simulate the boundary-layer characteristics in the adverse pressure-gradient regions at the rear of the airfoil. For Mach numbers of 0.90 and below (shown at the bottom of fig. 2), the boundary-layer trips on the outer wing panel were located from the 5-percent chord to the 8-percent chord on the upper surface and at the 31-percent chord on the lower surface. This forward trip arrangement on the upper surface was used at these Mach numbers to prevent laminar separation aft of the velocity peak that occurs near the leading edge. The trips on the upper surface of the inboard wing panel or "glove" region were moved forward because laminar flow could not be maintained in this region. For this reason, as well as the unscaled fuselage boundary layer near the wing root, boundary-layer scaling was not expected on the inboard wing regions.

INSTRUMENTATION AND PROCEDURE

The 248 flight wing surface pressures were transmitted to three wing instrument bays using 0.318-centimeter (0.125-inch) inner diameter tubing where the pressure measurements were made with scanivalves. All data were recorded on onboard tape and reduced by computer. During data runs, continuous in-flight scanivalve pressure transducer zeros were obtained. Data were taken during steady-state flight with several repetitive data cycles at each test condition. Data points were also repeated on successive flights, and checked well. The wind-tunnel and flight measurements were made with comparable accuracy.

RESULTS AND DISCUSSION

In the following figures, data are presented for selected conditions that are representative of the flight data obtained. Wind-tunnel results are compared with the flight data.

Figure 3 shows a wing pressure distribution (coefficient of pressure versus chord location) for both flight and wind-tunnel tests at a Mach number of 0.90 for a wing-panel normal-force coefficient of 0.30. (The wing-panel normal-force coefficient was obtained by integrating the span loads outboard of row 1.) In flight the right aileron was trimmed slightly down. The average deflection was 1.8°.

In general, the agreement between the flight and wind-tunnel pressure distributions is good for both the top and bottom surfaces. At these conditions, there is a high-velocity peak and a recompression region near the leading edge of the upper surface. As noted earlier, the boundary-layer trip was positioned near the leading edge of the upper surface of the model. In view of the good agreement, it is believed that the model trips had little effect on the pressure in this region.

Higher second-velocity peaks are more noticeable in the flight data at rows 3, 4, and 5. Although the deflected aileron may have contributed to these differences, it is not believed to have had a significant effect on the overall drag.

At the higher wing-panel normal-force coefficient of 0.53 (fig. 4), the agreement

between flight and wind-tunnel data is good, with recompressions occurring farther aft than at $C'_{N_{wp}} = 0.30$ (fig. 3) and at about the same chord location on the model and the airplane. Again, the second-velocity peak tends to be slightly higher in flight than in the wind tunnel. In both figures 3 and 4, trailing-edge pressure recovery is good for both the model and the airplane.

In figure 5 section normal-force coefficients for rows 2, 4, and 6 are shown as a function of angle of attack at a Mach number of 0.90. The angle-of-attack scale is offset for each row. The flight data were taken over a dynamic-pressure range from 8.14 kN/m^2 to 17.72 kN/m^2 (170 lb/ft^2 to 370 lb/ft^2), whereas the model data were obtained at 47.88 kN/m^2 (1000 lb/ft^2). It will be recalled that at a flight dynamic pressure of 9.58 kN/m^2 (200 lb/ft^2), the airplane wing shape was designed to correspond to the model wing at approximately 47.88 kN/m^2 (1000 lb/ft^2). The flight data appear to show a consistent trend, which suggests that dynamic pressure has little effect over this range.

As shown in figure 5, the flight section normal-force coefficients tended to be lower than the wind-tunnel data for the same angle of attack. (The solid symbols represent the flight section normal-force coefficients obtained from the pressure distributions shown in figures 3 and 4.) Some minor differences in the slopes also appear. The reasons for these differences are not understood. There could be discrepancies in either the model or the airplane angle-of-attack measurements, or both, that have not been detected.

Figure 6 shows a comparison of flight and wind-tunnel wing pressure-distribution data at a Mach number of 0.99 and a normal-force coefficient of 0.29, which is less than the design value. Flight data for rows 1 and 2, which were close to the fuselage where the boundary-layer-scaling conditions were not optimized, show good agreement with wind-tunnel results except that the second-velocity peaks are higher in flight. The second-velocity peaks are also higher in the flight data for the outboard rows.

At the design wing-panel normal-force coefficient of 0.35 (fig. 7), the trends are similar to those in figure 6. The higher flight second-velocity peaks occur on rows 1, 2, 3, and 4. On rows 5 and 6 there is a single recompression which occurs farther aft in flight than on the model. In the data of figures 6 and 7, the flight trailing-edge pressure did not recover as well as in the model tests. The reasons for these differences are discussed in paper 9.

The data in figure 8 are for a wing-panel normal-force coefficient of 0.49. Again, the comparisons generally show good agreement between the flight and wind-tunnel results for both the upper and lower surfaces. At this higher wing loading, both the airplane and model pressures show separated flow aft of the recompression, which is farther aft in flight than on the model. The more aft recompression results in a more rearward center of pressure on the wing in flight than on the model.

In figure 9 section normal-force coefficients at $M = 0.99$ for rows 2, 4, and 6 are shown as a function of angle of attack. The flight values are displaced with angle of attack relative to the wind-tunnel results, but because of the limited data, the curve is not well defined.

These data indicate that the pressure distributions shown previously for the lower wing loadings (solid symbols) are near a nonlinear region. This nonlinear region is believed to correspond to the condition where the boundary layer separates. This separation results from the aft location of the shock at this Mach number.

The variation of the shock position along the chord at one station, row 5, for a Mach number of 0.99 is shown in figure 10. The shock position is compared on the basis of section normal-force coefficient. The shock was identified by an abrupt change in pressure coefficient of approximately 0.30.

At the low section normal-force coefficient values, for both the model and in flight, there was a forward and an aft shock, as illustrated in the small schematic at the bottom right. The aft shock results from the second-velocity peak at these off-design section normal-force coefficients. On the model, as the forward shock moves rearward, the second-velocity peak and its subsequent recompression disappear. In flight, the second-velocity peak and its subsequent shock persisted through this region.

For section normal-force coefficients greater than 0.45, only one recompression takes place, on the aft region of the airfoil section, as illustrated in the small schematic at the upper right. The shock is approximately 10 percent farther aft in the flight data than in the wind-tunnel data. The shock moves slightly forward in both instances to a position which does not vary much with increasing section normal-force coefficient. This has beneficial effects in preventing separation from propagating forward. This effect is discussed further in paper 7.

These trends in shock location were also observed in the other outboard rows, except that in rows 3 and 4 the forward shock did not diminish until a slightly higher section normal-force coefficient was reached.

Both the position of the shock and the geometry of the trailing edge can influence the upper-surface pressure recovery at the wing trailing edge. Both the model and the airplane had a 1-percent-chord trailing-edge thickness, as illustrated in figure 11. As shown, the trailing-edge geometries did not differ significantly. On the airplane, orifice row 3 had a blunt trailing edge to accommodate future installation of a trailing-edge rake.

Trailing-edge pressures for both the model and the airplane are shown in figures 12 and 13. Data are compared at Mach numbers of 0.90, 0.97, 0.98, and 0.99 as a function of section normal-force coefficient.

In figure 12 the agreement in the trailing-edge pressure recovery on the inboard wing sections is considered good, even though the model boundary layer could not be properly simulated on the inboard wing and fuselage. The flight data tend to be slightly lower for row 1 and slightly higher for row 2, and the pressure-recovery levels tend to be higher near Mach 0.99 than Mach 0.90.

The trailing-edge pressure-recovery characteristics of the outboard wing sections (rows 3, 4, 5, and 6) are shown in figure 13. The significant difference between the data at the higher Mach numbers and the data at a Mach number of 0.90 is shown in the pressure-divergence trends of the model data. At a Mach number of 0.90, the trailing-edge pressures diverge at about the maximum section normal-force coefficient, indicating that separation spreads rapidly over the wing and causes the sections to stall.

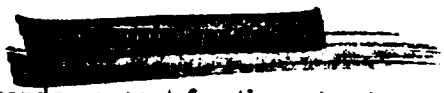

The flight data show the same trends, except for the outer two rows, where the maximum section normal-force coefficients for flight are higher than the model data. At Mach numbers of 0.97, 0.98, and 0.99, the sections do not stall until normal-force coefficients higher than shown are reached; however, the trailing-edge pressure coefficients diverge at section normal-force coefficients near 0.4. As noted previously, the aft shock associated with the higher Mach numbers prevents the spread of separation on the wing.

The model data indicate an optimum trailing-edge pressure-recovery condition near a section normal-force coefficient of 0.4 at Mach numbers of 0.97, 0.98, and 0.99. Although the flight data are incomplete at the lower section normal-force coefficients, there is some evidence that the airplane is showing the same trends as the model (rows 4 and 5, M = 0.99; and row 6, M = 0.97). However, it appears that the airplane trailing-edge pressures do not recover as well as on the model at the higher Mach numbers, and that this difference contributes to the increase in drag for the complete configuration.

In figure 14 span load distributions are shown at Mach numbers of 0.90 and 0.99 where the total wing-panel normal-force coefficients outboard of row 1 were the same for the model and the full-scale wing. In the span load distribution shown in the right plot, for the design condition of Mach 0.99, the flight data indicate that the position of the spanwise center of pressure would be slightly outboard of that on the model; however, the differences are small. At the off-design speed of Mach 0.90, in the left plot, there are even smaller differences. This suggests that the model and airplane have equivalent wing-stiffness characteristics for these conditions.

CONCLUDING REMARKS

In general, the degree of correlation between the model and airplane wing pressure measurements is believed to be good. Some differences are apparent, which can be summarized as follows. At off-design conditions the second-velocity peaks were higher on the airplane wing than on the model. At design conditions the shock was slightly farther aft on the airplane than on the model, and the trailing-edge pressure recovery was not as good. The inboard wing-panel loading on the airplane was slightly less than on the model, and because of the farther aft shock location, there was a more rearward center of pressure on the airplane wing.

SYMBOLS

b wing span, cm (ft)

$C'_{N_{wp}}$ wing-panel normal-force coefficient,

$$\int_{0.133}^{1} c_n \frac{c}{c_{av}} d\left(\frac{2y}{b}\right)$$

C_p pressure coefficient, $\frac{p - p_\infty}{q}$

[redacted]

c	local streamwise chord of basic wing panel, cm (in.)
c_{av}	average chord of wing panel, cm (in.)
c_n	section normal-force coefficient, $\int_{\text{Leading edge}}^{\text{Trailing edge}} \left(C_{p_l} - C_{p_u}\right) d(x/c)$
M	free-stream Mach number
p	local static pressure, N/m^2 (lb/ft^2)
p_∞	free-stream static pressure, N/m^2 (lb/ft^2)
q	free-stream dynamic pressure, N/m^2 (lb/ft^2)
x	chordwise distance rearward of leading edge, cm (in.)
y	distance perpendicular to the airplane centerline, cm (in.)
$\frac{2y}{b}$	semispan station
α	corrected airplane angle of attack, deg
δ_a	average aileron position between the inboard edge and outboard edge, positive trailing edge down, deg

Subscripts:

l	wing lower surface
te	wing trailing edge
u	wing upper surface

WING PRESSURE-SURVEY LOCATION

ROW	2y/b
1	0.133
2	.307
3	.480
4	.653
5	.809
6	.933

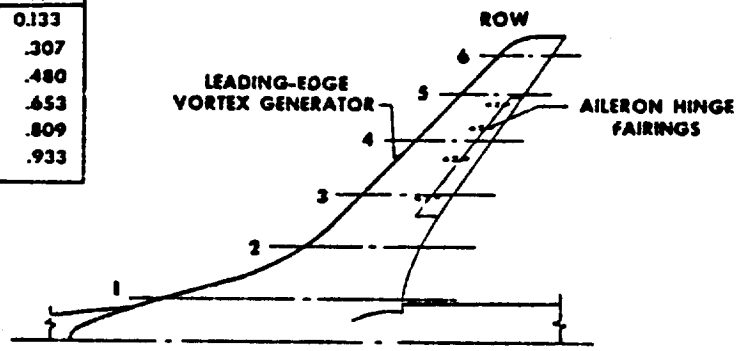

Figure 1

MODEL WING TRIP LOCATIONS

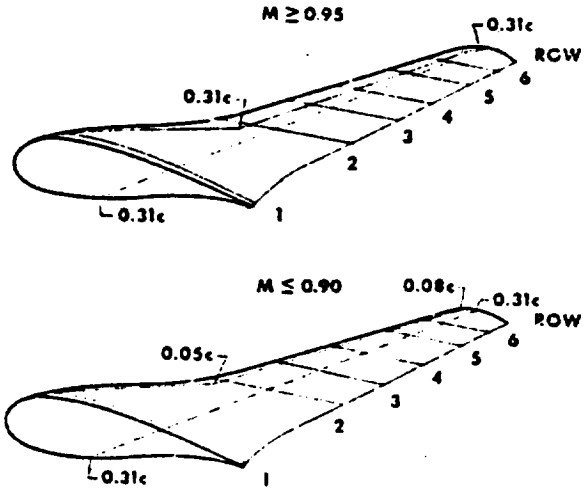

Figure 2

[redacted]

WING PRESSURE DISTRIBUTION

$M = 0.90,\ C'_{N_{wp}} = 0.30$

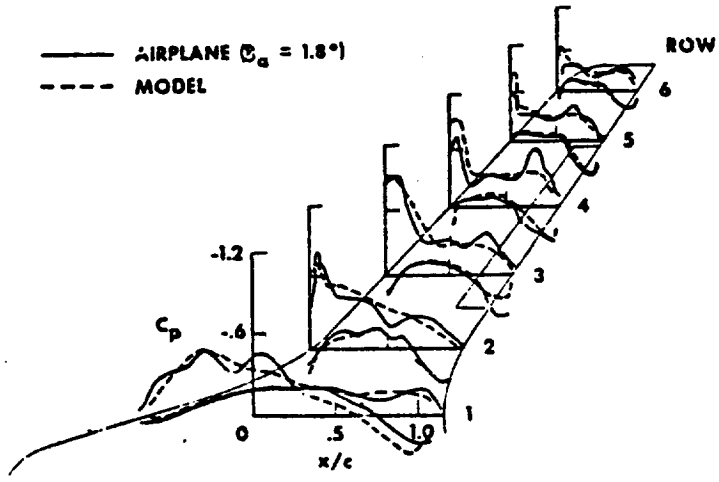

Figure 3

WING PRESSURE DISTRIBUTION

$M = 0.90,\ C'_{N_{wp}} = 0.53$

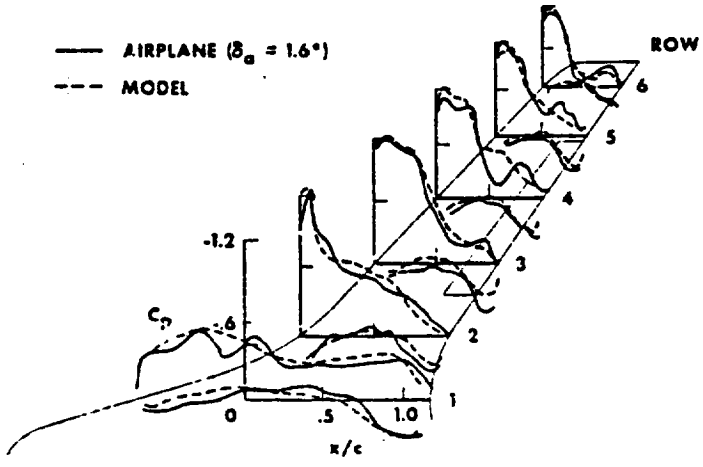

Figure 4

[redacted]

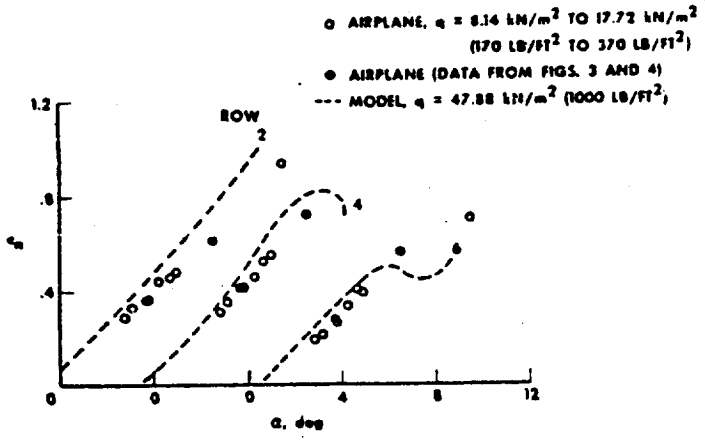

Figure 5

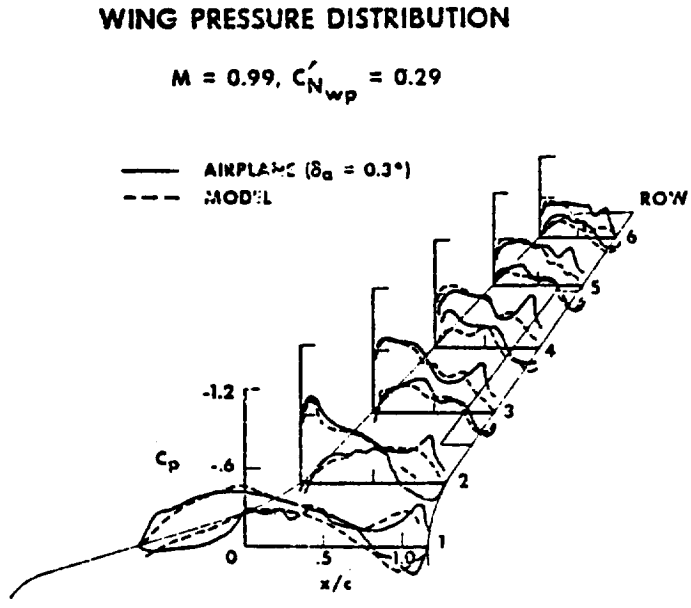

Figure 6

WING PRESSURE DISTRIBUTION

$M = 0.99,\ C'_{N_{wp}} = 0.35$

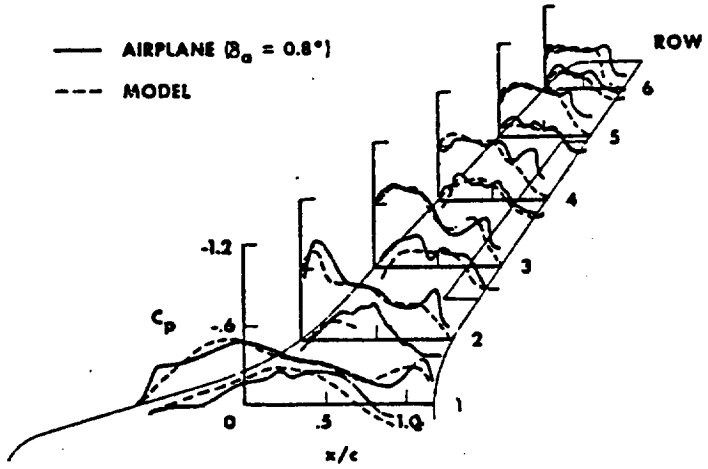

Figure 7

WING PRESSURE DISTRIBUTION

$M = 0.99,\ C'_{N_{wp}} = 0.49$

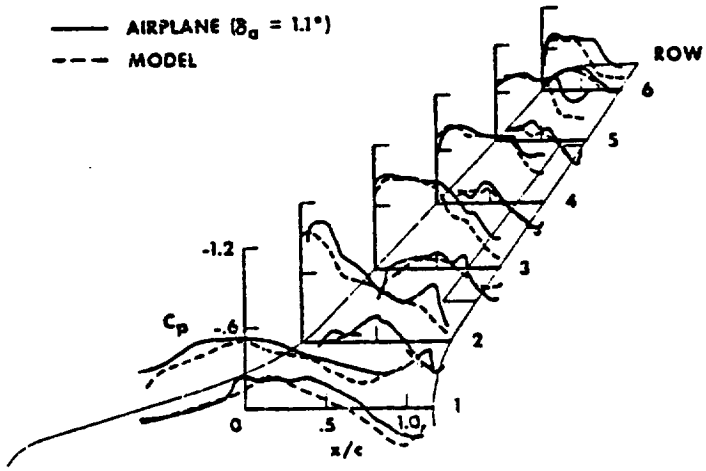

Figure 8

VARIATION OF SECTION NORMAL-FORCE COEFFICIENT
WITH ANGLE OF ATTACK

M = 0.99

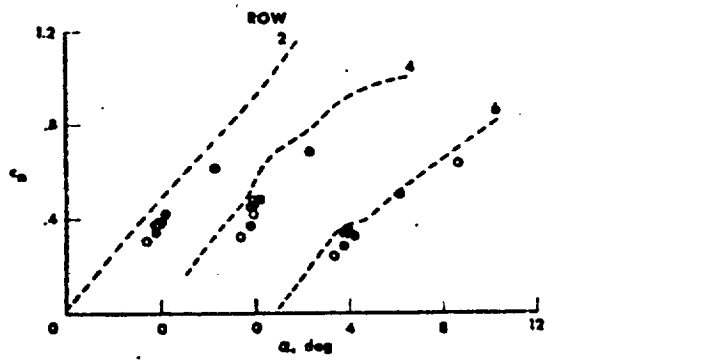

Figure 9

SHOCK LOCATION

M = 0.99, ROW 5

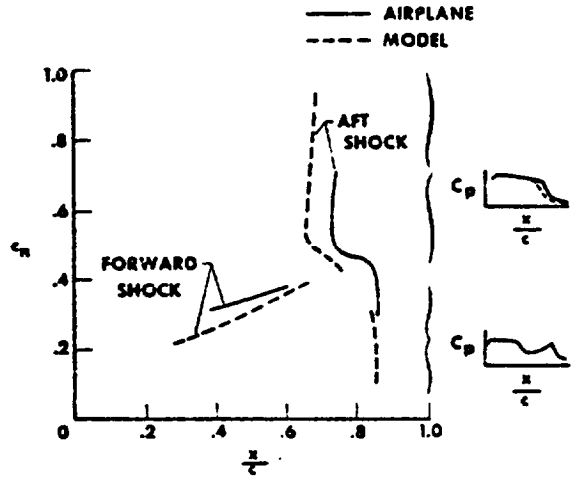

Figure 10

TRAILING-EDGE GEOMETRY AND ORIFICE LOCATIONS

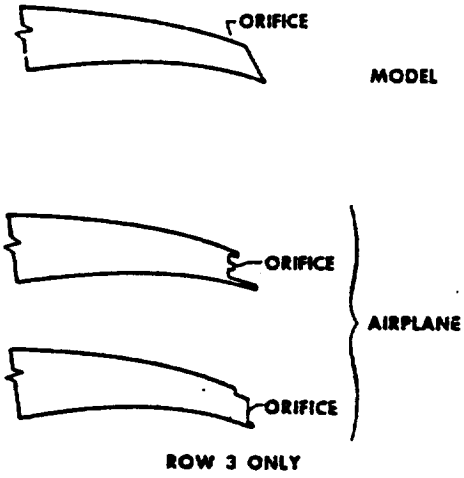

Figure 11

INBOARD WING TRAILING-EDGE PRESSURE RECOVERY

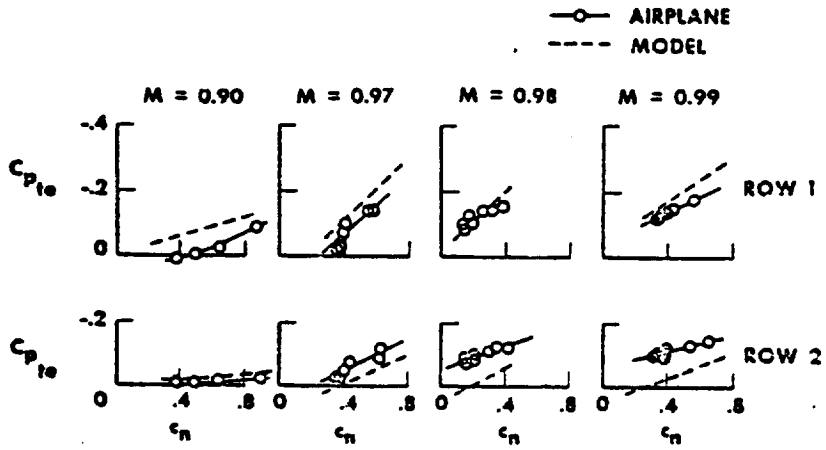

Figure 12

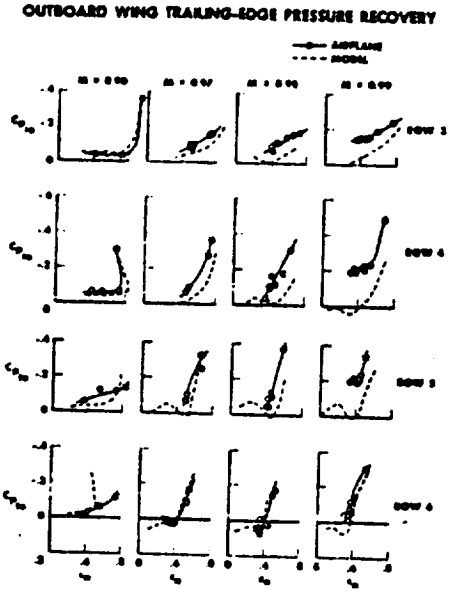

Figure 13

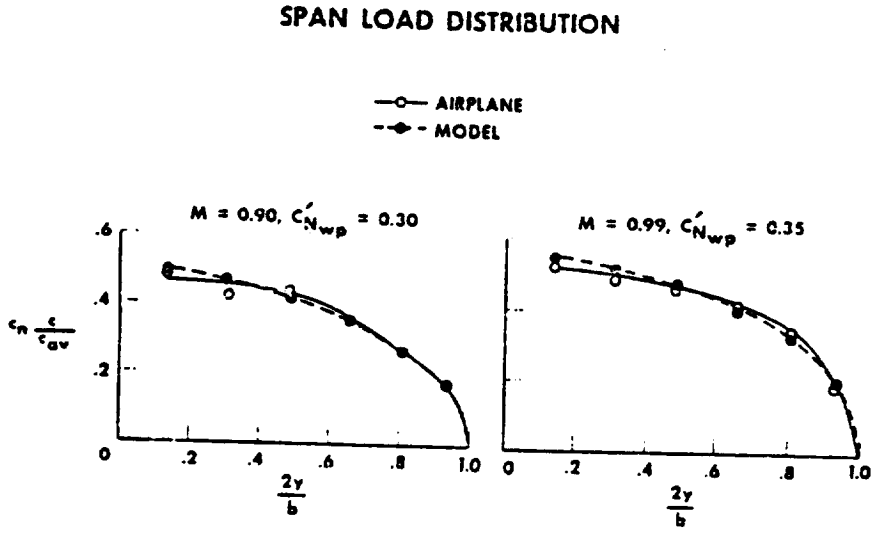

Figure 14

Preceding page blank

7. BUFFET CHARACTERISTICS OF THE F-8 SUPERCRITICAL WING AIRPLANE*

By V. Michael DeAngelis and Richard D. Banner
Flight Research Center

INTRODUCTION

Wing pressure measurements taken in flight have demonstrated the unique ability of the supercritical wing to maintain an aft shock location beyond the normal-force coefficient for flow separation. It was this feature of the upper-surface flow that held promise for improved, buffet-free flight at transonic speeds. In the F-8 supercritical wing flight program some airplane and wing structural response measurements were made to evaluate these potential improvements. This paper presents some of the preliminary results of that investigation. Wing structural response was used to sense the buffet of the wing, and these data are compared with wind-tunnel-model data and the wing flow characteristics at transonic speeds.

INSTRUMENTATION

The supercritical wing was instrumented with several different sensors, which permitted evaluation of the buffet-onset characteristics.

Figure 1 shows the type and location of the buffet instrumentation used in the study. Accelerometers were located at both wingtips, the pilot compartment, and near the center of gravity of the airplane. Strain gages were installed in the right-hand wing panel and outboard aileron segments to measure unsteady bending moments and unsteady aileron hinge moments, respectively. Pressure orifices were located in six rows on the right-hand wing panel as described in paper 6. A high-frequency pressure sensor was located on the upper surface of the right-hand wing panel at the outboard end of the aileron near the hinge line.

The pressure orifices and the strain gages used to measure wing-panel bending moment were common to both the flight vehicle and the wind-tunnel model.

DISCUSSION

Buffet Sensor Response

The flight buffet data were obtained from gradual windup-turn maneuvers. Typical time histories of the outputs of the various sensors during these maneuvers are

*Title, Unclassified.

presented in figure 2. The center-body accelerometer (near the center of gravity) has a response much like that of the cockpit accelerometer, but it is contaminated with inlet and engine noise and is, therefore, unusable. The pilot's indication of buffet onset is superimposed on the four traces. If buffet onset were selected as the point at which a definite increase in the unsteady oscillations of each signal was observable (shown by the dark arrows), the different sensors would indicate different times for buffet onset. This is to be expected, because buffet-intensity levels are a direct function of the characteristics of the structure and the location of the sensor. The responses of the sensors at the wingtip and aileron agree; the responses of the wing-panel bending moment and cockpit accelerometer also agree with one another and with the pilot's callout.

In general, the wingtip accelerometer was the most responsive, had the best resolution, and produced the most repeatable data points from flight to flight. In addition, it was believed that the wingtip response could best be related to the unsteady pressure forces which give rise to the structural buffeting. Therefore, the wingtip accelerometer was chosen as the basis for comparing and evaluating the structural buffeting characteristics of the supercritical wing.

Buffet Onset

Figure 3 shows the buffet-onset boundary based on the responses of the wingtip accelerometer for two values of dynamic pressure. The significance of this boundary is the apparent absence of a sharp drop in the buffet boundary which usually occurs between Mach numbers of 0.8 and 0.9 in conventional subsonic aircraft. When encountered during high-speed cruise, this form of buffeting is often termed Mach buffeting. The design cruise normal-force coefficient, C_{N_A}, of the supercritical wing is approximately 0.40 at Mach 0.99. It is apparent that the wing does not encounter buffeting at this value of C_{N_A} throughout the Mach range. All flight test data are presented for a center-of-gravity location at about 24 percent of the mean aerodynamic chord. If the data were obtained for the design center-of-gravity location, that is, at 35 percent of the mean aerodynamic chord, the buffet-onset curve would be raised by a normal-force coefficient of about 0.03.

The buffet-onset curve was not significantly altered by increasing the dynamic pressure from 9600 N/m^2 (200 lb/ft^2) to 19,200 N/m^2 (400 lb/ft^2).

Figure 4 shows how the buffet-onset boundary determined from the wingtip accelerometer data compares with the boundaries determined from the other sensors. As a basis for the comparison, the wingtip accelerometer data from figure 3 are faired and presented as a solid line. The symbols represent the buffet boundaries based on the aileron hinge moment, wing-panel bending moment, cockpit accelerometer output, and pilot callout. Data from the aileron hinge-moment gage agree most closely with the wingtip accelerometer data. The other three sources of data indicate a slightly higher buffet boundary than the wingtip accelerometer. The delay of buffet onset indicated by these other sensors is due generally to poor resolution and background noise. Refinements in the instrumentation and signal conditioning for these locations would be expected to provide results that agree better with the wingtip accelerometer data. In general, however, all indicators of buffet onset showed the same trends with Mach number.

Flight studies of buffeting characteristics of fighter aircraft have shown flaps to be effective in raising the buffet-onset boundary at transonic speeds. Therefore, it was of interest to examine the effects of flap deflection on the buffet boundary of the supercritical wing. Although the flaps were not designed as maneuvering flaps, the data might suggest regions where maneuvering would be improved by flap deflection. Figure 5 shows the effects of 5° of flap deflection on the supercritical wing buffet-onset boundary. At Mach 0.8 and 0.9 there is a slight gain in C_{N_A} before buffet onset, but above Mach 0.9 there is a slight loss in buffet-onset C_{N_A}. This slight loss is not unexpected, because the airfoil has already been optimized for these higher Mach numbers.

Flight and Wind-Tunnel Correlations

It is of interest to compare this flight buffet boundary with the boundary predicted from wind-tunnel data. In figure 6 a flight-determined buffet boundary is compared with two wind-tunnel-derived boundaries. The wind-tunnel buffet-onset data derived from the wing-panel bending-moment data are limited to Mach 0.9 and below. Above Mach 0.9 it was not possible to define reliable onset points. Of the six rows of pressure orifices, the three outboard rows were most sensitive to the initial flow separation and, therefore, were used to establish the trailing-edge pressure-divergence boundary. The lower bound of the I symbol indicates the initial divergence of any of the three outboard rows of trailing-edge pressures. The upper bound indicates the divergence of all three outboard rows of trailing-edge pressures.

At Mach 0.8 and 0.9, the wind-tunnel value of C_{N_A} for the upper bound of the trailing-edge pressure divergence and the bending-moment data agree fairly well with the flight data. In fact, the trends in buffet-onset C_{N_A} with Mach number are similar up to Mach 0.97. From Mach 0.97 to 0.99 the wind-tunnel data produce a boundary that drops off sharply. The difference between the two boundaries can be attributed to the fact that the wind-tunnel trailing-edge pressure divergence represents the initiation of an aerodynamic disturbance of forcing function, and that the flight-determined buffet boundary represents the initial measurable response of the wing structure to the aerodynamic disturbance.

The comparisons of the flight and wind-tunnel pressure data in paper 6 indicate that good agreement would be expected between the flight and wind-tunnel trailing-edge pressure-divergence boundaries. Therefore, it can be inferred that the trailing-edge pressure divergence from flight occurs at a lower C_{N_A} value than detected by the structural sensors.

To understand the difference between the trailing-edge pressure-divergence boundary and the initial structural-response boundary, it is necessary to examine the characteristics of supercritical flow near the cruise Mach number. Figure 7 illustrates the behavior of the flow on the outboard wing panel at Mach 0.99. The three inserts above the curve illustrate the upper-surface chordwise pressure distributions which correspond to the indicated portion of the section normal-force curve.

The section normal-force curve is characterized by two distinct linear ranges followed by the stalled region. In the initial linear range approaching the trailing-edge pressure divergence, the upper-surface pressure distribution is characterized by a shock aft of the midchord with an attached trailing-edge flow. The transition from the initial linear region to the second linear region begins with the trailing-edge pressure divergence. In this second linear region the upper-surface pressure distribution is characterized by a region of separated flow which is restricted to the area behind the shock. As the angle of attack increases in this region, the shock moves forward from about the 80-percent chord to about the 60-percent chord, thereby increasing the region of separated flow. Beyond the stall, the upper-surface flow separates over the entire chord. Without the vortex generator, the model data have shown that the section stalls at a much lower section normal-force coefficient. The flight-determined buffet-onset point is illustrated. From this figure it can be hypothesized that the shock is confining the initial separated flow region to an area sufficiently small that the structural sensors do not respond until a C_{N_A} value much larger than that for the trailing-edge pressure divergence is attained. In this Mach number range the trailing-edge pressure-divergence technique is not a good indicator of buffet onset as defined by the structural response, and, conversely, the buffet onset from structural response is not an indication of the initial flow separation. However, at the lower Mach numbers, that is, Mach 0.9 and below, the upper-surface shock does not affect the separated-flow region. Therefore the trailing-edge pressure-divergence boundary shows good agreement with the buffet boundary determined from structural sensor data.

Flow Studies

The extent of the separated flow on the wing at Mach 0.98 was determined during the flight tests from pressure data and tuft studies. Figure 8 illustrates the region of separated flow as restricted by the shock wave at approximately the condition corresponding to buffet onset as defined by the wingtip accelerometer. At the structural detection of onset, an appreciable area of separated flow exists. As shown, a high-frequency pressure sensor was installed near the shock location at the design cruise condition. This sensor was useful in studying the pressure fluctuations associated with the movement of the shock wave.

Presented in figure 9 are time histories of pressure fluctuations at Mach numbers of 0.90, 0.95, and 0.98. Corresponding C_{N_A} values are tabulated below each time history. At Mach 0.90 there is no evidence of a shock passing over the sensor with increasing values of C_{N_A}, and the buffet onset indicated by the pressure fluctuations agrees with that indicated by the wingtip accelerometer. At Mach 0.95 and a C_{N_A} of approximately 0.5, the shock passes aft of the sensor, as illustrated by the abrupt pressure drop. At a C_{N_A} of approximately 0.65, the shock begins to fluctuate behind and just over the sensor until a C_{N_A} of about 1.0 is attained when the shock begins to pass forward of the sensor. The flow behind the shock is separated, as shown by the large pressure fluctuations at C_{N_A} values of 1.2 and greater. The buffet onset defined by the wingtip accelerometer occurs slightly before the pressure sensor is excited.

The important difference at Mach 0.98 is that the shock is aft of the pressure sensor, as illustrated in figure 8. The shock approaches the sensor at a C_{N_A} of about 0.9. The onset of buffet defined by the wingtip accelerometer occurs at a C_{N_A} of 0.6, but the smoothness of the pressure-sensor data between the C_{N_A} values of 0.6 to 0.9 indicates that the shock is restricting the propagation of the separated flow region.

Buffet Intensity

In addition to the effect of the shock on the flow separation, the shock was found to also affect the intensity rise of the structural buffet response. Figure 10 presents the buffet-intensity data from the wingtip accelerometer as a function of the airplane normal-force coefficient. Data are presented for four Mach numbers. At Mach 0.90, where the shock is not prevalent, the intensity rises rapidly immediately after buffet onset. At Mach 0.95 the rate of intensity rise is lower just after buffet onset, becoming more pronounced at Mach 0.98. This moderate rate of intensity rise is encountered when the separated flow is restricted to the region behind the shock. The greater rate of intensity rise is encountered at higher C_{N_A} values when the entire outer wing panel begins to stall. Little flight data were obtained at Mach 1.1, but the wind-tunnel data indicate that the shock moved to the trailing edge. The flight test data obtained at a Mach number of 1.12 are presented for general interest. Little pressure data are available at this Mach number; therefore, no assessment of the effects of the shock can be made, but the buffet intensity rise does increase slowly immediately after onset.

Although the general effect of the shock on the intensity rise is shown in figure 10, one of the primary benefits of the supercritical wing on buffet is not readily apparent. To better illustrate this effect, the Mach 0.90 and 0.98 data are compared in figure 11. Although the buffet onset C_{N_A} value at Mach 0.98 is less than the C_{N_A} value at Mach 0.90, the intensity rise is much more gradual so that the intensity levels are considerably lower at higher values of C_{N_A}. Thus low intensity buffet maneuvering appears to be practical at transonic speeds.

CONCLUDING REMARKS

The buffet characteristics of the supercritical wing have been investigated by using various structural sensors and sensor locations. The wingtip accelerometer was found to provide the most accurate measurements of the structural response of the airplane.

The buffet-onset boundary from flight showed a high value of airplane normal-force coefficient, C_{N_A}, throughout the Mach range without the sharp drop which generally occurs in the higher transonic speeds.

Small deflections of the trailing-edge flaps produced moderate improvements in the buffet boundary at Mach 0.90 and below, but produced a slightly degrading effect at the higher transonic Mach numbers.

[redacted]

At Mach 0.90 and below, the wind-tunnel trailing-edge pressure-divergence boundary is in agreement with the flight-determined buffet boundary. Above Mach 0.90 the wind-tunnel data produced a considerably lower boundary, which suggests that for the supercritical wing the trailing-edge pressure divergence is not a valid indication of buffet onset as measured by structural-response sensors.

The unique flow characteristics of the supercritical wing at the higher transonic Mach numbers suggest that a maneuvering aircraft might attain high values of C_{N_A} with relatively low buffet-intensity levels.

SYMBOLS

a_n	normal acceleration, g units
Δa_n	filtered normal acceleration (high-pass filter), g units
C_{N_A}	airplane normal-force coefficient
c_n	section normal-force coefficient
c_p	pressure coefficient
g	acceleration due to gravity, m/sec^2 (ft/sec^2)
M	Mach number
Δp	difference between local static pressure and free-stream static pressure
q	free-stream dynamic pressure, N/m^2 (lb/ft^2)
x/c	chordwise distance normalized to local chord length
α	airplane angle of attack, deg
σ_{a_n}	root mean square of normal acceleration g units

[redacted]

BUFFET INSTRUMENTATION

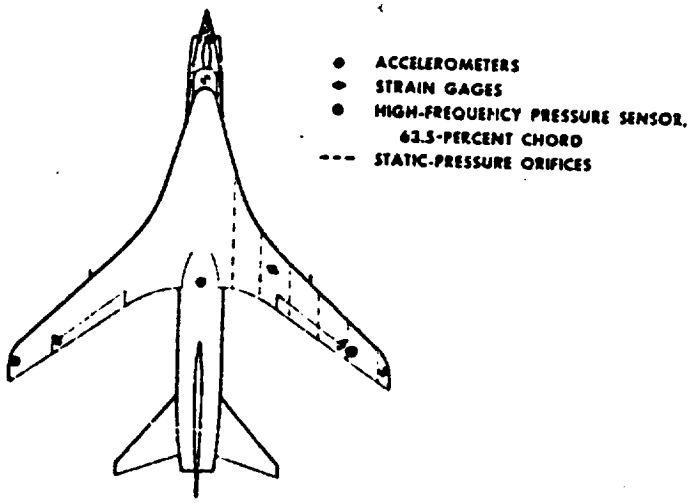

Figure 1

RESPONSE OF SENSORS DURING BUFFET

M = 0.95

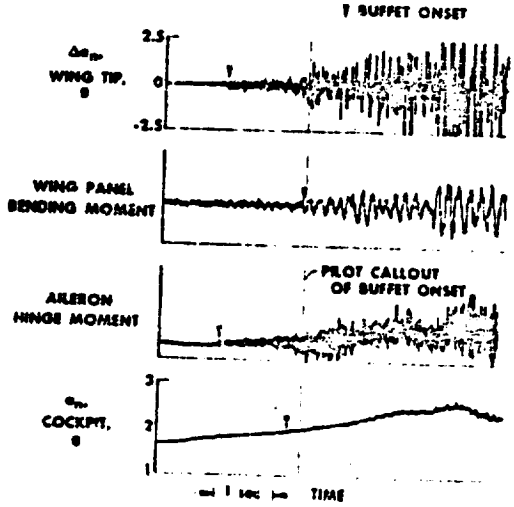

Figure 2

BUFFET-ONSET BOUNDARY

RIGHT-HAND WING-TIP ACCELEROMETER

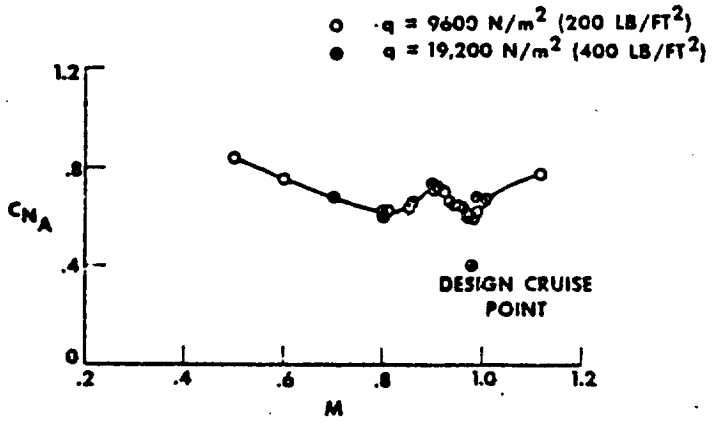

Figure 3

BUFFET-ONSET COMPARISONS FROM VARIOUS SENSORS

q = 9600 N/m² (200 LB/FT²)

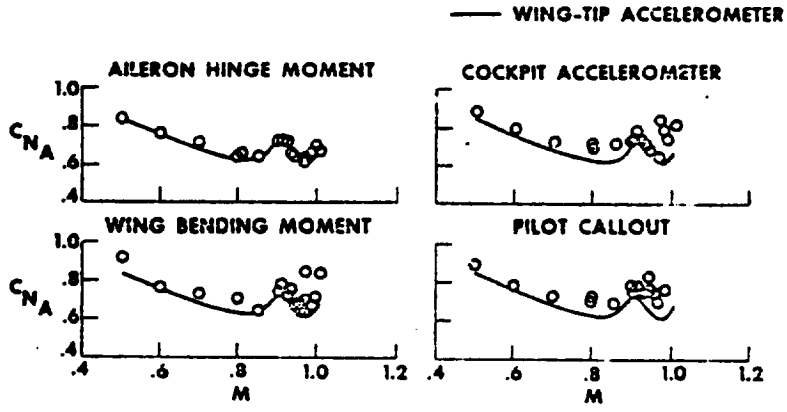

Figure 4

EFFECT OF FLAPS ON BUFFET-ONSET BOUNDARY

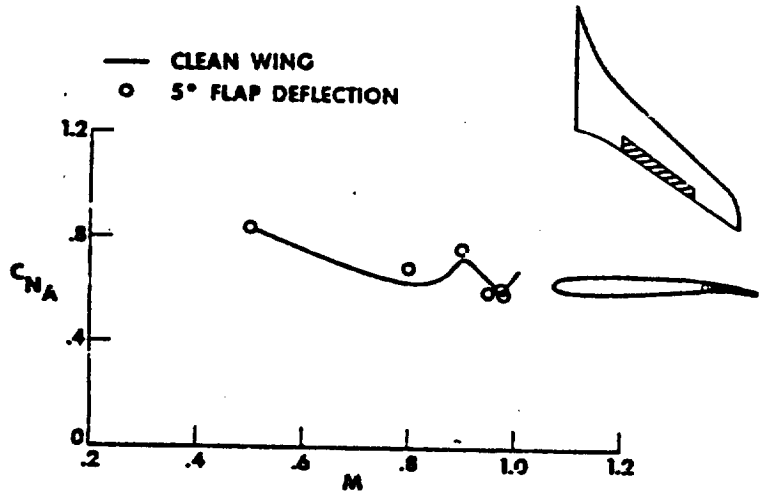

Figure 5

BUFFET BOUNDARY COMPARISONS

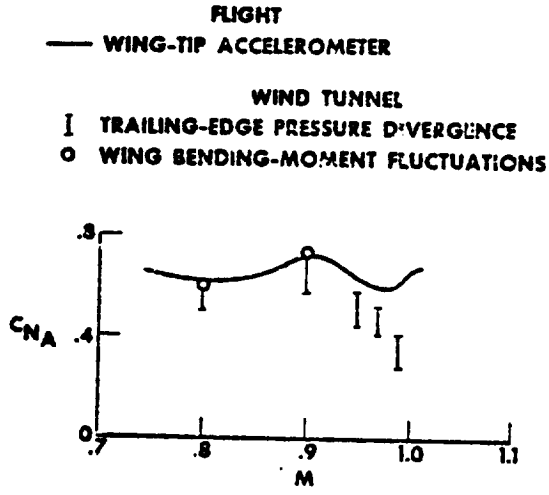

Figure 6

EFFECT OF FLOW ON OUTBOARD WING-PANEL CHARACTERISTICS

M = 0.99

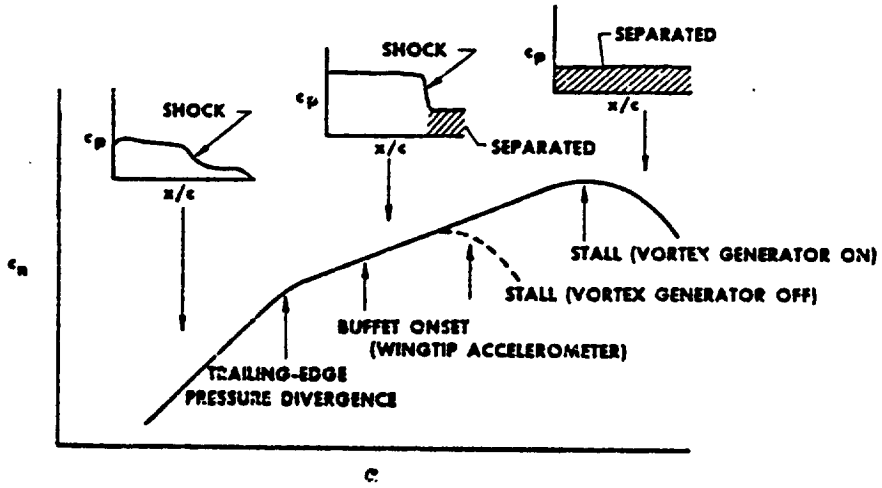

Figure 7

REGION OF SEPARATED FLOW AT BUFFET ONSET

FLIGHT DATA AT M = 0.98

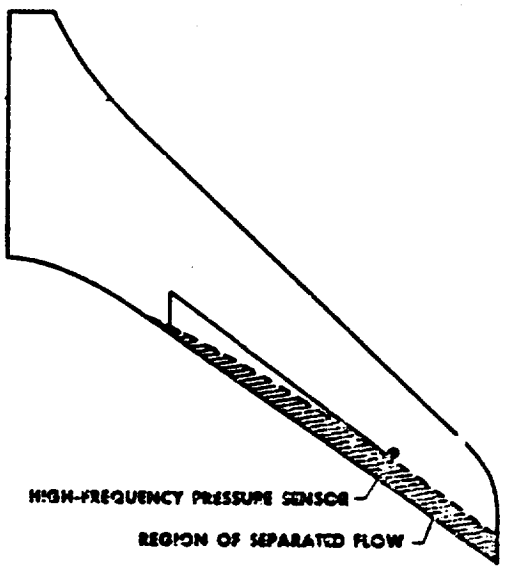

Figure 8

RESPONSE OF HIGH-FREQUENCY PRESSURE SENSOR

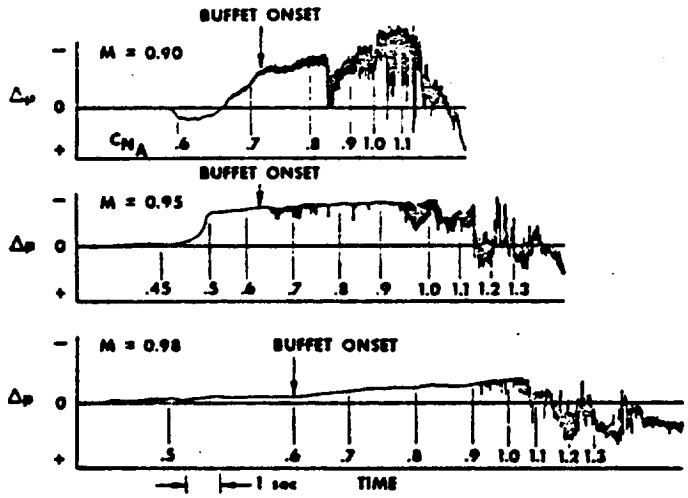

Figure 9

BUFFET INTENSITY CHARACTERISTICS
(ZERO POSITIONS SHIFTED FOR CLARITY)

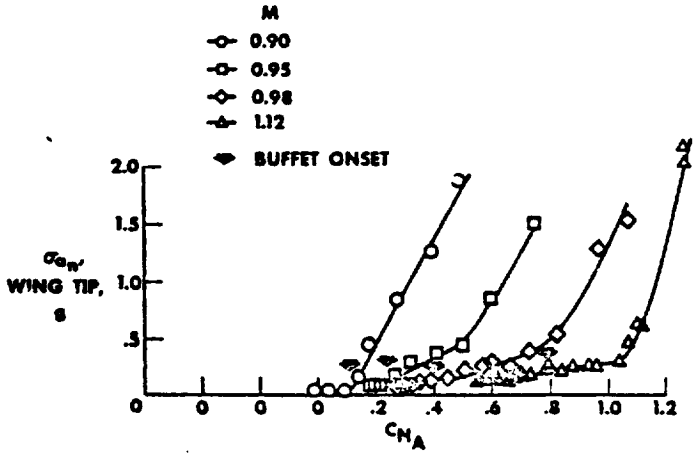

Figure 10

BUFFET INTENSITY COMPARISON

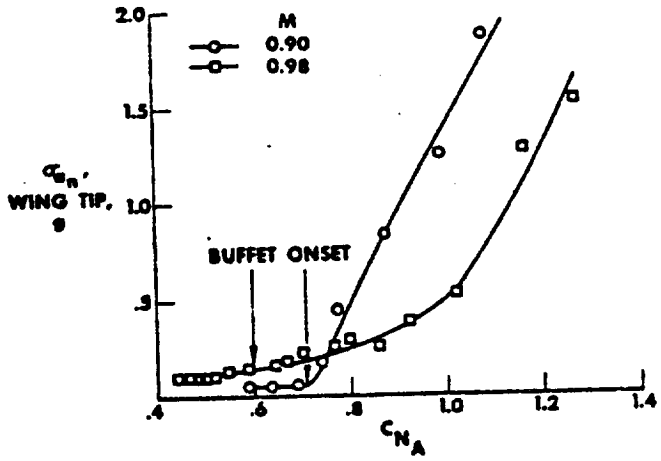

Figure 11

D8

[redacted]

X72-10204

8. PILOTING AND OPERATIONAL ASPECTS OF THE F-8 SUPERCRITICAL WING AIRPLANE*

By Thomas C. McMurtry, Neil W. Matheny, and Donald H. Gatlin
Flight Research Center

INTRODUCTION

One may well ask if a transport equipped with a supercritical wing can be flown routinely near Mach 1. Are there any unusual or unexpected characteristics that may introduce new operating problems? Although the F-8 supercritical wing test vehicle is not fully representative of a transport aircraft, it can provide some insight into the answers to these questions. The flight tests, therefore, have been patterned generally along the lines of typical transport operations, although consideration has also been given to the usefulness of the concept for other types of missions.

The range of altitudes and Mach numbers investigated covers present-day transport operating areas and includes the design cruise region near Mach ' as well as the design limit of Mach 1.2, as shown in figure 1. Within the test envelope, the vehicle trim and maneuvering characteristics, overspeed behavior, and overall stability and controllability have been evaluated, with particular emphasis on the transonic range. This paper considers both the overall handling characteristics of the test vehicle and the correlation of flight data with wind-tunnel results (refs. 1 and 2).

It should be pointed out that the basic intent of the program is to validate the wing concept and design approach. An effort was made to achieve acceptable handling qualities; however, time and cost constraints made it impossible to optimize them.

Although the test vehicle does not seem to be typical of a transport aircraft, because of its size and the location of the engine and wing (fig. 2), the wing and glove geometry, except for size, are nearly identical to those of proposed transport configurations. The ratios of aerodynamic and inertial moments are nearly the same as those of current transports except in the roll axis, where roll control power is high. Therefore, the vehicle response and handling characteristics in flight should provide some insight into the behavior of future transports designed around the supercritical wing concept.

PILOT COMMENTS

The first takeoff of the test vehicle was made from the dry lakebed at Edwards Air Force Base. The ground roll for nonafterburner takeoffs is approximately 2000 meters (6500 feet) and lift-off airspeed is 165 knots. All takeoffs are now made from the main

*Title, Unclassified.

[redacted]

runway. High takeoff and landing airspeeds are required because of the limited tailpipe clearance as well as the fixed incidence angle of the wing and the lack of high-lift devices. The only high-lift device provided is aileron droop. The handling qualities of the airplane during the takeoff and climbout are satisfactory in all respects.

In cruising flight the airplane has good stability and responds nicely to control inputs. Simulated collision-avoidance maneuvers have been performed with no adverse handling qualities noted. Maneuvers such as aileron doublets, rudder doublets, stabilizer pulses, wings-level sideslips, and windup turns have been made to obtain data for stability and control analysis. In simulated overspeed maneuvers performed near the design cruise condition, the control of the airplane was satisfactory in all respects.

An approach to a stall has been made up to an angle of attack of 17° (approximately 145 KIAS). The airplane was in the landing configuration. The approach was broken off when lateral response became poor. Light buffet was encountered during the maneuver. Control response was good up to an angle of attack of 17°.

The landing approach is made at approximately 8° angle of attack (170 KIAS). During the approach the ailerons are drooped 20° for a high-lift effect. The handling qualities are good during the landing approach. All landings are made on the dry lakebed because of the high approach airspeeds and the lack of deceleration devices. The high approach airspeed has not posed any problems other than requiring a longer runway.

The airplane generally displays conventional handling qualities throughout its operating envelope.

A simulator was used to prepare for the flight program using wind-tunnel-derived aerodynamic characteristics. It was fixed base and had limited cockpit features, but it did provide the pilot with an adequate representation of the aircraft response to control inputs and the control activity required to perform the various flight-test maneuvers. The flight characteristics agreed well with the simulated characteristics.

The airplane has an irreversible flight control system which includes stability augmentation. The use of an irreversible flight control system is not unique; at least two current transports have similar systems with no manual reversion. A command augmentation system incorporating blended pitch rate and normal acceleration feedback (C* system) was used in the pitch axis. It was required to compensate for reduced longitudinal stability at advanced load factors. The roll and yaw augmentation systems are similar to those of the basic F-8 airplane.

The test airplane has been flown at some trim conditions without stability augmentation and still has acceptable handling qualities.

LONGITUDINAL RESPONSE

In considering the vehicle response to longitudinal control inputs, it is convenient to refer to the current Military Specification (ref. 3) requirement for transport aircraft as shown in figure 3. This specification calls for a combination of short-period frequency and normal acceleration per unit angle of attack to be within the bounds for level 1 operations. Level 1 refers to "up and away" flight with all systems functioning. Levels 2

and 3 pertain to partial systems failures which increase the pilot's workload and, at level 3, lead to mission termination. The flight data represent the unaugmented airplane for the transonic range and are about midway between the level 1 bounds. The pilots considered the longitudinal response to be satisfactory. Also, the flight data are in good agreement with predictions based on wind-tunnel tests. The Military Specification also calls for certain damping levels. The augmented airplane meets the damping criteria; however, with augmentation off, the damping falls short of the minimum requirement, and the airplane is lightly damped and tends to overshoot.

The two principal longitudinal stability derivatives—C_{m_α} and $C_{m_q} + C_{m_{\dot{\alpha}}}$—with corresponding wind-tunnel data in the transonic range are shown in figure 4. The flight values of the derivatives were determined by a digital computer technique for matching time histories of the aircraft responses (ref. 4). The flight data for C_{m_α} show a generally higher trend than predicted from wind-tunnel data. The differences, however, do not cause significant increases in the frequency levels shown in figure 3. The damping derivatives from flight agree well with the wind-tunnel estimates, except in the range from Mach 0.9 to 1.0. In either instance the differences are minor and not apparent to the pilot.

TRANSONIC TRIM VARIATION

Trim variation during transonic accelerations is another area of interest to the transport pilot. In the past, tucking at high subsonic Mach numbers required compensation in one form or another. The supercritical wing vehicle, however, shows no noticeable tuck. Figure 5 illustrates the variation of stabilizer angle for trim with Mach number for a level acceleration-deceleration maneuver performed at 13,700 meters (45,000 feet) altitude. A tuck was predicted between Mach 0.99 and 1.02. The flight data show, however, that nearly neutral speed stability exists between Mach 0.9 and 1.05. The stick-force variation is not shown because the pitch augmentation system provides apparent neutral speed stability for all conditions. Below Mach 1.0, the trim angle requirement in flight is slightly greater than predicted from model tests. Part of the discrepancy can be attributed to the higher trend of the flight values for C_{m_α} noted in figure 4. In addition, some of the discrepancy is believed to be due to differences in zero-lift pitching moment, C_{m_o}. Figure 6 compares the flight values for C_{m_o} with those obtained from wind-tunnel measurements. The flight values were estimated from measurements of aerodynamic-center location and stabilizer effectiveness. Below Mach 0.95 the comparison indicates a considerable difference in zero-lift pitching moments, with the flight data showing a larger nose-down moment. A contributing factor to this difference is the more negative pressure measured along the wing trailing edge, as noted in paper 5.

TRANSONIC MANEUVERING CHARACTERISTICS

The maneuverability of the test airplane is satisfactory in the transonic range, particularly at the design cruise Mach number. The principal factors that affect

maneuverability are shown in figure 7. The upper boundary shows the highest normal-force coefficients obtained in flight so far. The vehicle exhibits a pitchup that occurs well above normal transport operating conditions and is in fair agreement with the wind-tunnel predictions. The sharp rise in this boundary above Mach 0.9 is attributed to a rearward shift of the wing shock wave to the vicinity of the trailing edge. This shock is stabilized at the aft location and acts as a barrier to forward spreading of flow separation. This delays the occurrence of large lift losses on the outboard wing sections at high angles of attack. Buffet onset also occurs well above the normal operating conditions.

The basic parameters relating to longitudinal maneuverability are shown in figure 8, a comparison of flight and predicted normal-force and pitching-moment characteristics for a fixed stabilizer position at a Mach number of 0.95. The flight results were obtained from known stabilizer effectiveness and measurements of stabilizer angle during a gradual windup turn. The trends of the flight and wind-tunnel results are similar. In particular, the normal-force curves agree well. The pitching moments from flight, however, show slightly higher stability and, as noted in figure 6, more negative values. A decrease in stability is indicated in the flight data at approximately 7° angle of attack. This is followed by an abrupt pitchup at about 11° angle of attack. The wind-tunnel data also exhibit a nose-up tendency at about 7° angle of attack and an abrupt pitchup near 13° angle of attack. Buffet onset is generally observed in flight at the first break in the pitch curve. These variations in stability are masked by the pitch command augmentation system.

UPSET-OVERSPEED BEHAVIOR

Another factor of concern to the transport pilot is the controllability of the aircraft in an upset or overspeed condition. Several upset maneuvers have been performed with the test vehicle starting from wings-level and banked attitudes near the design cruise speed. A time history of the most severe maneuver, with the aircraft banked approximately 45°, is shown in figure 9. An upset was initiated by pushing over to near 0 g, holding for about 5 seconds with fixed throttle, and then recovering with a 1.5g to 2.0g pullup.

Figure 10 shows the altitude and Mach number excursions resulting from three different upset maneuvers performed with the stability augmentation system on. Two of the maneuvers were started from level flight at approximately Mach 0.97, one from approximately 14,000 meters (46,000 feet), and the other from 15,000 meters (49,000 feet) altitude. The maneuver starting at 15,000 meters (49,000 feet) was held at 0.5g for 10 seconds before recovery was initiated; the others were held for only 5 seconds. Because of the further increase in drag beyond the cruise point, neither of the excursions from level flight extended much beyond the sonic speed. The banked maneuver was performed to exceed Mach 1, but was no more difficult to control.

The recovery in each maneuver was easy to perform, and the aircraft response was normal in all respects. Control power was adequate, and there were no tendencies for wing drop or control reversal. The airplane has been accelerated to a supersonic condition many times and has handled nicely. When the drag rise was encountered in flight, the indications to the pilot seemed to be the same as those in any other airplane; that is, the airplane just stopped accelerating. This was not an abrupt change, but it

was an obvious one.

LATERAL CONTROL POWER

As pointed out earlier, roll control is provided by conventional midspan ailerons. These surfaces have dimensions of approximately 25 percent of the wing chord by 40 percent of the wing semispan and were sized to permit landings in strong crosswinds. They are about double the relative sizes of the ailerons on the 707 airplane. However, most current transports also have spoilers in addition to ailerons for lateral control. The roll capability of the test vehicle is shown in figure 11, a plot of maximum available control power as a function of roll time constant. The boundaries apply to transport aircraft and were determined by using the Flight Research Center variable-stability JetStar airplane (ref. 5). The flight data are in generally good agreement with predictions based on wind-tunnel tests, although both the flight and predicted control power are greater than the satisfactory range indicated for transport aircraft. This higher trend is considered to be satisfactory for experimental flight purposes.

Figure 12 presents the variation of the two principal roll-response derivatives in the transonic range. The aileron effectiveness and damping-in-roll derivatives obtained from flight tests and faired wind-tunnel data are shown as functions of Mach number. The roll power is proportional to aileron effectiveness, $C_{l_{\delta_a}}$, which is higher in flight than predicted from wind-tunnel tests at Mach numbers below about 0.95. The damping derivative, C_{l_p}, also shows a slightly higher trend than predicted. These differences are not apparent in the comparisons of roll power shown in figure 11.

LATERAL-DIRECTIONAL COUPLING

Good roll response also requires minimum coupling between the roll and yaw axes. In figure 13 flight data are compared with predicted roll response in terms of ω_φ, which contains the yaw-due-to-aileron derivative, a principal contributor to roll-yaw coupling, and ω_d, the Dutch roll frequency. When ω_φ is equal to ω_d, a pure roll response is obtained. High ratios of ω_φ to ω_d lead to a pilot-induced oscillation (PIO) tendency, whereas low ratios result in sluggish roll response. The flight and predicted responses are again in good agreement and are in a region considered to be satisfactory. These trends are consistent with the pilots' evaluations of the roll performance as excellent at transonic speeds.

The agreement between flight and predicted roll-yaw coupling is reflected in the comparisons of the dihedral-effect derivative, C_{l_β}, and yaw-due-to-aileron derivative, $C_{n_{\delta_a}}$, shown in figure 14. The dihedral effect from flight is slightly higher than the wind-tunnel result. The value of the yaw-due-to-aileron derivative is small and shows a more adverse trend than predicted. The differences, however, are not sufficient to produce an unsatisfactory roll response. Therefore, an interconnect between the aileron

and rudder to reduce roll-induced yaw was not needed in the cruise region.

CONCLUDING REMARKS

The F-8 supercritical wing program has indicated that the piloting tasks and procedures at cruise speeds in the vicinity of Mach 1 should be no less routine than in present-day transport operations. Some differences do exist between flight and wind-tunnel measurements of the stability and control characteristics; however, the handling qualities were predicted well. No unexpected or violent control characteristics have been encountered.

This brief assessment of the stability and control characteristics of the F-8 supercritical wing test vehicle can perhaps be summarized in one overall observation: The introduction of the supercritical wing is not expected to create any serious problems in day-to-day transport operations.

REFERENCES

1. Harris, Charles D.; and Bartlett, Dennis W.: Wind-Tunnel Investigation of Effects of Underwing Leading-Edge Vortex Generators on a Supercritical-Wing Research Airplane Configuration. NASA TM X-2471, 1972.

2. Bartlett, Dennis W.; and Re, Richard J.: Wind-Tunnel Investigation of Basic Aerodynamic Characteristics of a Supercritical-Wing Research Airplane Configuration. NASA TM X-2470, 1972.

3. Anon.: Flying Qualities of Piloted Airplanes. Mil. Spec. MIL-F-8735B(ASG), Aug. 7, 1969.

4. Iliff, Kenneth W.; and Taylor, Lawrence W., Jr.: Determination of Stability Derivatives From Flight Data Using a Newton-Raphson Minimization Technique. NASA TN D-6579, 1971.

5. Holleman, Euclid C.: Flight Investigation of the Roll Requirements for Transport Airplanes in Cruising Flight. NASA TN D-5957, 1970.

SYMBOLS

a_n	normal acceleration at the center of gravity, g
C_{l_p}	damping-in-roll derivative, rad^{-1}
C_{l_β}	effective dihedral derivative, deg^{-1}

$C_{l_{\delta_a}}$	rolling-moment coefficient per degree of aileron deflection, deg^{-1}
C_m	pitching-moment coefficient
$C_{m_q} + C_{m_\alpha}$	effective damping-in-pitch derivative, rad^{-1}
C_{m_o}	pitching-moment coefficient at zero lift and $\delta_h = 0$
C_{m_α}	pitch stability derivative, deg^{-1}
C_N	normal-force coefficient
$C_{n_{\delta_a}}$	yawing-moment coefficient per degree of aileron deflection, deg^{-1}
h_p	pressure altitude, m (ft)
$L_{\delta_a}\delta_{a_{max}}$	maximum rolling acceleration due to aileron deflection, sec^{-2}
M	Mach number
n/α	normal acceleration per unit angle of attack, g/rad
q	dynamic pressure, kN/m^2 (lb/ft^2)
α	angle of attack, deg
γ	flight-path angle, deg
δ_a	aileron deflection, deg
δ_h	horizontal-stabilizer deflection, deg
τ_r	roll-mode time constant, sec
φ	bank angle, deg
ω_d	Dutch roll natural frequency, sec^{-1}
$\omega_{n_{sp}}$	natural frequency of the longitudinal short-period oscillation, sec^{-1}
ω_φ	frequency of the numerator of the φ/δ_a transfer function, sec^{-1}

[redacted]

FLIGHT TEST ENVELOPE

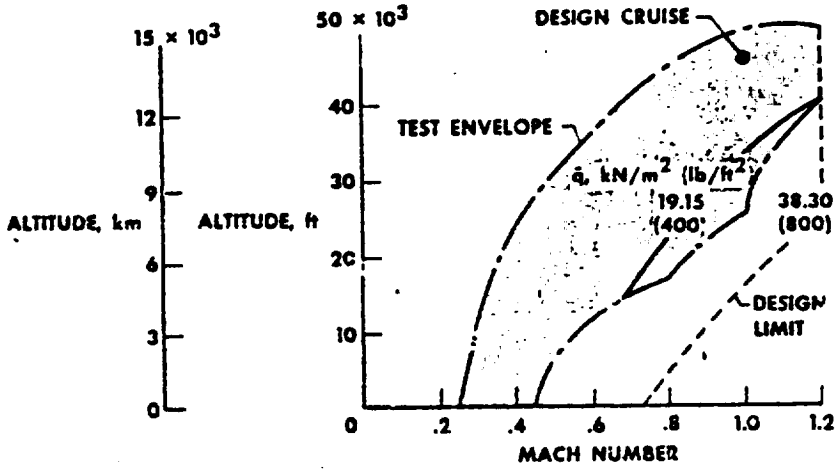

Figure 1

F-8 SUPERCRITICAL WING TEST-BED AIRPLANE

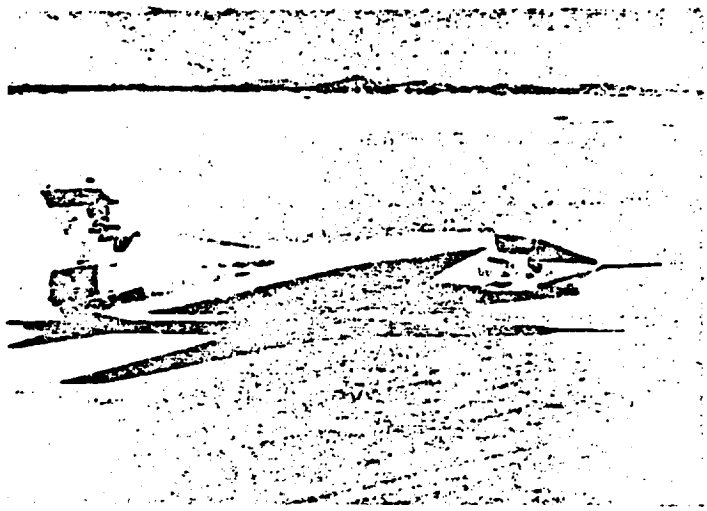

Figure 2

[redacted]

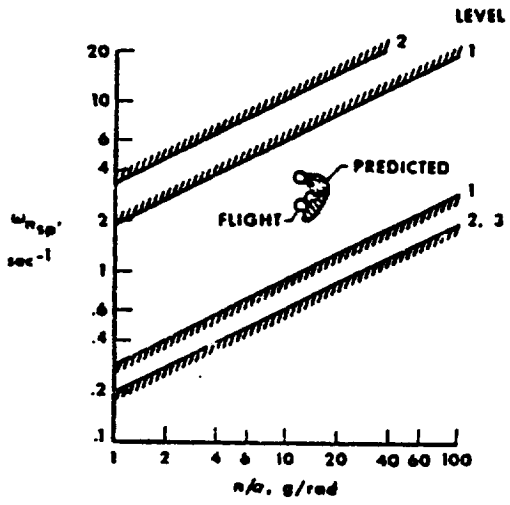

Figure 3

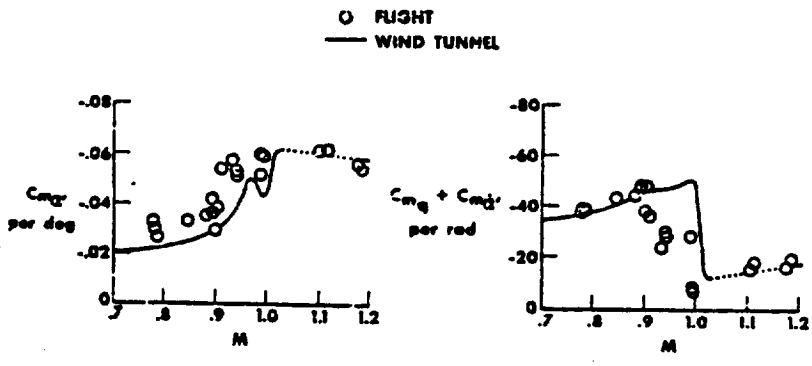

Figure 4

TRANSONIC TRIM VARIATION

h_p = 13,700 METERS (45,000 FEET), C.G. = 22 PERCENT

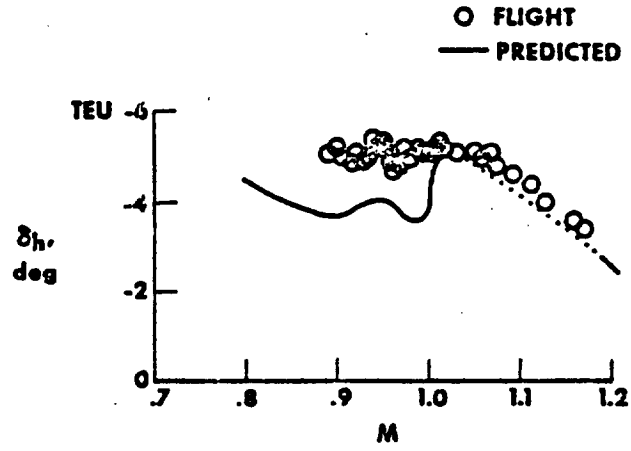

Figure 5

ZERO-LIFT PITCHING MOMENT

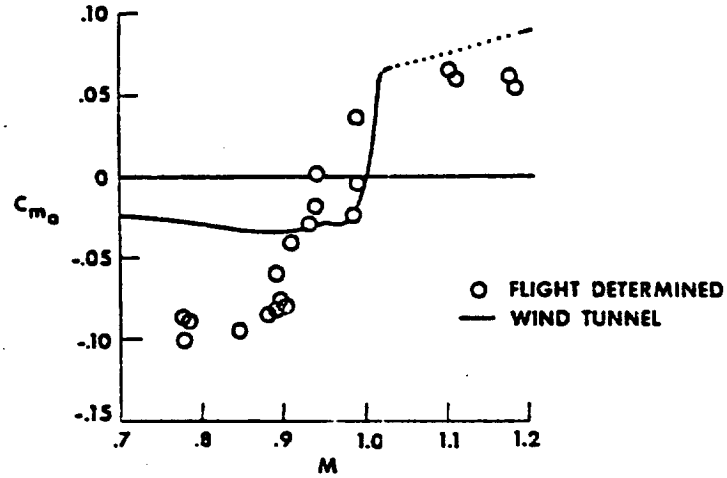

Figure 6

MANEUVERING CHARACTERISTICS

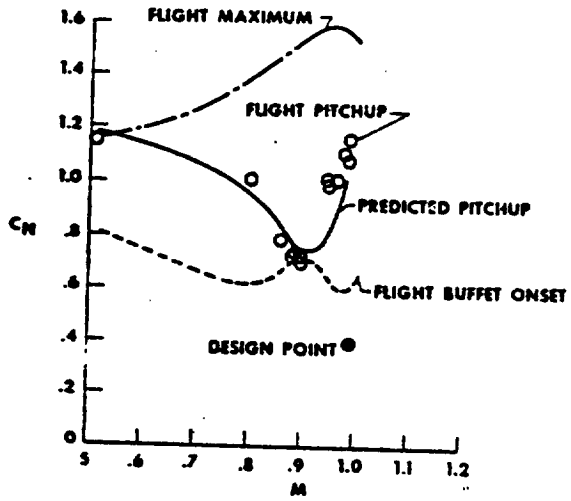

Figure 7

LONGITUDINAL CHARACTERISTICS

M = 0.95, δ_h = −2.5°, C.G. = 25 PERCENT

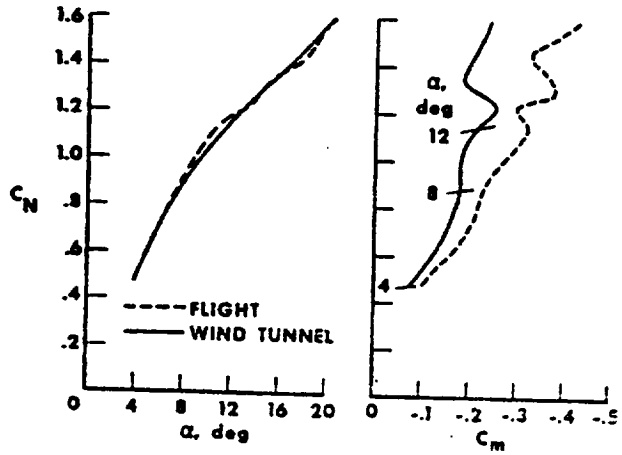

Figure 8

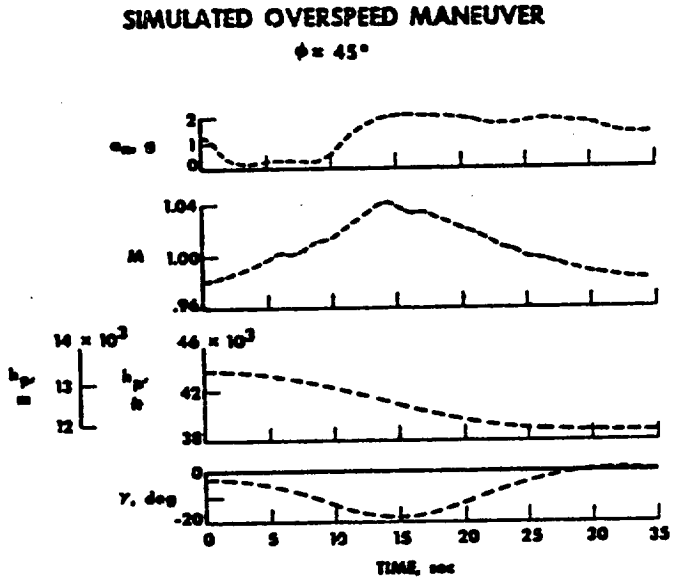

Figure 9

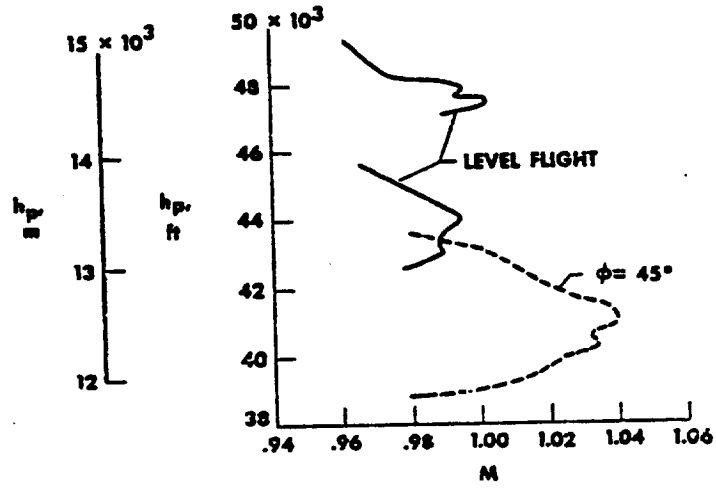

Figure 10

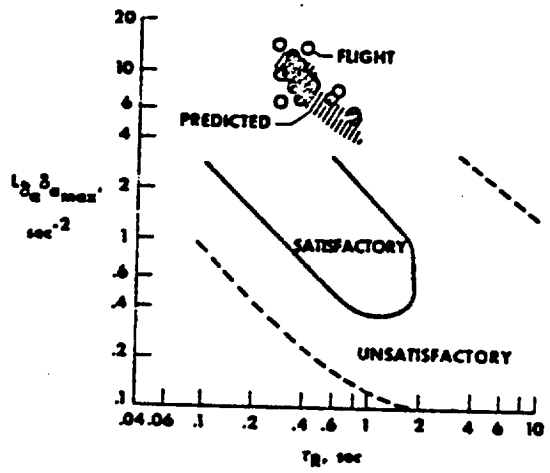

Figure 11

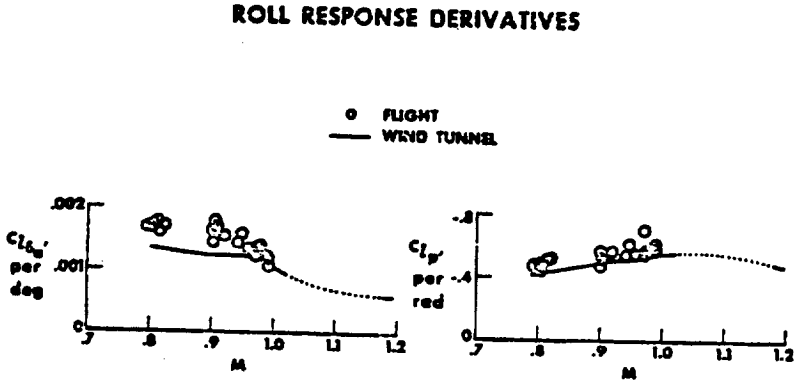

Figure 12

[redacted]

LATERAL-DIRECTIONAL COUPLING

M = 0.8 TO 1.0

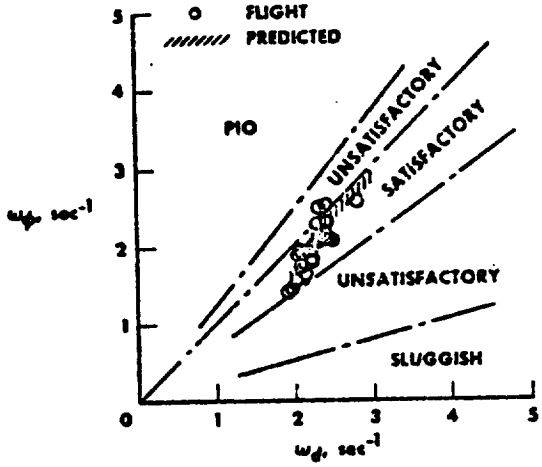

Figure 13

LATERAL-DIRECTIONAL DERIVATIVES

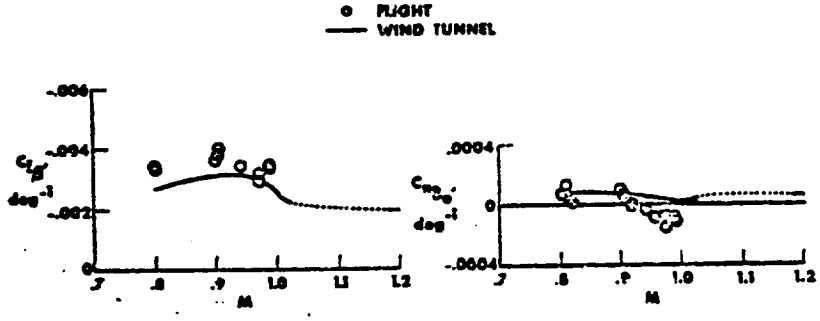

Figure 14

D9

[redacted] X72-10205

9. COMMENTS ON WIND-TUNNEL—FLIGHT CORRELATIONS FOR THE F-8 SUPERCRITICAL WING CONFIGURATION*

By Richard T. Whitcomb
Langley Research Center

INTRODUCTION

As the results presented in the previous papers have indicated, the flight programs to this point have demonstrated the essential practicality of the supercritical wing concept and, generally, have shown good agreement between the wind-tunnel and flight results over the flight envelope. However, several obvious differences between the flight and wind-tunnel pitching moment, drag polars, drag rise, and pressure distribution results for the F-8 program require some further analysis and discussion. The primary differences can probably be attributed to Reynolds number effects and wind-tunnel-wall interference. The wall interference particularly influences the transonic drag rise.

EFFECT OF REYNOLDS NUMBER

For this brief discussion of Reynolds number effect a figure from paper 6 for a Mach number of 0.90 is repeated as figure 1. As noted previously, the loadings on the aft regions of the sections are greater in flight than in the wind tunnel. The aileron deflection of 1.8° in flight contributes to these differences in the region of the aileron. However, analysis of more recent flight data for various aileron angles indicates that the effect of an aileron deflection of this magnitude is secondary. Apparently, the effective aft camber is greater in flight than in the wind tunnel. This effect may cause, at least in part, the more negative pitching moments at this Mach number noted in paper 8 and the relative rotation of the drag polars shown in paper 5. This difference in camber may be associated with the influence of Reynolds number on the strong boundary-layer effects for supercritical airfoils discussed in paper 1. As noted in papers 3 and 6, the technique used during the wind-tunnel tests to attempt to simulate full-scale Reynolds numbers was not practical for lower speed conditions such as those of the present case. The wing-wake surveys planned for the wind-tunnel model and the airplane in flight should help greatly in clarifying the Reynolds number effect.

EFFECT OF TUNNEL WALL ON DRAG RISE NEAR MACH 1.0

To more clearly define the drag rise, the drag results presented in paper 5 were

*Title, Unclassified.

[redacted] Downgraded at 3 year intervals; declassified after 12 years

reduced to incremental form by subtracting the drag coefficients measured at a Mach number of 0.90 and are shown with a significantly expanded scale in figure 2. To eliminate the effect of the tail angle in the comparison, the wind-tunnel results presented are for the same tail angles as those required for trim in flight. As noted in paper 5, at Mach numbers near 1.0 the drag rise for the 1/11.5-scale model in the Langley 8-foot tunnel is less than that for the airplane. A smaller 1/16-scale model in the 8-foot tunnel has a drag rise at these speeds similar to that for the larger model. Results obtained at the Arnold Engineering Development Center (AEDC), the Boeing Co., and the Langley Research Center strongly suggest that this variation is due primarily to the strong effects of the wind-tunnel wall on the extensive supersonic flow field produced by the displacement of the total airplane model at these speeds. Some Langley results (ref. 1) are shown in figure 3. A supercritical body of revolution of a fineness ratio of approximately 9 has been tested in the 8-foot tunnel and the 16-foot tunnel and free-dropped. This fineness ratio is greater than that for the F-8 airplane. As for the F-8 data, the results have been reduced to an incremental form. In this instance the drag coefficients are based on the body frontal area. Differences in drag for Mach numbers approaching 1.0, similar to those for the F-8 airplane, may be noted, with the drag increments for the two model-to-tunnel sizes being approximately equal but significantly lower than for the flight test. However, for the F-8 configuration the differences between wind-tunnel and flight occur at somewhat lower Mach numbers than for the ideal body of revolution because of the lower fineness ratio and nonoptimum area distribution, as described in paper 3.

The severity of this wall interference problem is illustrated by results from tests of a group of finless bodies of different ratios of model to wind-tunnel cross-sectional area in the 8-foot and 16-foot tunnels (fig. 4). For the range of model sizes usually used for high subsonic speed wind-tunnel tests, such as for the configuration of figures 2 and 3, the drag increment at $M = 0.99$ is approximately constant at a level substantially less than the free-drop value, noted by the level at zero body size. The drag-rise increment for the tunnel results does not reach that for the drop test until the ratio of body cross-sectional area to tunnel area is made very small. The smallest ratio shown is for a 6.3-centimeter (2.5-inch) diameter body in the 16-foot tunnel. Figure 4 also illustrates the abruptness of the onset of the problem. At a slightly lower Mach number of 0.98, the small drag increment is approximately the same over a range of the smaller body sizes.

ANALYSIS OF TUNNEL WALL EFFECT NEAR MACH 1.0

Pressure distributions for the bodies of the previous figure indicate the source of this drag difference near $M = 1.0$ (fig. 5). The pressures along the aft parts of the larger bodies are more positive than those on the smallest bodies. As with other mixed-flow problems, a complete explanation of this effect is involved. However, some explanation is in order. At these speeds, the induced supersonic field of the body grows rapidly. When this field approaches the wall, the relieving flow through the slots retards its growth and the supersonic field is less extensive than in free air. The effect is roughly similar to reduction in effective Mach number. It is interesting to note that the pressure distribution for the rear portion of the largest body is similar to that on the smallest body at a lower Mach number.

For an airplane with lift and a nonoptimum area distribution such as the F-8 supercritical wing airplane the problem is more complex. Presented in figure 6 is a comparison of the fuselage pressure distribution for the F-8 airplane at a Mach number of 0.99 and a lift coefficient of 0.23. As for the bodies of revolution, the pressures over the rear portion of the fuselage are more positive for a larger ratio of model-to-tunnel size. The wall effect also influences the wing pressures, as indicated in figure 7. The wing pressures obtained in the 8-foot and 16-foot tunnels for the same condition as for the previous figure are shown. The pressures on the aft portions of the inboard region and the entire chords of the outboard region are more positive in the 8-foot tunnel than in the 16-foot tunnel. The wind-tunnel flight comparisons presented in paper 6 for a Mach number of 0.99 but at a somewhat higher lift coefficient indicate roughly similar differences (fig. 8). However, the wind-tunnel results of figure 7 indicate similar trailing-edge pressure recoveries for the two tunnels, whereas the recoveries for the flight tests are significantly worse than for the 8-foot tunnel at this Mach number (fig. 8). These latter differences were described in detail in paper 6. This situation is probably due to the substantially greater magnitudes and more rearward locations of the second-velocity peaks in flight than in either of the wind-tunnel tests. Obviously, for flight the boundary layer must move through larger, steeper pressure gradients near the trailing edge, resulting in a greater tendency toward separation. These excessive second-velocity peaks for the flight data at this Mach number are not due primarily to a difference in effective Reynolds number, as for $M = 0.90$, but to the fact that the model was "tuned" in the wrong environment because of the wind-tunnel-wall effect. The results indicate that the aft camber is excessive for the most effective operation at cruise for full-scale flight conditions.

DRAG CREEP

The effect of the tunnel wall on the drag at lower Mach numbers must also be considered. As indicated in figure 2, the drag creep for the 1/11.5-scale F-8 supercritical wing airplane model in the 8-foot tunnel is greater than in flight. Also, the body of revolution in the 8-foot tunnel experiences a drag creep not indicated for the body in free drop (fig. 3). Comparison of the wind-tunnel and flight results for the F-8 airplane indicates that the difference is caused by variations of the pressure on the aft portion of the fuselage. These differences in drag creep are associated with classical subsonic wind-tunnel blockage, which increases very rapidly as Mach number is increased toward 1.0. The results shown in figures 2 and 3 indicate that, in contrast to the severe wall problem for Mach numbers near 1.0, this blockage effect is essentially eliminated by moderate reductions of model size. The 1/16-scale model of the F-8 airplane in the 8-foot tunnel has about the same creep as the flight vehicle, and the creep for the body of revolution in the 16-foot tunnel is similar to that for the drop body.

Wind-tunnel experiments at AEDC, Boeing, and Langley have indicated that the wall effect near $M = 1.0$ can be substantially reduced by reducing the porosity of the tunnel walls. Experiments in the 8-foot tunnel indicate that the creep can be essentially eliminated for large models by increasing tunnel porosity to the relatively large value which theoretically produces zero subsonic blockage, which leads to a dilemma: slots must be wide for one speed range and narrow for another. Extensive experiments in the 8-foot tunnel have not yielded a simple solution. Variable porosity will probably be required.

APPLICATION OF WING TO A TRANSPORT CONFIGURATION

The wall effect for the F-8 configuration at near-sonic speeds is confused at present by the fairly complex shock field of the nonoptimum longitudinal cross-sectional area distribution. Such a distribution is not representative of an actual transport airplane design, because any configuration designed for this speed range would undoubtedly have a more nearly optimum area distribution. To make the area distribution for the F-8 airplane configuration more representative, side fairings will be added to the fuselage. The effect of these side fairings on the area distribution of the F-8 airplane is shown in figure 9. The added area provides the physical cross-sectional area shown by the short-dashed line. In the region of the wing, the area added is less than that required to achieve the area distribution for an ideal supercritical body of revolution. The difference in area allows for the nonlinear expansion of the supersonic stream tubes above the upper surface of the wing. With the fuselage additions, the shock strengths and drag at Mach numbers near 1.0 are substantially reduced. However, it should be noted that ideally the additional physical indentation required to compensate for this effect should be concentrated on top of the fuselage rather than on the sides, as will be done for the F-6 airplane because of the high location of the wing.

Even with the addition of the side fairings, the drag rise for the flight configuration will probably be greater than that required for efficient cruise at Mach numbers above approximately 0.97. For a transport configuration with a higher fineness ratio and a more refined area-rule application than that used for the F-8 airplane, this limiting value probably would be about 0.98 in flight. This fact, together with the problems associated with wind-tunnel testing near a Mach number of 1.0, as just discussed, suggests that the design of the wing for the F-8 airplane was overly ambitious. The wing should have been designed for a Mach number of 0.98 rather than for near 1.0, as indicated in paper 3. An analysis of the wing pressure distributions measured in the wind tunnel and flight suggests that a wing designed for this lower Mach number, used in conjunction with an optimumly area-ruled fuselage, would have about 2° less sweep than that of the wing now on the F-8 airplane.

CONCLUDING REMARKS

The preceding discussion has indicated that wind-tunnel-wall interference results in lower drag in the tunnel than in flight at Mach numbers near 1.0 but causes a greater drag creep at lower Mach numbers; the aft camber of the supercritical wing now on the F-8 airplane is excessive for most efficient cruise in full-scale, free-air flight; and with our present knowledge and wind-tunnel equipment it appears impractical to attempt to develop a transport airplane with an efficient cruise Mach number higher than 0.98.

REFERENCE

1. Usry, J. W.; and Wallace, John W.: Drag of a Supercritical Body of Revolution in Free Flight at Transonic Speeds and Comparison With Wind-Tunnel Data. NASA TN D-6580, 1971.

SYMBOLS

A	cross-sectional area, m^2 (ft^2)
C_D	drag coefficient
C_L	lift coefficient
$C'_{N_{wp}}$	normal-force coefficient for wing panel outboard of first row of pressure orifices
C_p	pressure coefficient
c	local streamwise chord of basic wing panel, cm (in.)
i_t	horizontal-tail incidence relative to fuselage reference line, deg
M	Mach number
x	chordwise distance rearward of leading edge along the chord, cm (in.)
Δ	increment
δ_a	aileron deflection, deg

WING PRESSURE DISTRIBUTION

$M = 0.90, C'_{N_{wp}} = 0.30$

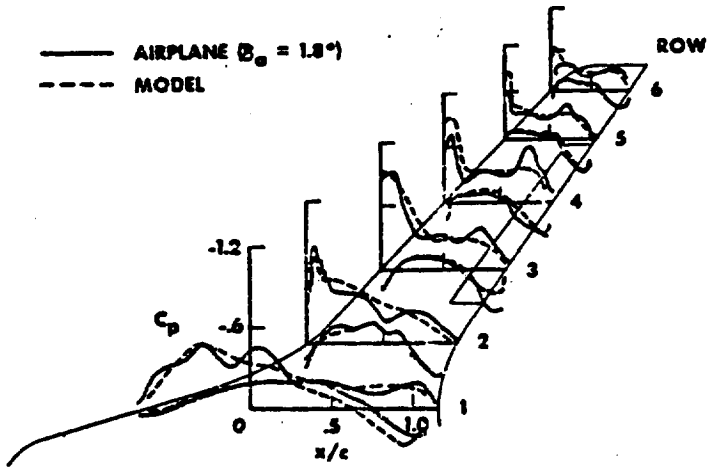

Figure 1

COMPARISON OF DRAG RISE INCREMENT FOR F-8 SUPERCRITICAL WING

$C_L = 0.4$, i_t EQUAL

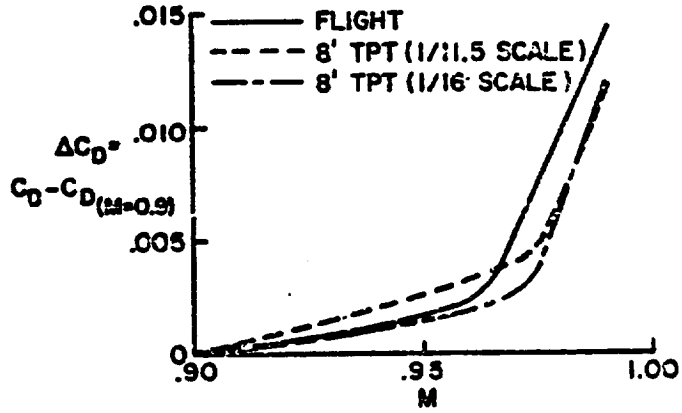

Figure 2

EFFECT OF WIND-TUNNEL WALL ON BODY DRAG RISE

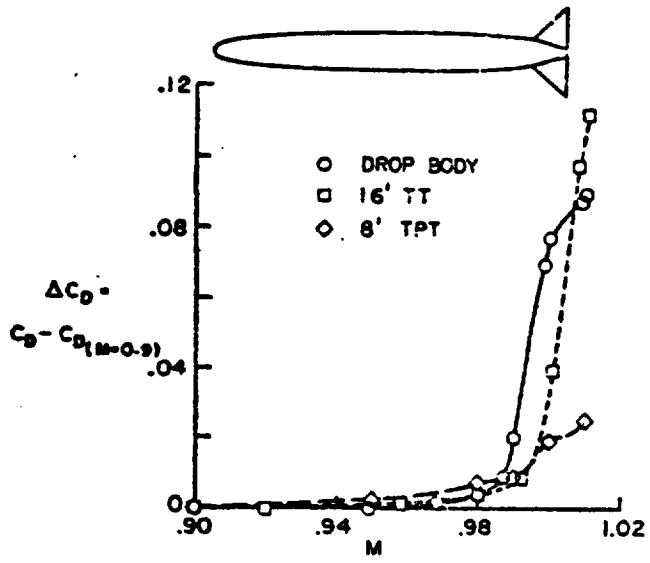

Figure 3

EFFECT OF RELATIVE BODY SIZE ON DRAG RISE

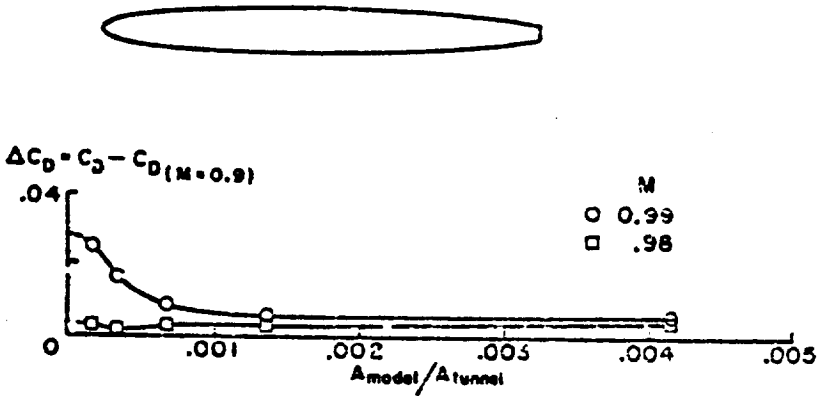

Figure 4

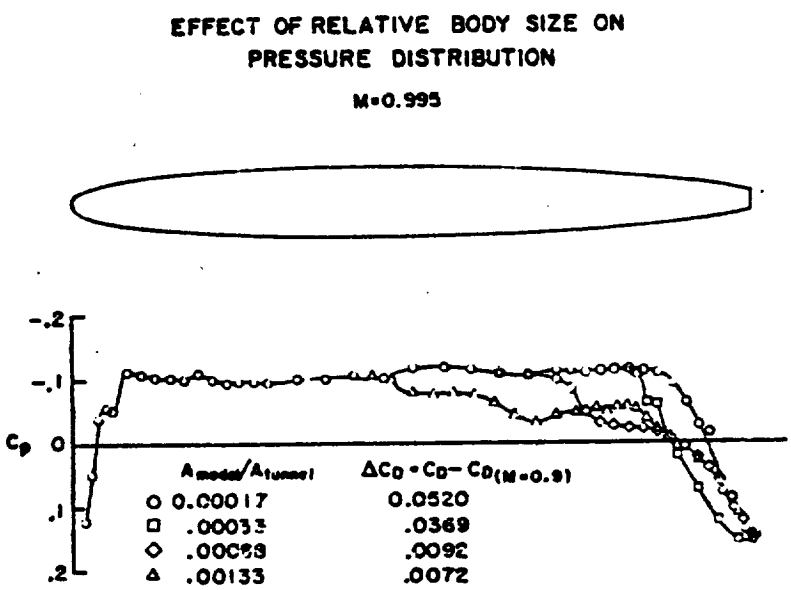

Figure 5

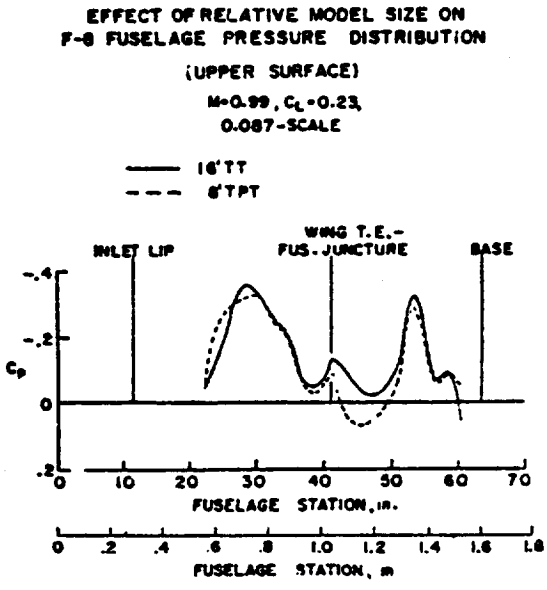

Figure 6

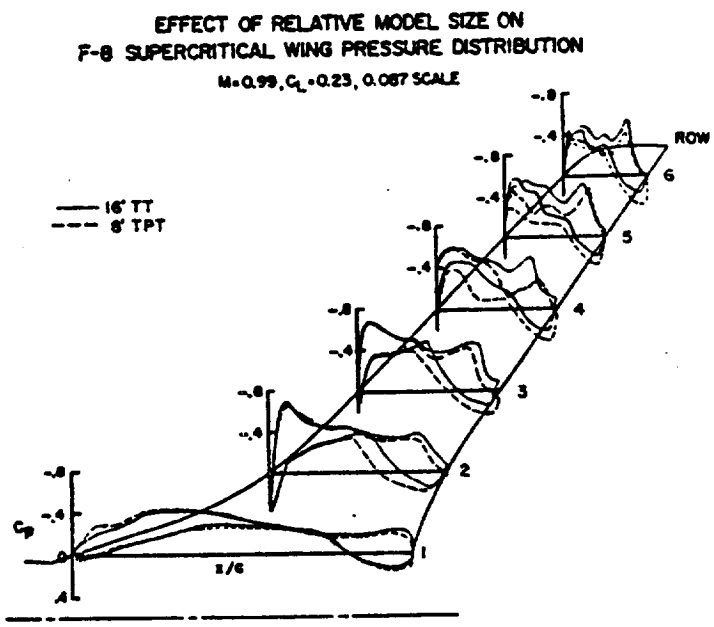

Figure 7

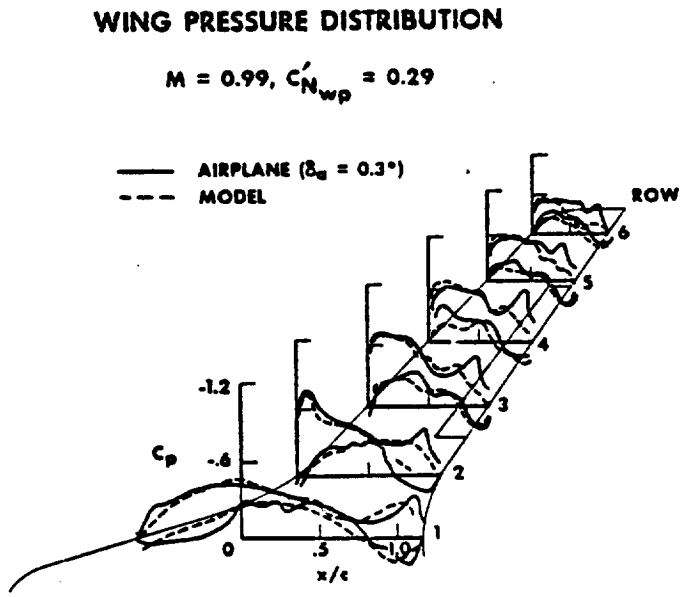

Figure 8

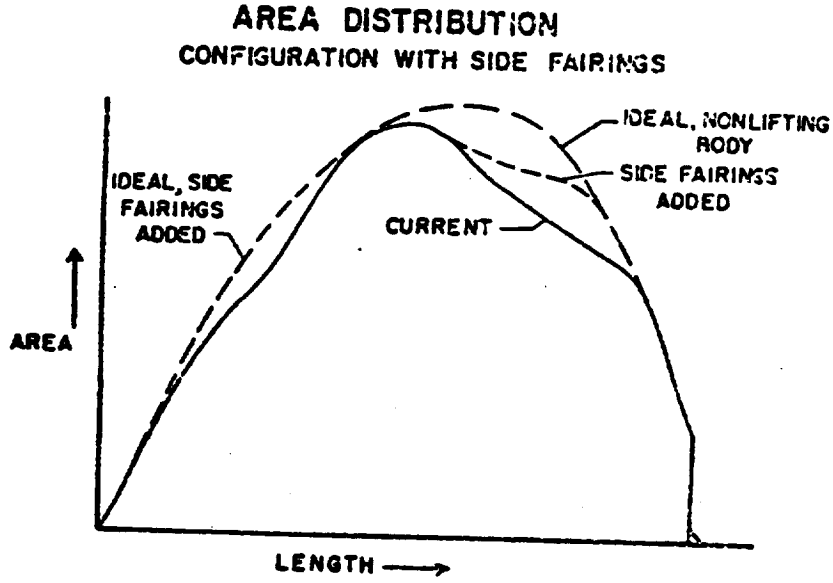
AREA DISTRIBUTION
CONFIGURATION WITH SIDE FAIRINGS
IDEAL, NONLIFTING BODY
SIDE FAIRINGS ADDED
IDEAL, SIDE FAIRINGS ADDED
CURRENT
AREA
LENGTH

Figure 9

10. SUMMARY AND FUTURE PLANS*

By Joseph Weil

Flight Research Center

and Richard C. Dingeldein

Langley Research Center

INTRODUCTION

In this final paper I will try to summarize where we have been and where we think we may be going in supercritical wing proof-of-concept flight testing.

Let us reexamine the objectives of the F-8 supercritical wing flight program. When the program was conceived in 1968, hopes were high that the promising characteristics indicated from wind-tunnel results would also be achieved at higher Reynolds numbers in flight. But there were some who felt that the gains might be as elusive and sensitive to the flight environment and practical airplane construction tolerances as the drag bucket predicted for low-drag airfoils in low-turbulence wind tunnels 30 years ago. We were particularly concerned about the difficulty of obtaining accurate wind-tunnel and flight correlations because the region of greatest interest is close to Mach 1. At and near Mach 1 the wind-tunnel results are subject to maximum uncertainties, and obtaining accurate flight data in this speed range can also be difficult.

Specifically, we were interested in determining gross indicators of design achievement, such as the transonic drag-rise Mach number, buffet, and stability and control characteristics. In the last category we wondered whether any unexpected and perhaps violent flight behavior might be triggered by flow separation at transonic speeds, especially in regard to operating margins relative to transports. As another objective, and to supplement this information, we planned to obtain detailed chordwise pressure distributions at six spanwise locations and to perform limited boundary-layer and wake surveys. Of course, in all the objectives a primary concern was the ability to predict flight behavior from wind-tunnel data. Also, we were anxious to determine the sensitivity of the flight results to aileron deflection, wing-surface roughness, and waviness. How did the attained performance deviate with departure from the wing profile design condition of a lift coefficient of 0.40 at Mach 0.99?

*Title, Unclassified.

SUMMARY OF F-8 SUPERCRITICAL WING RESULTS

The key F-8 supercritical wing results discussed in the earlier papers may be summarized as follows: I feel the overall performance goals of Richard T. Whitcomb, as demonstrated by delayed drag-rise Mach number and a relatively high lift coefficient for the onset of significant separation, have been achieved.

Figure 1 compares wind-tunnel and flight drag data at a lift coefficient of 0.40. Differences in flight and wind-tunnel fuselage base and boattail pressures and horizontal-tail deflection have been accounted for, so that any dissimilarity in the data shown should be associated with effects on the wing. Two points are worthy of mention. First, the drag-rise Mach number for both wind-tunnel and flight data is approximately the same (0.96). Second, the drag obtained in the Langley 8-foot tunnel at Mach 1 is significantly lower than the drag obtained in flight. The more gradual drag rise in the 8-foot tunnel data was shown in paper 9 to be primarily the result of tunnel wall interference.

Figure 2 shows the flight-derived buffet-onset boundary in terms of airplane normal-force coefficient and Mach number. There is no significant decrease of the C_{N_A} for buffet onset at transonic speed, and, actually, at the design Mach number of 0.99, the C_{N_A} for buffet onset increases with Mach number. Up to Mach numbers slightly in excess of 0.90 it would appear that means are available to adequately correlate flight buffet onset with wind-tunnel indicators. Near design Mach number a reliable method for predicting buffet onset is lacking, and additional effort is required to improve existing techniques.

There have been some discrepancies in pressure distributions determined in wind-tunnel tests and in flight, which may suggest slight modifications to design techniques when the reasons for these differences are better understood, although here again the overall agreement is believed to be fairly good. Figure 3 compares flight and wind-tunnel pressure distribution near the design C_L condition at Mach 0.99. It was at this condition that the maximum attempt was made at model scaling of outboard-wing-panel boundary-layer conditions, and total wing twist was comparable. In general, the flight and wind-tunnel pressure distributions agree fairly well, although the shock location was farther aft and trailing-edge pressure recovery was not as good in flight as in the tunnel.

Even though there have been some differences in predicted and flight-determined stability and control derivatives, the handling qualities were estimated quite well and there have been no unexpected or violent flight control incidents.

Although not a stated objective of the program, the F-8 supercritical wing investigation has enabled us to contribute to the important area of wind-tunnel test techniques near Mach 1.

FUTURE PLANS FOR F-8 SUPERCRITICAL WING PROGRAM

Where does the F-8 program go from here? Although we feel we have presented a meaningful progress report, much data are already in hand that will require additional analysis. This should enable us to better separate some of the variables that are now ill-defined and hence were not discussed.

The additional tasks remaining in the current flight test program include making boundary-layer and wake measurements, determining the effect of wing-surface variables, and evaluating the Mach 1 fairings.

The locations of the boundary-layer rake and swinging probe for the wake surveys are shown in figure 4. Upper-surface boundary-layer data will be obtained with a 12.7-centimeter (5-inch) rake at the two spanwise locations shown. Somewhat more extensive wake surveys will be possible at the same spanwise locations with the rotating pitot probe. These surveys, which may help explain some of the differences between predicted and flight results, are the next scheduled objectives for the flight program. Later this year we plan to increase the number of high-response pressure orifices, as shown in figure 4, to obtain more information on the mechanism of the shock—turbulent-boundary-layer interaction and its contribution to the separation phenomenon, which, in turn, will contribute to the development of predictive techniques for mixed flows.

One of the original objectives that has not yet been achieved is the determination of the sensitivity of the supercritical wing pressure distribution to various types of roughness and simulated production imperfections. Figure 5 illustrates the scope of projected tests. The upper surface of the outboard wing region, shown crosshatched, would be modified so that the effects of such surface variables as spanwise gaps, aft-facing steps, waviness, and simulated screw or rivet heads could be examined. Another possibility involves removing the sealing devices now at the aileron hinge.

Early this summer the Mach 1 fairings shown in figure 6 will be installed. The main purpose of these fairings is to produce a weaker shock pattern near Mach 1. It will be interesting to see whether this will provide a better correlation between 8-foot wind-tunnel data and flight results in this Mach range.

Also being considered is a modification to the trailing edge of the present wing to reduce the magnitude of the second pressure peak and thus possibly produce results closer to the lower Reynolds number wind-tunnel data.

It is fairly well known that the Langley Research Center is sponsoring a number of systems studies to determine the role that advanced technology might play in providing more efficient long-haul transport aircraft which can cruise at very high subsonic Mach numbers. These studies, although not yet complete, have indicated some promising areas which might provide the basis for additional flight demonstrations. Because of the economies that can be achieved by using the F-8 test-bed, a new supercritical wing for this vehicle incorporating more representative advanced transport features is being

studied. Some of the design considerations for the wing are composite structures, high-lift devices, and active controls.

The use of composite structures would make it possible to improve strength and stiffness at reduced weights by choosing the location and direction of load-carrying fibers so that they are most effective. Studies indicate that a much lighter wing of given geometry—perhaps up to 25 percent lighter than possible with conventional metal construction methods—can be fabricated by using composite materials. Moreover, for a given wing-sweep angle, area, and thickness distribution, this weight-saving could be traded to achieve a higher-aspect-ratio composite wing than could be constructed from metal alone for the same weight. It may become practical to obtain the benefits of high aspect ratio—as high as 9—for transport aircraft. Figure 7 illustrates how an aspect-ratio-9 wing would look on the F-8 test-bed. With this configuration for an advanced transport, large gains in cruise efficiencies would be expected to translate directly into airline profits. Use of composites for major portions of the wing structure as well as high-lift devices and control surfaces is, therefore, an important design consideration. This flight application and the resulting structural and aerodynamic evaluation could provide data that are not available elsewhere. Benefits from improved surface smoothness and contour control are also expected, but the relatively few flight hours for the experimental airplane would not allow assessment of service life of composite structures.

Inasmuch as the present F-8 supercritical wing program has increased our confidence in predicting the aerodynamic characteristics of an almost ideal wing at transonic speeds, a follow-on program would not be complete without proper attention to low-speed characteristics. Any new wing will be designed to incorporate advanced high-lift devices. Thus the program will provide means of evaluating all the factors that must be considered for transport operation from takeoff to landing. The improvements in low-speed performance, as well as the effects of retracted high-lift devices on cruise drag, will be an important part of this program.

One of the most questionable areas resulting from tailored structural characteristics using composites is in aeroelasticity. Such problems as flutter and response to turbulence may adversely affect the safety or service life of the aircraft. However, numerous studies have shown that many of these dynamics problems can be alleviated through the use of active control systems. Although these active control systems offer promise in suppressing gust loads and flutter and improving ride qualities and maneuver loads, this area represents the design consideration least capable of definition at this time.

A broad, NASA-wide research activity in this area is being formulated. Although it is too early to be specific, the possible application of active controls to a new F-8 wing could provide early flight validations of such advanced concepts. Hydraulically actuated spoilers would be a candidate control for wing-load alleviation, a single-slotted flaperon for load alleviation and gust suppression, and an outboard-tip flaperon for flutter suppression. In addition, these devices could be used to produce variable camber and twist to provide better wing geometry for off-design performance improvement.

The cost effectiveness of several alternate approaches to a new experimental airplane is being studied.

[redacted]

TRANSONIC AIRCRAFT TECHNOLOGY PROGRAM

The work that has been accomplished and is planned on the T-2C and F-8 airplanes to provide basic supercritical wing technology will be augmented by a program that was approved about a year ago—the Transonic Aircraft Technology or TACT program. This program will provide additional proof of concept in supercritical wing technology using an F-111A variable-sweep tactical aircraft as the test-bed. The wing will have much more representative elastic characteristics than provided by the boilerplate F-8 construction and will seek higher angle-of-attack maneuvering performance optimization.

The results of this joint NASA/USAF program should have direct application to future high-performance combat aircraft. Figure 8 is a comparison of the basic F-111A and the TACT F-111 airplanes. The TACT concept development was a joint endeavor of General Dynamics and Richard T. Whitcomb. The TACT wing panel is of lower aspect ratio, less tapered, and of lower maximum sweep than the basic F-111 wing. Some of these changes in geometry were dictated by a design objective of optimizing the cruise and maneuvering performance in the 0.85 to 0.90 Mach range for the intermediate sweep configurations. The TACT F-111 airplane has a single-slotted flap rather than the double-slotted flap of the conventional F-111A airplane. The flap system on the supercritical wing does not yield a maximum lift coefficient as high as that of the basic F-111 airplane but was selected on the basis of simplicity and minimum cost.

Some of the detailed program objectives are as follows:

To demonstrate transonic maneuverability by -
- Evaluating buffet onset and intensity
- Ascertaining energy-maneuverability capability
- Assessing overall handling qualities from gunsight tracking

To determine overall performance and handling qualities such as -
- Drag-rise Mach number, drag polars
- Effects of wing sweep and external stores
- Low-speed handling qualities with high-lift devices

To define local aerodynamics through -
- Pressure distribution studies of the effects of wing sweep and external stores and the effects of flaps, spoilers, and leading-edge flaps

To determine wake drag

We are particularly anxious to evaluate the potential of the supercritical wing for raising the buffet-onset lift coefficient and reducing its intensity, together with the expected reduction in drag at elevated g, which is so important for a highly maneuverable aircraft.

In overall performance and handling we are interested in determining the sensitivity of the supercritical wing characteristics to small changes in sweep. Will the supersonic

[redacted]

performance at maximum sweep be penalized by the presence of the supercritical airfoil? Much more emphasis will be placed on determining the performance and low-speed handling qualities with high-lift devices than in the F-8 program.

In the study of local aerodynamics, systematic pressure distributions will be obtained to help us understand effects of wing sweep, external stores, and high-lift devices and to obtain data for design loads.

In all these areas flight results will be carefully correlated with wind-tunnel data.

The management, technical direction, funding, and contract monitoring of the TACT program is the responsibility of the Air Force Flight Dynamics Laboratory. As mentioned previously, much of the conceptual testing and development of the design was done in the 8-foot tunnel at the Langley Research Center. Most of the final detailed wind-tunnel work is being done at the Ames Research Center.

General Dynamics has the role of designing, fabricating, and installing the new wing on an F-111 fuselage. They will also support the entire program, including the flight test phase as needed.

The Flight Research Center is responsible for flight test instrumentation and data reduction and the conduct of the flight test program. This latter effort will be a joint endeavor with the Air Force Flight Test Center, which will actively participate with test pilots, flight planning, and data analyses.

The time schedule for the F-111 program is shown in figure 9. Program approval was obtained in February 1971. Final wind-tunnel testing and wing design and fabrication will be completed by next fall. The F-111A airplane that will ultimately accept the new wing is being instrumented at the Flight Research Center to enable some additional performance and maneuverability baseline data to be obtained starting in late spring. These tests will end in October when the airplane is scheduled to be sent to Fort Worth, Texas, for the mating of the new wing and other preflight activities. The actual flight test program is scheduled to start in May 1973, and these tests and analyses will continue at least through calendar 1974.

CONCLUDING REMARKS

Significant strides have been made as a result of the simple, minimum-cost T-2C and F-8 supercritical wing programs in bringing the supercritical wing from a promising wind-tunnel development to the point where the designer can have greater confidence based on flight-proved technology. The T-2C program has shown that almost a 50-percent increase in airfoil thickness is possible with no reduction in drag-rise Mach number. The F-8 program has demonstrated that drag-rise Mach numbers near 1 are attainable for subsonic transport wings. Data for the T-2C airplane, which is closer to a two-dimensional configuration than the F-8 airplane, have shown a somewhat better overall correlation with wind-tunnel predictions. Although not quite as close correlation was obtained with the F-8 data, for the most part the correlations were good, considering the much more complicated three-dimensional flow problem associated with the highly swept wing and the difficult problem of obtaining reliable data near Mach 1 in either a wind-tunnel or flight environment. We plan to extend the scope of the F-8

program in the coming months, as described earlier. Data to be obtained in the F-111 supercritical wing program will add a new dimension with the application of supercritical wing technology to a tactical variable-sweep airplane.

Finally, lest we leave the impression that we are overly smug and complacent, I would like to say that the F-8 program has shown several areas where predictive techniques need substantial improvement. Also, this program has reaffirmed the requirement for developing improved test techniques near Mach 1. It is hoped that the current and projected supercritical wing tests will serve as a catalyst to achieve some of these goals.

SYMBOLS

b	wing span, m (ft)
C_D	drag coefficient
C_L	lift coefficient
C_{N_A}	airplane normal-force coefficient
$C'_{N_{wp}}$	wing-panel normal-force coefficient, $\int_{0.133}^{1} c_n \frac{c}{c_{av}} d\left(\frac{2y}{b}\right)$
C_p	pressure coefficient, $\frac{p - p_\infty}{q}$
c	local streamwise chord of basic wing panel, cm (in.)
c_{av}	average chord of wing panel, cm (in.)
c_n	section normal-force coefficient, $\int_{\text{Leading edge}}^{\text{Trailing edge}} \left(C_{p_l} - C_{p_u}\right) d(x/c)$
M	Mach number
M_{DR}	drag-rise Mach number
p	local static pressure, N/m^2 (lb/ft^2)

[redacted]

p_∞	free-stream static pressure, N/m^2 (lb/ft^2)
q	free-stream dynamic pressure, N/m^2 (lb/ft^2)
x	chordwise distance rearward of leading edge, cm (in.)
y	distance perpendicular to the airplane centerline, cm (in.)

Subscripts:

l	wing lower surface
u	wing upper surface

[redacted]

COMPARISON OF ADJUSTED DRAG RESULTS

$C_L = 0.4$

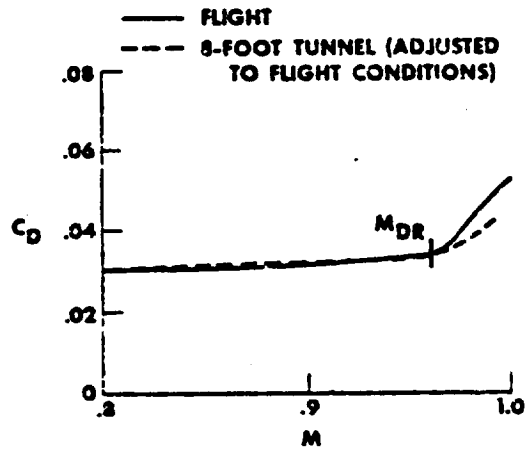

Figure 1

F-8 SUPERCRITICAL WING BUFFET ONSET

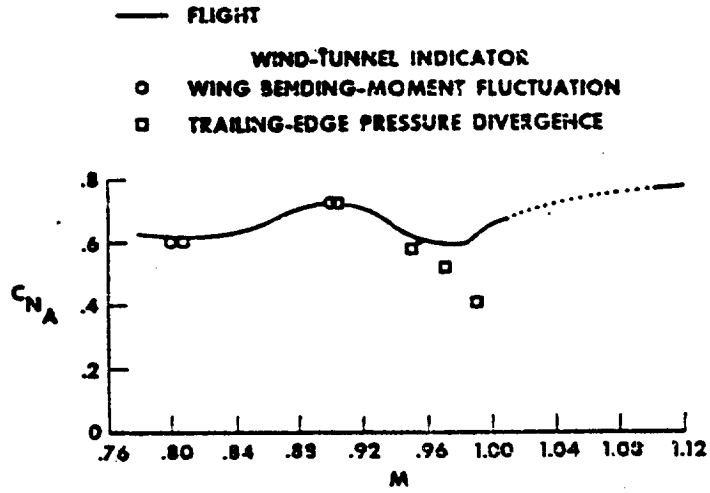

Figure 2

F-8 SUPERCRITICAL WING PRESSURE DISTRIBUTION

$M = 0.99,\ C'_{N_{wp}} = 0.35$

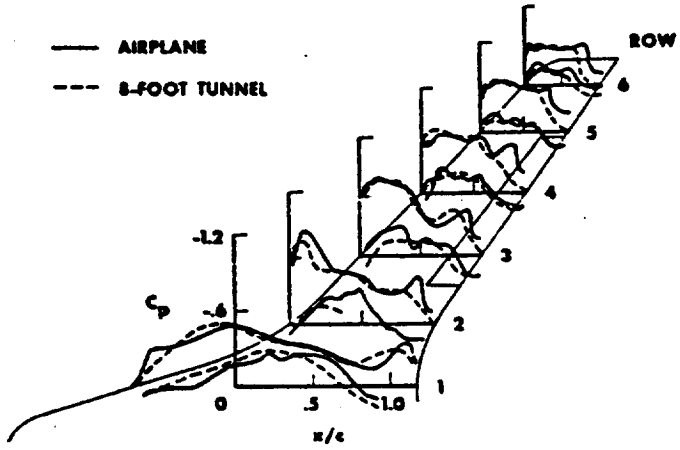

Figure 3

BOUNDARY LAYER AND WAKE SURVEY LOCATIONS ON F-8 SUPERCRITICAL WING

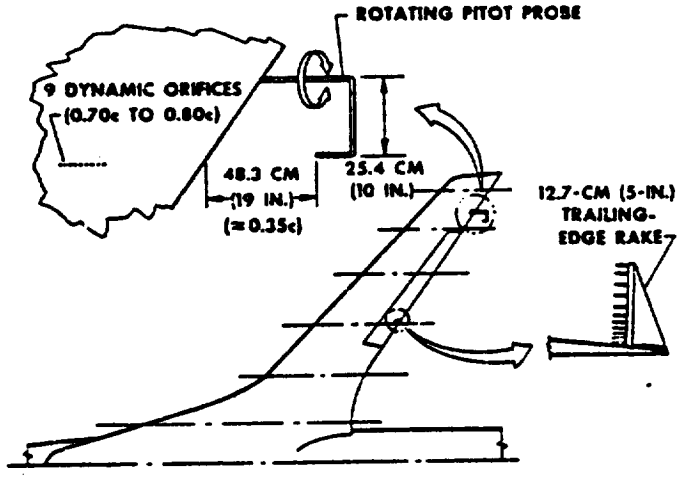

Figure 4

WING SURFACE VARIABLES

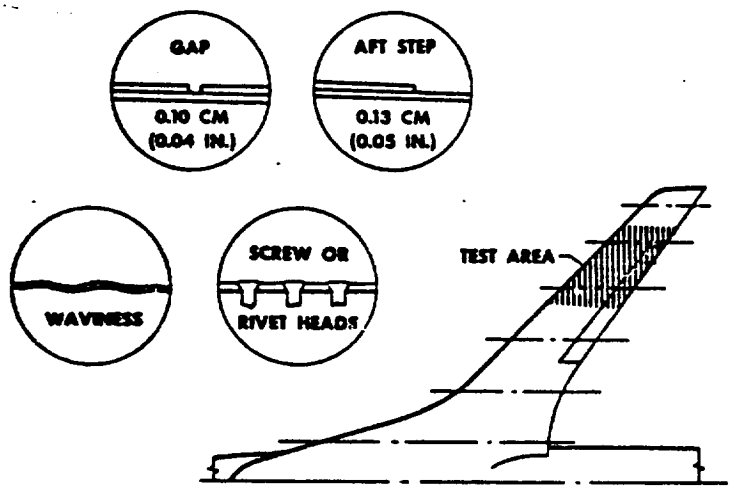

Figure 5

MACH 1 FAIRING FOR F-8 SCW

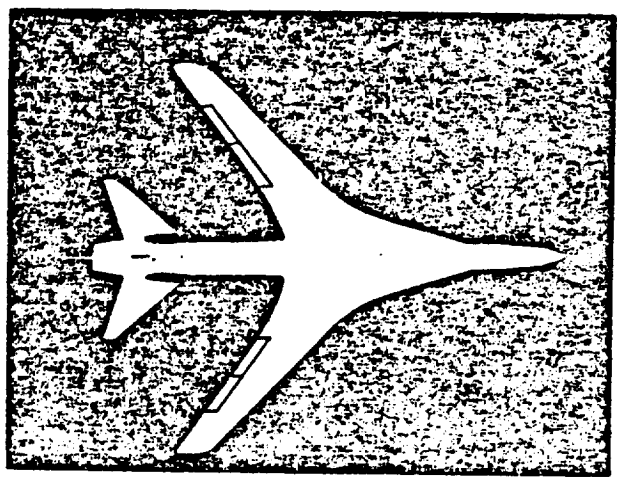

Figure 6

[redacted]

POSSIBLE NEW WING FOR F-8

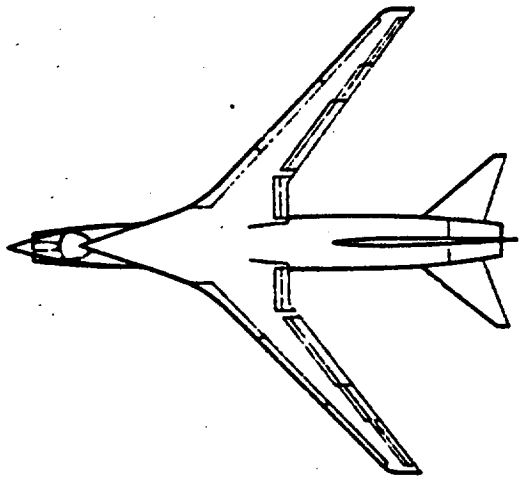

Figure 7

AIRPLANE COMPARISON

PARAMETER	TACT	BASIC
WING		
AREA, M^2 (FT^2)	56.1 (604)	48.8 (525)
MAC, CM (IN.)	219.5 (125.8)	275.6 (108.5)
ASPECT RATIO	5.83	7.56

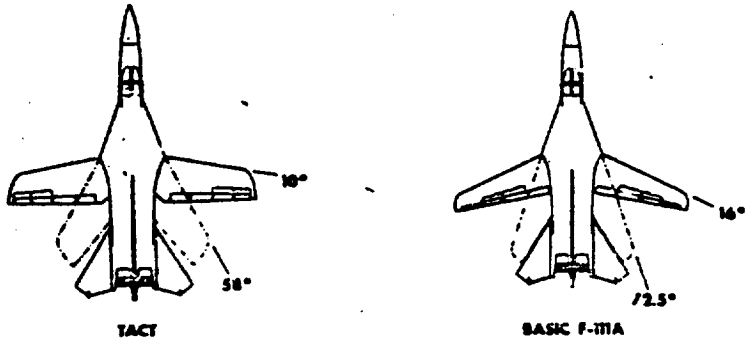

Figure 8

[redacted]

[redacted]

TACT PROGRAM SCHEDULE

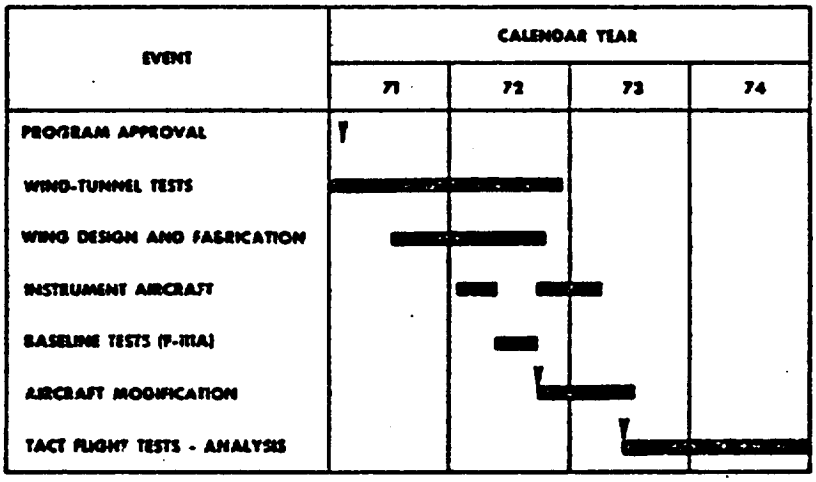

Figure 9